1987

Split-peak determination of protein adsorption kinetics in high-performance affinity chromatography

David Scott Hage
Iowa State University

Hage, David Scott

SPLIT-PEAK DETERMINATION OF PROTEIN ADSORPTION KINETICS IN HIGH-PERFORMANCE AFFINITY CHROMATOGRAPHY

Iowa State University PH.D. 1987

PLEASE NOTE:

In all cases this material has been filmed in the best possible way from the available copy. Problems encountered with this document have been identified here with a check mark __✓__.

1. Glossy photographs or pages _____
2. Colored illustrations, paper or print _____
3. Photographs with dark background _____
4. Illustrations are poor copy _____
5. Pages with black marks, not original copy _____
6. Print shows through as there is text on both sides of page _____
7. Indistinct, broken or small print on several pages ✓
8. Print exceeds margin requirements _____
9. Tightly bound copy with print lost in spine _____
10. Computer printout pages with indistinct print _____
11. Page(s) _____ lacking when material received, and not available from school or author.
12. Page(s) _____ seem to be missing in numbering only as text follows.
13. Two pages numbered _____. Text follows.
14. Curling and wrinkled pages _____
15. Dissertation contains pages with print at a slant, filmed as received _____
16. Other _____

_____

_____

University
Microfilms
International

Split-peak determination of protein adsorption kinetics in high-performance affinity chromatography

by

David Scott Hage

A Dissertation Submitted to the
Graduate Faculty in Partial Fulfillment of the
Requirements for the Degree of
DOCTOR OF PHILOSOPHY

Department: Chemistry
Major: Analytical Chemistry

Approved:

Signature was redacted for privacy.

In Charge of Major Work

Signature was redacted for privacy.

For the Major Department

Signature was redacted for privacy.

For the Graduate College

Iowa State University
Ames, Iowa

1987

TABLE OF CONTENTS

GENERAL INTRODUCTION

Principles and History of Affinity Chromatography

The purification and determination of biological macromolecules is an area which has long been of interest. This has resulted in the development of a number of separation techniques for such compounds as proteins and nucleic acids. Most of these methods are based on physiochemical differences in the molecules being separated, including their size, shape, and charge. Examples of such techniques are electrophoresis, ion-exchange chromatography, and size exclusion chromatography (1-3).

In biomacromolecular separations, the molecule of interest may only occur in small amounts or in the presence of a large number of similar compounds. As a result, a multistep procedure based on several different techniques may be needed to obtain a good separation. This approach not only requires a great deal of time and effort, but may also give the desired compound in only a low yield (4,5).

One alternative approach is to use affinity chromatography. Affinity chromatography may be defined as a chromatographic technique based on the selective, reversible interactions of biologically active molecules (4). In other words, it is based on a functional property, the ability of biolog-

ical molecules to bind selectively with other molecules. This type of interaction is characteristic of many biological systems, such as the binding of enzymes with substrates, antibodies with antigens, and hormones with hormone receptors (6).

In affinity chromatography, these interactions are used by attaching a molecule able to selectively bind the analyte, or molecule of interest, to a solid support. This immobilized molecule is called the affinity ligand. Although the ligand is usually of biological origin, compounds including synthetic dyes (7), metal chelates (8), thiol groups (9), and apolar groups (10) have also been used.

Once the ligand has been immobilized, the support is packed in a column and used in a separation scheme such as shown in Figure 1. First, sample is applied to the column under conditions which allow the analyte to bind to ligand. This is known as the adsorption step. Since, ideally, the ligand binds only with the analyte, other components of the sample are eluted from the column and appear in the non-retained peak.

The analyte is eluted by changing the mobile phase composition to dissociate the analyte-ligand complex. This may be done through nonspecific methods which cause conformational changes in the analyte or ligand. These methods include changing the pH, ionic strength, or organic solvent

Figure 1. Separation scheme for affinity chromatography

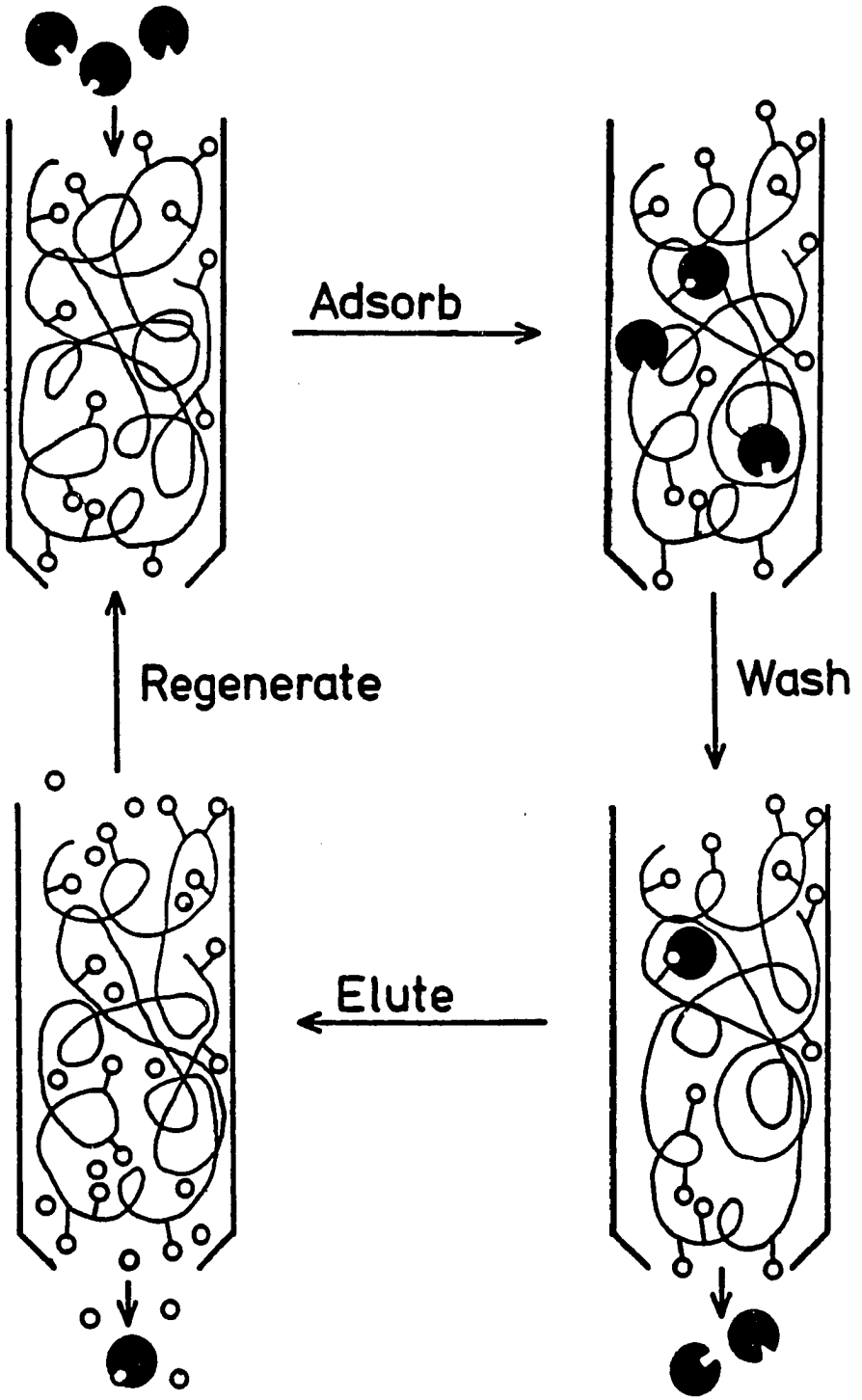
Adsorb
Wash
Elute
Regenerate

content of the mobile phase. The analyte can also be eluted by using a technique known as biospecific elution. In this case, a compound is added to the mobile phase that competes for active sites on the analyte or ligand, forcing the analyte off the column by mass action (11). For example, enzyme retained on an immobilized inhibitor column may be eluted by adding free inhibitor to the mobile phase. After the analyte has been eluted by one of these methods, the mobile phase is changed back to its original composition, the column regenerated, and the entire process repeated with the next sample.

Based on this technique, a large number of analytes have been purified and studied. These have included enzymes, antibodies, and nucleic acids, as well as cells and viruses (4,5,11). In many cases, the high selectivity of affinity chromatography allows these separations to be performed in only one or two steps, with typical purifications of a hundred- to thousand-fold (4,5). In work with hormone receptors, a purification in excess of 500,000-fold has even been reported (4).

The first reported use of affinity chromatography was in 1910, when Starkenstein used insoluble starch to purify α-amylase (12). In 1924, it was proposed that such a technique, in which analyte binds to a "fixed partner", would be useful as a general method for the separation of active biological

compounds (13). However, the first use of immobilized ligands was not reported until 1951, when Campbell et al. used antigens attached to a solid support for the purification of antibodies (14). Affinity chromatography was soon used to purify a number of other compounds, including tyrosinase (15), flavokinase (16), and avidin (17).

Despite this work, the technique did not enjoy widespread use until the 1960s. Several important breakthroughs occurred at this time. One was the introduction of better affinity chromatographic supports, such as beaded agarose (18). Another was the development of the cyanogen bromide method (19), a general technique for the coupling of proteins and other ligands to these supports through primary amine groups. Both developments were used in 1968 by Cuatrecasas et al. to produce what are considered the first modern affinity chromatographic separations (20).

Affinity chromatography has since become a popular tool for biochemical separations, with its use being reported in more then 3,500 papers over the past 19 years. During this time, agarose and other soft gels have been the supports most commonly used. These nonrigid supports have limited most of the reported applications to the use of low flowrates and pressures, resulting in typically long analysis times (11,21).

More rapid separations were made possible by the development of diol-bonded silica in 1976 by Regnier and Noel (22). Diol-bonded silica is a rigid, uniform support material. This makes it more chromatographically efficient than agarose and allows it to be used at higher flowrates. Also, it does not adsorb most proteins, unlike normal silica (23), and yet can be easily modified for ligand attachment. These properties make it an almost ideal affinity chromatographic support. The potential of diol-bonded silica in affinity chromatography was demonstrated in 1978 by Ohlson et al., who used it to obtain several affinity separations with analysis times of only 5 min (24). This was the beginning of the technique known as high-performance affinity chromatography (HPAC).

Because HPAC combines the selectivity of affinity chromatography with the speed of high-performance liquid chromatography (HPLC), a great deal of interest has been expressed in developing HPAC as a viable analytical technique. Although still an area of active research, a number of analytical applications using HPAC have already been developed. These include the profiling of urine samples (25), the measurement of immunoglobulins in cerebrospinal fluid (26) and serum (27), and the development of reusable immunoassays (28). In some cases, such separations are possible in as little as one to three minutes (21,27). This work will examine some of the

practical and fundamental aspects of using HPAC in analytical applications, but most of the principles discussed will apply to low-performance affinity chromatography as well.

Review of Previous Work

In affinity chromatography, a number of factors must be considered in obtaining good separations. These include choosing a suitable ligand and immobilization method, selecting the correct mobile phase conditions for analyte adsorption, and determining how to elute analyte from the column without irreversibly damaging the immobilized ligand (5,11,29). Another factor which can be important is the amount of time allowed for adsorption. Failure to consider this can result in a significant amount of analyte eluting in the nonretained peak. This occurs due to what is known as the split-peak effect.

The split-peak effect occurs when injection of even a small amount of pure analyte results in two fractions: a non-retained peak and a strongly-retained peak. This is believed to be a result of the kinetic nature of the chromatographic process and is characterized by a change in the relative size of the nonretained peak with flowrate and/or column size.

The theoretical basis of this effect dates back to 1955, when it was shown by Giddings and Eyring that a molecule

undergoing simple first-order adsorption on a column has a probability $e^{-k\ t}$ of eluting without being retained, where k is the first-order adsorption rate constant and t is the void time of the column (30). It was later demonstrated by DeLisi et al. in computer simulations that this effect can also be produced by slow mass transfer processes within the column, such as diffusion of the analyte into and out of the pores of the support (31).

The earliest recognized report of this phenomenon was made by Cuatrecasas, Wilchek, and Anfinsen in 1968 (20), the same work in which the first modern affinity chromatographic separations were presented. This effect was seen when they attempted to purify staphylococcal nuclease on an immobilized inhibitor column. In this experiment, it was found that a small amount of nuclease sometimes appeared in the nonretained fraction. Although partly related to the sample concentration used, the amount of nonretained nuclease was also found to be flowrate dependent, with nonretained nuclease tending to appear when fast flowrates were used (20).

The time dependence of analyte adsorption was studied in more detail by Lowe et al. in 1974 (32). In this work, the binding of lactate dehydrogenase and glycerokinase to an AMP-Sepharose column was examined as a function of adsorption time. Although the column had the same capacity for both

enzymes, significant differences were noted in the amount of each enzyme that bound to the column as the adsorption time was varied. For the lactate dehydrogenase, essentially all of the enzyme was found to bind over adsorption times of 1, 20, and 67 hours. Glycerokinase, however, gave nonretained fractions ranging from 41 to 74% under the same time and sample size conditions, with the amount of nonretained glycerokinase increasing as the adsorption time decreased. It was also noted that the time required for adsorption at a given flow-rate could be varied by changing the column size, in that even nonretained lactate dehydrogenase could be obtained if sufficiently small columns were used. In explaining these effects, it was suggested that they were somehow related to the rate of interaction of the enzymes with the immobilized ligand (32).

Since the presence of nonretained analyte is undesirable in any type of chromatographic separation, it was not long after this effect was observed that a number of methods were proposed for dealing with it. One suggested technique was to simply use low flowrates in order to allow sufficient time for analyte adsorption (29,33). Another was to stop the flow of analyte through the column during the adsorption step (29,32), again resulting in an increase in the adsorption time. Although these techniques were potentially useful in reducing the split-peak effect, they did so at the cost of increasing

the overall separation time. Despite the fact that a better understanding of this effect could have allowed the extent of this increase to be minimized, little further work was done in this area for some time.

It was shortly after the introduction of HPAC that a renewed interest in this effect appeared. The first report of the split-peak effect in HPAC was in 1980 by Sportsman and Wilson, where it was observed in both the retention of immunoglobulin G (IgG) on immobilized anti-IgG antibodies and in the binding of insulin to a similar anti-insulin support (34). The effect was soon reported in a number of other HPAC systems. These included the adsorption of trypsin and α-chymotrypsin to immobilized soybean trypsin inhibitor (35,36), the binding of leukocyte A interferon to immobilized anti-interferon antibodies (37), the adsorption of acetylcholinesterase to immobilized procainamide (38), and the binding of glusose oxidase antibody conjugates to antigen previously adsorbed on an affinity column (28).

Since the goal of HPAC is to provide faster separations than are obtained with low-performance affinity chromatography, the guidelines previously used in dealing with the split-peak effect were no longer adequate. Instead, a better understanding of the relationship between retention and the adsorption time was needed, allowing the amount of analyte

retained in a given amount of time to be optimized. One study examining this effect more closely was the work of Roy et al. (37). The goal of this study was to develop an HPAC system for the fast purification of recombinant interferon. One of the factors considered in the design of this system was the amount of interferon retained as a function of flowrate. This was studied by applying known amounts of analyte to anti-interferon columns at various flowrates. The amount of retained interferon was then determined and plotted as a function of flowrate and sample load. From these plots, it was possible to determine what flowrate conditions were needed to produce a given degree of analyte adsorption at a particular load. Although an entirely empirical approach, this method was effective in quantitativly dealing with the split-peak effect (37).

A more fundamental approach was suggested by the work of Sportsman et al. (34,39). In this case, the split-peak effect was related directly to the reactions involved in analyte adsorption. This was first done by describing the adsorption process in terms of an equilibrium between the bound and free analyte (34). This system was chosen since the ratio of the bound to free analyte (b/f) obtained on immunoaffinity columns was found to vary with sample size in a manner similar to that seen in immunoassays, which are usually described by an equi-

librium model. Based on this model, plots of b/f vs. sample size were used to give an apparent equilibrium constant, K', for each of the systems studied. Although it was predicted that such plots should give a linear response, significant curvature was actually seen. It was suggested that this curvature was due to antibody heterogeneity, but the additional fact that K' varied with flowrate indicated that this model did not adequately describe the split-peak effect for the systems studied (34).

A different model was used in the second series of experiments. In this case, analyte adsorption was described in terms of a second-order reversible rate expression (39). This model was then used to study the binding of insulin to an immunoaffinity column by measuring the amount of nonretained insulin as a function of flowrate. The data were then plotted according to the rate expression for the model, using the column void time as the time of reaction. To obtain kinetic data from this plot, it was also necessary to determine the value of the equilibrium binding constant. This approach did give an adsorption rate constant comparable to that obtained in batch kinetic studies, but the plots again showed significant deviations from the predicted response (39). Although neither this nor the previous model appeared to adequately describe the data, this work did suggest that a more funda-

mental description of the split-peak effect might be possible. This work also suggested that the effect might be useful in the determination of such physical parameters as adsorption rate constants.

Statement of the Problem

It has already been shown that the split-peak effect can be an important consideration in the use of affinity separations. It has also been shown that a good quantitative description of this effect has not yet been developed. One goal of this work, then, was to study the split-peak effect and to develop a theoretical model by which it could be quantitated or measured. Once developed, this model was tested by using it to characterize the split-peak behavior of IgG on protein A affinity columns, as described in Section I.

Another goal of this work was to explore any possible analytical applications of the split-peak effect and the model used to describe it. One such application is the optimization of analyte adsorption. This is illustrated in Section II, where the equations developed in this work are used in the design of an HPAC system for the determination of two serum proteins. Two other applications, the comparison of the kinetic properties of affinity supports and the determination of chromatographic rate constants, are discussed in Section I.

Finally, some fundamental aspects of the split-peak effect are also considered. One of these is the effect of nonlinear elution conditions on the amount of nonretained analyte. This was examined through the use of computer simulations. The results of this study are presented in Section III.

THEORETICAL DESCRIPTION OF THE SPLIT-PEAK EFFECT

Chromatographic Model

To obtain a method for quantitating the split-peak effect, it was first necessary to derive an equation that could be used to describe it. This was accomplished using the same chromatographic model as presented earlier (31,40-43). In this model, the column is divided into three distinct phases. The first is the stationary phase, which contains the immobilized ligand or analyte adsorption sites. The second is the mobile phase directly in contact with the ligand. This includes any eluent within the pores of the support or on its surface and is referred to as the stagnant mobile phase. The volume of this phase is given by V_p, the pore volume. The third phase is the eluent which freely flows through the column. This includes any mobile phase located outside of the pores of the support and is referred to as the flowing mobile phase. The volume of this phase is given by V_e, the elution volume of a solute totally excluded from the pores.

As analyte E travels through the column in the flowing mobile phase, it is viewed in this model as undergoing the following reactions leading to its adsorption:

$$E_e \underset{k_{-1}}{\overset{k_1}{\rightleftharpoons}} E_p \qquad (1)$$

$$E_p + L \underset{k_{-3}}{\overset{k_3}{\rightleftharpoons}} E_p\text{-}L \qquad (2)$$

In these reactions, E_e and E_p represent the analyte in the flowing mobile phase and stagnant mobile phase, respectively, and L is the immobilized ligand. Mass transfer of E between the flowing and stagnant mobile phases is described by the first-order rate constants k_1 and k_{-1}. The binding of E with L is described by the second-order adsorption and first-order desorption rate constants, k_3 and k_{-3}.

The values of k_1 and k_{-1} are related to the excluded volume and pore volume, V_e and V_p, by

$$K_1 = \frac{k_1}{k_{-1}} = \frac{V_p}{V_e} = \frac{m_{E_{p\infty}}}{m_{E_{e\infty}}} \qquad (3)$$

where $m_{E_{p\infty}}$ and $m_{E_{e\infty}}$ are the moles of E_p and E_e at equilibrium and K_1 is the mass transfer equilibrium constant. Also, k_3 and k_{-3} are related to K_3, the equilibrium constant for the binding of analyte to ligand, by

$$K_3 = \frac{k_3}{k_{-3}} = \frac{[E_p\text{-}L]}{[E_p]\,[L]} \qquad (4)$$

where [] represents the concentration of the given species in the stagnant mobile phase.

Derivation of the Split-Peak Equation

The split-peak effect was described using a special case of the system given in Equations 1 and 2. In this special case, it is assumed that linear elution conditions are present (i.e., $[L] \gg [E_p]$) and that E adsorbs irreversibly on the time scale of the experiment (i.e., $k_{-3} \cong 0$ or the binding of E to L is sufficiently strong to allow the nonretained and retained peaks to be resolved from one another). The net result of these assumptions is that Equation 2 reduces to the simple first-order reaction

$$E_p \xrightarrow{k_3 [L]} E_p\text{-}L \qquad (5)$$

where $k_3 [L]$ is the apparent first-order adsorption rate constant.

Based on this system, the relative amount of analyte in the nonretained peak can be obtained using procedures similar to those given in References 31 and 40 through 43. This is accomplished by determining the distribution of analyte in the column as a function of time. To do this, the location of analyte in the column is described by the variable x, where $x = 0$ at the column outlet and $x = h$, the column length, at its inlet. Time is described by the variable t, where $t = 0$ at the time of injection.

The distribution of analyte in the column is given by the functions p(x,t), q(x,t), and r(x,t). These represent the probabilities of finding analyte in the flowing mobile phase, stagnant mobile phase, and stationary phase, respectively, at any given time and column location.

By using a conservation of mass approach along with the reactions given in Equations 1 and 5, the following system of partial differential equations are obtained describing the change in these probabilities with time and distance along the column:

$$\frac{\partial p}{\partial t} = u_e \frac{\partial p}{\partial x} - k_1 p + k_{-1} q \tag{6}$$

$$\frac{\partial q}{\partial t} = k_1 p - k_{-1} q - k_3 [L] q \tag{7}$$

$$\frac{\partial r}{\partial t} = k_3 [L] q \tag{8}$$

where u_e is the linear velocity of an excluded, nonretained solute and all other parameters are as defined previously.

To solve the above equations, it is assumed that the injection volume of analyte is small vs. the total column volume. This allows the initial layer of analyte on the column to be viewed as an instantaneous source of analyte, which may be described by a Dirac delta function. Using this gives the initial conditions for $0 \leq x \leq h$ as being

$$p(x,0) = \delta(x - h) \tag{9}$$

$$q(x,0) = 0 \tag{10}$$

$$r(x,0) = 0 \tag{11}$$

Since there are no molecules at the inlet of the column once the initial layer leaves, the boundary conditions for $t > 0$ are

$$p(h,t) = 0 \tag{12}$$

$$q(h,t) = 0 \tag{13}$$

$$r(h,t) = 0 \tag{14}$$

By integrating Equations 6 through 8 from zero to infinity with respect to t and using the initial conditions given in Equations 9 through 11, the following results are obtained:

$$r(x,\infty) = k_3 [L] \int_0^\infty q(x,t)\, dt$$

$$= k_1 \int_0^\infty p(x,t)\, dt - k_{-1} \int_0^\infty q(x,t)\, dt \tag{15}$$

$$\int_0^\infty q(x,t)\, dt = k_1/(k_{-1} + k_3 [L]) \int_0^\infty p(x,t)\, dt \tag{16}$$

$$u_e \frac{\partial}{\partial x} \int_0^\infty p(x,t)\, dt = -\delta(x - h) - r(x,\infty)$$

$$= -\delta(x - h) - k_1/(1 + k_{-1}/k_3 [L]) \int_0^\infty p(x,t)\, dt \tag{17}$$

Letting $y = h - x$, Laplace transforms can be used to solve Equation 17 with the boundary conditions in Equations 12 through 14 to give

$$\int_0^{\infty} u_e\, p(x,t)\, dt = e^{-c(h - x)} \tag{18}$$

$$r(x,\infty) = c\, e^{-c(h - x)} \tag{19}$$

in which c is defined by the expression

$$c = (k_1/u_e)/(1 + k_{-1}/k_3\, [L]) \tag{20}$$

Note that $u_e\, p(0,t)$ is simply the elution profile of the analyte and $r(x,\infty)$ is the distribution of retained molecules in the column. This means that integration of $u_e\, p(0,t)$ over times of zero to infinity will give the total relative amount of analyte eluting in the nonretained peak, or the free fraction (f). Similarly, integration of $r(x,\infty)$ over the entire length of the column will give the total relative amount of retained or bound analyte (b). When this is done, the following results are obtained:

$$f = \int_0^{\infty} u_e\, p(0,t)\, dt = e^{-c\, h} \tag{21}$$

$$b = \int_0^{h} r(x,\infty)\, dx = 1 - e^{-c\, h} \tag{22}$$

Substituting in the definition of c given in Equation 20 and rearranging terms, Equation 21 can be written in the following form:

$$\frac{-1}{\ln f} = \frac{u_e}{h}\left(\frac{1}{k_1} + \frac{k_{-1}}{k_1\, k_3\, [L]}\right) \tag{23}$$

Since [L] is defined as the concentration of ligand sites in the stagnant mobile phase, it can be related to m_L, the total moles of ligand in the column, by the expression

$$[L] = m_L/V_p \tag{24}$$

It is also possible from the model to relate u_e to the flow-rate (F) through the relationship (42)

$$u_e = F\ h/V_e \tag{25}$$

By substituting these expressions for [L] and u_e into Equation 23 along with the fact that $V_p/V_e = k_1/k_{-1}$ from Equation 3, the following result is obtained:

$$\frac{-1}{\ln f} = F\left(\frac{1}{k_1\ V_e} + \frac{1}{k_3\ m_L}\right) \tag{26}$$

The above equation predicts that a plot of $-1/\ln f$ vs. F will give a straight line with an intercept of zero and a slope equal to $(1/k_1\ V_e + 1/k_3\ m_L)$. This relationship is what will be referred to as the split-peak equation.

As stated earlier, two experimental conditions must be met to apply this equation. One is that linear elution conditions are present, or that the relative amount of free and bound analyte is independent of sample size. The second is that adsorption must be essentially irreversible on the

time scale of the experiment, or that the nonretained and retained peaks are sufficiently resolved to allow the bound and free fractions to be measured independently from one another. Another assumption made in the derivation is that the injection volume is negligible vs. the total column volume, allowing sample input to be represented by a Dirac delta function. However, this is not a necessary experimental requirement since larger injection volumes may be regarded as a series of delta functions, in each of which the same fraction f elutes without retention.

These are also a number of assumptions made in using this particular chromatographic model. One is that the system can be described by a single set of rate constants, or by a homogeneous system. The possible affect of deviations from this, or the presence of column heterogeneity, will be discussed in both Sections I and III. The model also assumes that the effect of processes other than adsorption or mass transfer between the stagnant and flowing mobile phases, such as mass transfer of analyte within the flowing mobile phase or extracolumn band-broadening, is negligible. The validity of this assumption will be discussed in Section III.

Despite these possible limitations, Equation 26 is useful in qualitatively explaining many of the previous observations made regarding the split-peak effect. For example, it pre-

dicts an increase in the amount of nonretained analyte with flowrate, as seen in earlier studies (20,32,35-37,39). This occurs since both f and -1/ln f increase with F. Equation 26 also predicts an increase in f as the column size decreases, as observed by Lowe et al. (32). This is expected since a decrease in column size causes a proportional decrease in both V_e and m_L. The result is an increase in the slope of Equation 26 and the flowrate dependence of f.

Although the model used in this derivation is applicable to any type of liquid chromatography involving analyte adsorption as the retention mechanism, split-peaks are only commonly reported in affinity chromatography. A closer examination of the parameters in Equation 26 reveals why this is the case. One possible reason is that m_L is often much smaller for affinity supports than other chromatographic matrices. This is related not only to the column size, but also to its surface area and ligand density. Under the same column size and support conditions, affinity columns may have between 10- to 1000-fold fewer ligands than ion-exchange or reversed-phase columns. This is due to the larger size of the ligands typically used in affinity chromatography. For example, an immobilized protein may cover up to 10^4 Å^2 of the surface area of the support, while each of the alkyl groups commonly used in reversed-phase supports occupy only about 40 Å^2 per

molecule (44). Since the slope of Equation 26 increases as m_L decreases, the lower ligand density of affinity columns tends to make split-peaks more likely to occur.

Split-peaks are also more likely to observed as the mass transfer rate constant k_1 decreases. In this model, k_1 is directly proportional to the diffusion coefficient (D), as will be shown in Section I. This makes split-peaks more likely to occur when slowly diffusing analytes, such as macromolecules, are chromatographed. This takes place since k_1 may decrease by 10- to 100-fold in going from a small solute, with a molecular weight of 100 or less and a diffusion coefficient of approximately 10^{-5} cm^2/sec, to analytes such as proteins, which have diffusion coefficients of 10^{-6} to 10^{-7} cm^2/sec (45).

Overall, this indicates that the reason why split-peaks are not usually observed in most types of liquid chromatography is that the split-peak slopes for these techniques (i.e., the slope term of Equation 26) are much smaller than those usually obtained in affinity chromatgraphy. These smaller slopes result in most forms of chromatography having only negligible free fractions (i.e, $f \cong 0$) under normal operating conditions. However, it will be shown that split-peaks can also be observed in areas other than affinity chromatography if the proper operating conditions are used.

SECTION I.

STUDIES OF THE IMMOBILIZATION-DEPENDENT ADSORPTION KINETICS OF PROTEIN A

INTRODUCTION

It was shown earlier how the equations developed in this work agree qualitatively with previous experimental observations of the split-peak effect. This makes them useful in explaining the split-peak effect and in developing guidelines that can be used to minimize it. To be useful for an application such as the optimization of analyte adsorption, however, it is also necessary that they agree quantitatively with the experimental results. To determine whether or not this is the case, one purpose of this study was to compare the flowrate dependence of adsorption predicted by the model to that actually seen with an experimental system. The particular system used for this was the adsorption of rabbit IgG on immobilized protein A.

Protein A is a 42,000 molecular weight protein from the cell walls of Staphylococcus aureus (46,47). It is made up of a single polypeptide chain arranged in an elongated structure. This structure consists of four immunoglobulin binding sites at the N-terminal end and a cell wall binding region at the C-terminal end (48). Rabbit IgG is a 150,000 molecular weight protein (49). It is the most abundant type of antibody in rabbit serum (49) and consists of only one known subclass (50). Each IgG molecule is made up of four polypeptide chains: two identical H or heavy chains, each with a

molecular weight of about 50,000, and two identical L or light chains, each with a molecular weight of approximately 25,000 (49). These are joined by disulfide bonds to give a structure made up of two antigen binding sites, or F_{ab} regions, and one constant, or F_c, region (49). Protein A binds primarily with F_c region (50).

Since it was first described by Verwey in 1940 (51), protein A has become a popular biochemical tool. This is due to its ability to bind immunoglobulins from several mammalian species (50). One use of protein A has been as an affinity ligand for the purification and separation of immunoglobulins (52,53). Such separations are usually performed by allowing immunoglobulins to bind to protein A at a pH of 7.0 to 7.4 and later dissociating the resulting complex by going to more acidic elution conditions (50). Protein A can also be used as an antibody-binding reagent for a number of different immunotechniques. One characteristic of protein A that makes it especially attractive for this is that it binds primarily with the F_c region of antibodies, allowing the adsorbed antibodies to retain their antigen-binding activity (50). This makes protein A useful as a reagent in indirect immunoassays (52) and as an antibody coupling reagent for the preparation of a variety of immunoaffinity supports (54).

The IgG-protein A system was chosen for this study not only for its practical importance, but also due to the fact that split-peaks for this system have already been observed. For example, in one previous study it was shown that significant amounts of nonretained human IgG were obtained when nonoverloading samples were injected in 6 mm protein A HPAC columns (55), while the same system exhibited normal chromatographic behavior when 5 cm columns were used (27). In another study, it was observed that the amount of canine immunoglobulin bound to protein A Sepharose columns could be increased by recycling sample through the column (56), in effect increasing the analyte adsorption time.

Besides verifying the equations developed in the previous chapter, another goal of this study was to examine the kinetic properties of the IgG-protein A system. The use of affinity chromatography for the determination of physical parameters, such as rate constants and equilibrium constants, is an area known as quantitative affinity chromatography. The first reported use of this technique was by Andrews et al. in 1973 (57). In this study, affinity chromatography was used to determine the equilibrium constants for the interaction of human galactosyltransferase with glucose and N-acetyl-glucosamine (57). This technique has since been used to determine equilibrium constants for a large number of other systems, as

reviewed by Dunn (58) and Chaiken (59). Systems that have been studied with this technique include the binding of psychoactive drugs to bovine glutamate dehydrogenase (60), the interaction of lactate dehydrogenase with the dye Cibacron Blue (61), and the binding of immunoglobulin A F_{ab} fragments with phosphorylcholine (62).

Although widely used for the determination of equilibrium constants, only a few studies have been reported using affinity chromatography for the determination of rate constants (35,39,59,63-65). This is typically done by relating the kinetics of analyte-ligand interactions to band-broadening of the analyte peak as it isocratically elutes from an affinity column. Even though the theoretical basis for this is well-developed (42,43,66-68), the experiments involved in these studies are complicated by a number of factors. These factors include extracolumn band-broadening (67), measurement errors in the statistical moments used to determine band-broadening (69), and dependence of some theoretical terms on the degree of analyte retention (67,70,71). As suggested by the work of Sportsman et al. (39) and the equations derived in this work, the split-peak effect may allow an alternative approach to obtaining affinity rate constants, in that it allows the kinetics of the analyte-

ligand interaction to be related to a more easily measured parameter, the peak area.

In this study, the split-peak effect was used to examine the kinetic properties of protein A supports prepared by different immobilization methods. Changes in the properties of protein A as a result of immobilization have been previously noted by Nilsson et al. (72). In this earlier study, it was found that protein A immobilized on agarose had different binding specificities for rat IgG than found with native bacteria-bound protein A. This was seen in that the binding strength of immobilized protein A for two subclasses of rat IgG was larger than that obtained for native protein A, while binding to two other subclasses was not affected (72).

THEORY

Equation 26 was used to compare the flowrate dependence of analyte adsorption predicted by the model to that actually seen with the IgG-protein A system.

$$\frac{-1}{\ln f} = F\left(\frac{1}{k_1 V_e} + \frac{1}{k_3 m_L}\right) \qquad (26)$$

As pointed out previously, this equation predicts that a plot of $-1/\ln f$ vs. flowrate will give a linear relationship with an intercept of zero and a slope equal to $(1/k_1 V_e + 1/k_3 m_L)$. Note that the first term in the slope, $1/k_1 V_e$, is related to diffusion or mass transfer of analyte from the flowing mobile phase to the stagnant mobile phase, while the second, $1/k_3 m_L$, is related to analyte adsorption. If diffusion is the rate-limiting step in retention (i.e., $k_3 [L] >> k_1$ and k_{-1}), the first term dominates. If adsorption is rate-limiting (i.e., $k_3 [L] << k_1$ and k_{-1}), the second term dominates. Intermediate cases can also occur.

One way in which Equation 26 was used in this experiment was to compare the kinetic properties of different affinity supports. This can be done by comparing the overall slope obtained for each support under equivalent operating conditions or by performing further experiments to determine the values of the individual rate constants. For example,

the value of k_3 can be obtained from the slope of Equation 26 if values of V_e, m_L, and k_1 are already known. V_e can be determined by measuring the elution volume of a large, excluded solute. Breakthrough curves or other means can be used to measure m_L.

Two different approaches can be used to estimate k_1. In the first, split-peak measurements are made under conditions in which the term $1/k_3\ m_L$ is negligible, or diffusion is rate-limiting. Under these conditions, Equation 26 reduces to

$$\frac{-1}{\ln f} = F\left(\frac{1}{k_1\ V_e}\right) \qquad (27)$$

which predicts that a plot of $-1/\ln f$ vs. F for a diffusion-limited system will give a straight line with an intercept of zero and a slope of $1/k_1\ V_e$. Thus, k_1 can be determined from this slope once V_e has been measured.

One system that may exhibit the split-peak effect under diffusion-limited conditions is the adsorption of proteins on reversed-phase columns (73). This system would be expected to be diffusion-limited since reversed-phase supports typically have a large value of m_L due to the small amount of surface area required by each ligand, as discussed previously. Another possible factor is that k_3 may be larger for protein-ligand interactions in reversed-phase chromatography than in a

technique such as affinity chromatography. This would be expected since affinity ligand-analyte interactions are typically very site specific, requiring a particular orientation of both the analyte and ligand in order for binding to occur (29), while protein retention on reversed-phase columns involves a less specific mechanism, the adsorption of analyte on a large hydrophobic surface (73).

Equation 27 can be applied to obtain $1/k_1$ V_e for affinity columns by making split-peak measurements on reversed-phase supports prepared using the same original support material. Under equivalent application conditions, both systems would be expected to exhibit similar protein mass transfer kinetics. Thus, the reversed-phase results can be used to calculate k_1 for the affinity supports or to provide an estimate of their diffusional slope term.

A second estimate of k_1 can be made by measuring the band-broadening of the analyte peak under isocratic elution conditions. Band-broadening in chromatography is usually expressed in terms of H, the plate height, which may be defined as follows (74):

$$H = \sigma^2/L \qquad (28)$$

where L is the column length and σ^2 is the variance of the peak expressed in units of column length.

Various processes contribute to the width of peaks in chromatography. These processes are usually assumed to be independent of one another, allowing them to be described by separate variance or plate height terms. These terms are then added together to give the total plate height, H (74). For an adsorption technique such as affinity chromatography, H can be represented as the sum of the following terms:

$$H = H_{ec} + H_l + H_m + H_{sm} + H_k \qquad (29)$$

In this expression, H_{ec} represents the plate height contribution of extracolumn effects, such as band-broadening within the tubing of the system or dispersion caused by the use of large sample loops. H_l gives the plate height due to longitudinal diffusion (i.e., diffusion parallel to solvent flow). H_m represents the plate height contribution of mass transfer effects in the flowing mobile phase, such as sample dispersion caused by the presence of multiple flow paths through the column (i.e., eddy diffusion) and nonuniform flow profiles. H_{sm} gives the contribution due to mass transfer between the flowing and stagnant mobile phases and H_k gives the plate height due to the kinetics of analyte adsorption/desorption (74,75).

One of the main goals of chromatographic theory has been to relate these various plate height terms to fundamental

properties of the chromatographic system and the column operating conditions (74). The results have usually been expressed in terms of equations relating plate heights to the linear velocity of analyte through the column (u). Examples of such equations include those developed by van Deemter et al. (76), Giddings (66), and Kennedy and Knox (77). Using the same model as presented here, Hethcote and DeLisi have derived equations for H_{sm} and H_k in the case of affinity chromatography (42,43). Based on these, the following plate height expression can be written for the system given in Equations 1 and 2 (75):

$$H = H_{ec} + H_m + \frac{2\ u\ V_p\ (1 + V_m\ k'/V_p)^2}{k_{-1}\ V_m\ (1 + k')^2} + \frac{2\ u\ k'}{k_{-3}\ (1 + k')^2} \qquad (30)$$

where the two linear velocity terms represent the plate height contributions due to H_{sm} and H_k, respectively, and k' is the capacity factor, a measure of analyte retention. The H_k term in this equation is identical to that derived by others (66, 67,78). The H_{sm} term is also equivalent to previous expressions (66,67,71,78), given the fact that the values of k_1 and k_{-1} in this model are really combinations of geometric and diffusional factors, as shown by Equation 31.

$$k_{-1} = k_1\ (V_e/V_p) = \frac{60\ \tau\ \rho\ D_m}{d_p^2} \qquad (31)$$

In this relationship, d_p is the particle diameter of the packing material and D_m is the diffusion coefficient of analyte in the bulk mobile phase. The other two parameters, τ and ρ, are the tortuosity factor (66) and the restricted-diffusion factor (71), constants correcting for the slower diffusion of solute once within the pores of the support.

Note in Equation 30 that both the H_{sm} and H_k terms show a first-order relationship between the plate height and u, while the contributions due to H_{ec} and H_m are considered to be either small or flowrate independent. It is also important to note that H_l is not considered in Equation 30. This is due to the fact that longitudinal diffusion in liquid chromatography is often insignificant, making this term negligible (74).

To determine k_1 using Equation 30, column conditions are adjusted so that analyte is not retained on the column (i.e., $k' = 0$). An example of such a system is the elution of protein on a column containing diol-bonded silica. Under these conditions, Equations 3 and 30 can be combined to yield the following expression:

$$H = H_{ec} + H_m + \frac{2\ u\ V_p^2}{k_1\ V_e\ V_m} \qquad (32)$$

which predicts that a plot of H vs. u will give a straight line with an intercept of $(H_{ec} + H_m)$ and a slope equal to

$(2\ V_p^2)/(k_1\ V_e\ V_m)$. Thus, from this slope an estimate of k_1 can be obtained for a given analyte on a particular support. Note that this requires that the values of V_e and other parameters again be known. V_e is determined as described previously and V_m, the elution volume of analyte from the column, can be measured in the same experiment used to generate the peak height data. V_p is obtained by simply calculating the difference between V_m and V_e.

EXPERIMENTAL

Reagents

The protein A, rabbit IgG, and sodium cyanoborohydride were from Sigma (St. Louis, MO) and were the purest grades available. The 1,1'-carbonyldiimidazole (CDI), 1-cyclohexyl-3-(2-morpholinoethyl)carbodiimide metho-p-toluenesulfonate (CMC), and morpholine were obtained from Aldrich (Milwaukee, WI). The LiChrospher SI 500 (10 μm diameter, 500 Å pore size) and Nucleosil (10 μm diameter, 50 Å pore size) were from Alltech (Deerfield, IL). The N-Hydroxysuccinimide was from Eastman (Rochester, NY), the n-octyldimethylchlorosilane from Petrarch (Bristol, PA), and the carboxylate microspheres (0.1 μm diameter) from Polysciences (Warrington, PA).

Instrumentation

The chromatographic system consisted of a Series 344 gradient elution chromatograph (Beckman, Berkeley, CA) and a V^4 detector (ISCO, Lincoln, NE) operated at 280 nm. Data were collected and processed with an Apple IIe computer and ADALAB interface (Interactive Microware, State College, PA). The columns were of a published design (79), with the outer connector modified as a water jacket. A Model 705 stirred-slurry column packer (Micrometrics, Norcross, GA) and Haskel

air-driven pump from Alltech were used in column packing by the upward-slurry pack method.

Procedures

Preparation of protein A supports

The diol-bonded LiChrospher and Nucleosil were prepared as described previously (80). Three methods were used to immobilize protein A on these supports. In each case 1 to 2 mL of 0.1 M potassium phosphate buffer was added to 0.1 g of activated silica. This mixture was degassed under sonication and aspirator vacuum for 15 min. A total of 10 mg of protein A/g silica was then added and the mixture shaken at 4 °C for 3 to 6 days.

The first immobilization technique used was the Schiff base (SB) method, as summarized in Figure 2. In this method, diol-bonded silica, shown at the top of Figure 2, is oxidized with periodic acid to produce aldehyde groups on the surface of the support. When protein is added to a suspension of this silica, free amine groups on the protein react with these aldehyde groups to form a Schiff base. In the presence of a mild reducing agent, such as sodium cyanoborohydride, the Schiff base is reduced upon formation to give a stable secondary amine linkage between the protein and the support (25).

Figure 2. The Schiff base immobilization method

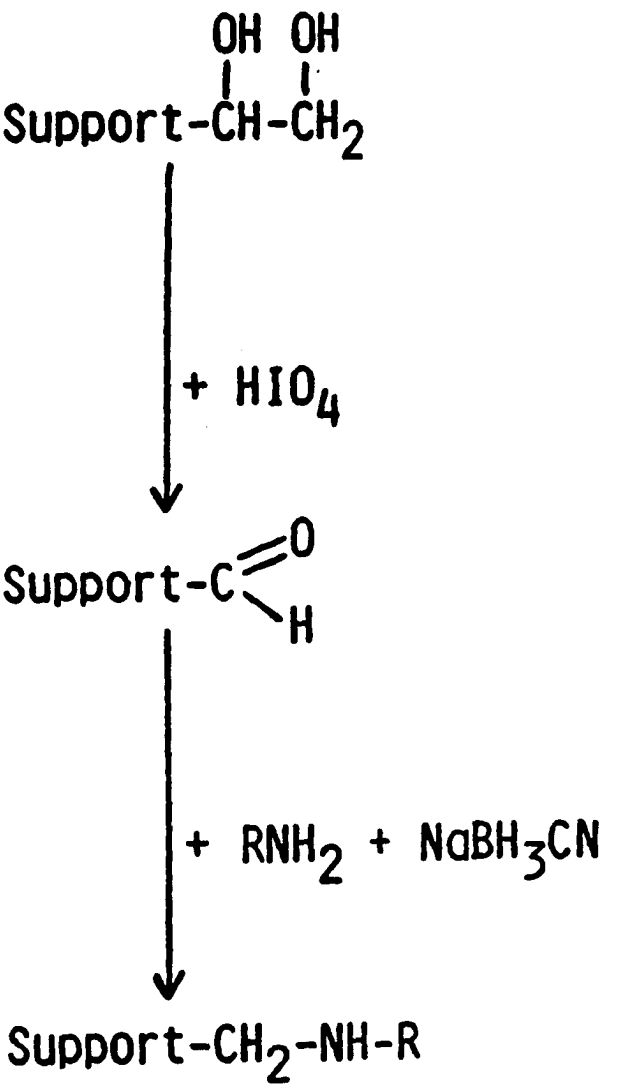
OH OH
Support-CH-CH2
+ HIO4
Support-C=O
H
+ RNH2 + NaBH3CN
Support-CH2-NH-R

The Schiff base method used in this experiment was a modified version of the procedure developed by Larsson and co-workers (25). The support was activated with aldehyde groups by adding 0.1 g diol-bonded silica to 5 mL of a solution containing 5 mg/mL periodic acid in 80% acetic acid. This mixture was degassed as described previously and shaken at room temperature for 30 min. The silica was then collected by filtration, washed with methanol, and dried under aspirator vacuum. Next, the silica was placed in pH 5.7 phosphate buffer along with 200 mg sodium cyanoborohydride/g silica and degassed. After degassing, the protein A was added and allowed to react with the silica for 6 days.

The second immobilization technique used was the CDI method, shown in Figure 3. Diol-bonded silica is also the starting material for this method but in this case is activated by reacting it with CDI to place imidazolyl carbonate groups on its surface. When protein is added to a solution containing this activated silica, free amines on the protein displace these groups to form alkyl carbamate bonds between the protein and the support (81).

The CDI supports in this experiment were synthesized according to a previously-published procedure (81). The activated matrices were prepared as described in the

Figure 3. The CDI immobilization method

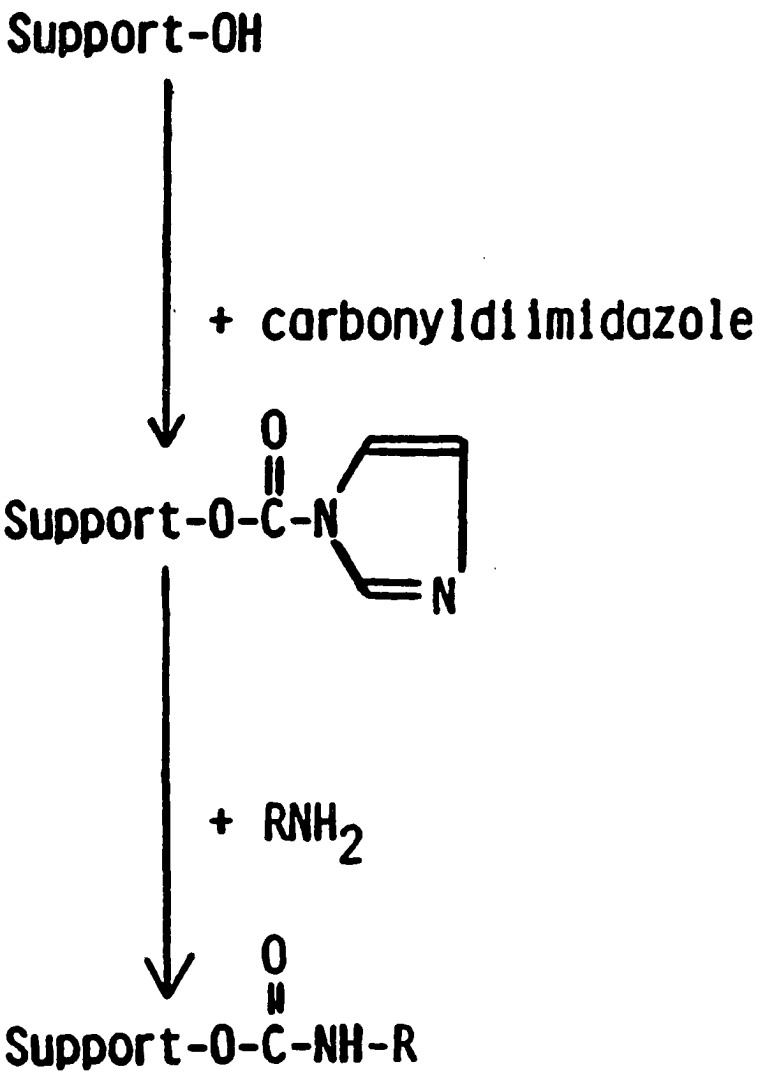
Support-OH
+ carbonyldiimidazole
Support-O-C-N
N
+ RNH2
Support-O-C-NH-R

reference, placed along with protein A in phosphate buffer at pH's ranging from 4.0 to 8.0, and allowed to react for 6 days.

The last method used was the ester-amide (EA) method, given in Figure 4. In this technique, diol-bonded silica is activated through a series of reactions which place N-hydroxysuccinimide groups on its surface. In the presence of free amines, these groups are displaced forming an amide bond between protein and the support material.

The EA procedure used was based on that developed by Landgrebe et al. (44). In this method, a mixture of 0.1 g of diol-bonded silica, 0.25 g of succinic anhydride, and 5 mL of 0.001 M hydrochloric acid in dioxane was prepared and refluxed for 48 h. The silica was then filtered, washed with warm dioxane, and dried under aspirator vacuum. This was activated by combining it with 20 mg of N-hydroxysuccinimide, 75 mg of CMC, and 1.0 mL of dioxane followed by degassing and shaking for 2 h at room temperature. The product was filtered, washed with dioxane and methanol, and dried under aspirator vacuum. The silica was then placed in pH 6.0 phosphate buffer along with protein A and allowed to react for 3 days.

After coupling, the protein A silicas prepared by each immobilization method were centrifuged, washed with 2 M sodium chloride and water, and stored at 4 ^{o}C in 0.1 M pH 7.0 phosphate buffer. A portion of each sample was washed with

Figure 4. The ester-amide immobilization method

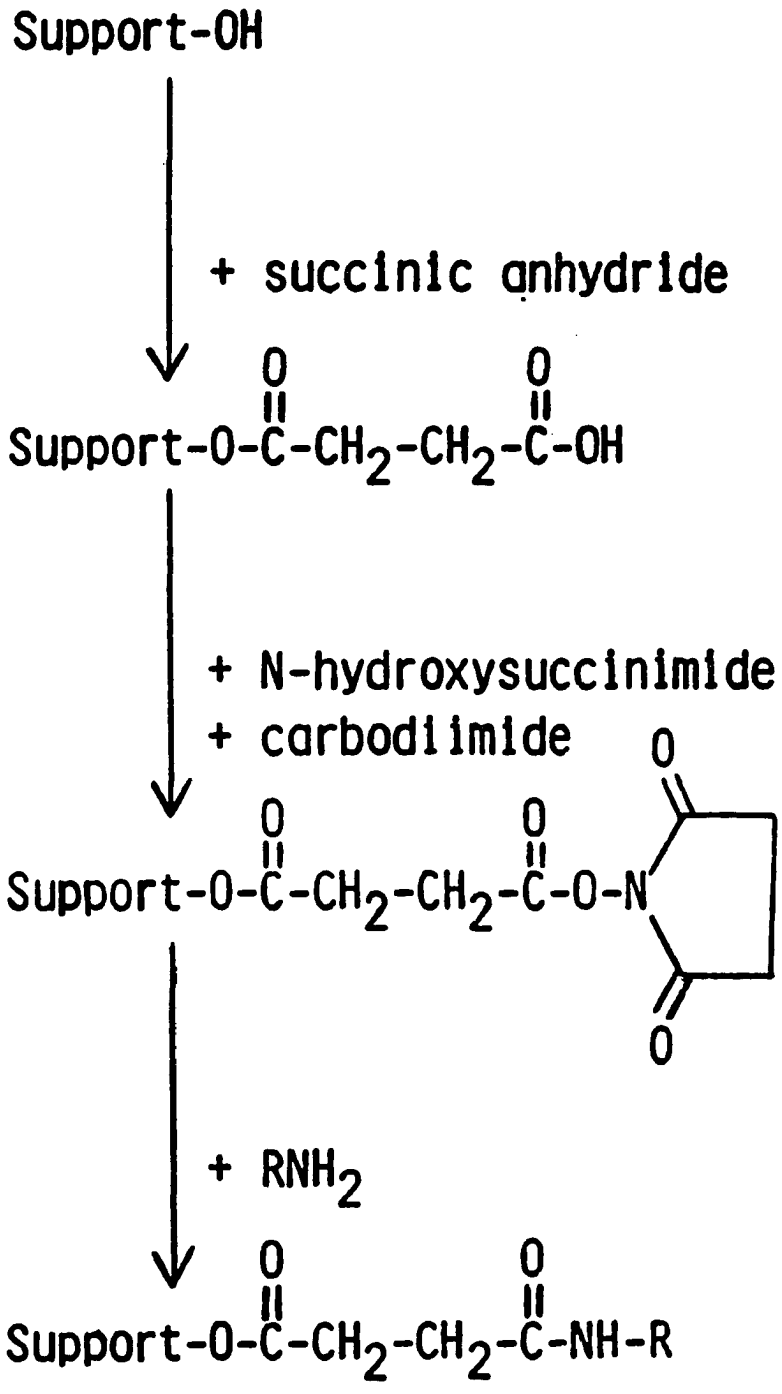
Support-OH
+ succinic anhydride
Support-O-C-CH2-CH2-C-OH
+ N-hydroxysuccinimide
+ carbodiimide
Support-O-C-CH2-CH2-C-O-N
+ RNH2
Support-O-C-CH2-CH2-C-NH-R

water and vacuum-dried at room temperature. These were later assayed for protein content in triplicate by the Lowry method (82) using protein A as the standard and diol-bonded silica as the blank. The remainder of each protein A silica was vacuum slurry-packed (83) into 6.35 mm x 4.1 mm I.D. and 6.35 mm x 2.1 mm I.D. columns.

Under the reaction conditions given, all three of the immobilization methods were found to introduce approximately a monolayer of active groups onto the support. The diol coverages of the supports prior to activation were determined using the periodate oxidation method (84,85). This gave diol coverages of 760 μmol/g silica for the Nucleosil, 200 μmol/g for the LiChrospher used in the SB and EA methods, and 250 μmol/g for the LiChrospher used in the CDI method.

Preparation of reversed-phase supports

The LiChrospher and Nucleosil reversed-phased supports were prepared according to published procedures (83,86) by placing 0.2 g of silica in 1.0 g of n-octyldimethylchlorosilane and 10 g of carbon tetrachloride. The LiChrospher and Nucleosil supports were then vacuum slurry-packed into 6.35 mm x 1 mm I.D. and 2.55 mm x 1 mm I.D. columns, respectively.

Chromatography

The application buffer for the protein A columns was 0.1 M potassium phosphate buffer (pH 7.0). All IgG solutions applied to the protein A affinity columns were prepared in this buffer. The elution buffer for these columns was 0.1 M potassium phosphate buffer (pH 3.0). Elution of adsorbed IgG was accomplished by means of a step change in pH.

The weak mobile phase for the reversed-phase columns was 0.02 M ammonium acetate (pH 7.0) containing 0.01% (v/v) morpholine. All IgG solutions used in the reversed-phase work were prepared in this buffer. Elution of retained protein from the reversed-phase columns was accomplished by using a linear 5 min gradient from 0 to 100% 2-propanol.

Kinetic studies on both the protein A and reversed-phase supports were performed at 25 °C. All other chromatography was done at room temperature.

The static adsorption capacity of each protein A support was found by continuously applying 0.1 mg/mL IgG to the 6.35 mm x 2.1 mm I.D. column prepared for each sample. The capacity was determined by integrating the resulting break-through curves (87) and correcting for the void volume of the system. All protein A columns were pretreated several times in this manner to eliminate any residual active groups or irreversible adsorption sites.

The split-peak behavior of the protein A supports was examined using the 6.35 mm x 4.1 mm I.D. columns. For each column, 10 μL injections of IgG were made at 3 to 5 concentrations ranging from 0.14 to 2.2 mg/mL. These studies were done over flowrates of 0.25 to 4.0 mL/min for the SB- and EA-immobilized protein A columns and 0.02 to 0.40 mL/min for the CDI-immobilized protein A support. The areas of both the retained and nonretained peaks were determined by computer integration and, in some cases, checked with a planimeter. These areas were then normalized vs. flowrate. The nonretained peak areas were corrected for an inactive impurity in the IgG, which made up a maximum of 2.0% of the total IgG area. The retained peak areas were corrected for a previously-noted impurity in the phosphate buffer (88), which concentrated on the column at pH 7 but eluted when the pH was decreased to 3. The area resulting from this impurity was easily calculated since it was a linear function of the volume of pH 7 buffer applied. This peak is believed to be caused by the retention of transition metal ions on the support since its size could be reduced by first passing the buffer through a chelating resin.

A check on these integration and correction procedures was made by normalizing the total area of both peaks vs. the flowrate and the amount of IgG applied. By doing this, it was

determined that the total normalized area varied randomly by less than 6% (1 standard deviation) during the course of the experiments, confirming the validity of the procedures used.

The nonretained fraction f of IgG eluting from the protein A columns was calculated by dividing the corrected nonretained peak area by the total corrected area of the nonretained and retained peaks. This was possible since it was found that the IgG peak area increased linearly with sample size over the entire concentration range studied.

The value of k_1 was measured isocratically by injecting IgG on diol-bonded silica columns, to which IgG does not adsorb. The columns used were 10 cm x 4.1 mm I.D. and were packed at 3000 p.s.i. using the upward slurry-pack method. Using pH 7.0 phosphate buffer as the mobile phase, 10 µL injections of 2.2 mg/mL IgG were made on the column at flowrates of 0.25 to 3.0 mL/min. The statistical moments of each peak were determined using the Gaussion approximation method (69). Corrections for the extracolumn volume were made by injecting 10 µL of 16 µg/mL uracil, a small nonretained solute, on the system with the column removed. The void and excluded volumes of the columns were measured by injecting 10 µL of 2.2 mg/mL IgG and 0.25% carboxylate microspheres, respectively. In the case of the microspheres, the mobile phase was deionized water, which was also used to prepare

the sample solution. This was used to prevent agglomeration of the microspheres.

The split-peak estimate of k_1 was obtained by injecting IgG on reversed-phase columns. For the reversed-phase LiChrospher supports, a 3 μL sample of 0.90 to 1.50 mg/mL IgG was injected while a 3 μL sample of 0.25 to 0.50 mg/mL IgG was used for the Nucleosil. These studies were done over flowrates ranging from 0.20 to 2.0 mL/min. The nonretained peak area was found as described earlier and the fraction f was calculated by dividing this area by the total area of the sample, corrected for the inactive impurity, when injected through an open tube. This was possible since it was found that the peak area for IgG in the ammonium acetate buffer increased linearly with sample size over the entire concentration range studied.

RESULTS AND DISCUSSION

Static Properties of Immobilized Protein A

In the first part of the experiment, the static properties of the various protein A supports were determined. In describing these supports, each will be referred to in terms of the immobilization method and support material used to prepare it. For example, protein A immobilized on LiChrospher SI 500 by the Schiff base method will be referred to as the SB-500 support.

The static properties of the protein A supports are given in Table I. The intervals used in this and in all following tables represent a range of one standard deviation. The rather large standard deviations reported are due to the small sample sizes (0.6 to 3 mg silica) used in the protein assay and variability caused by the silica support. Despite this, it is clear from the data that all three methods resulted in the immobilization of 86 to 100% of the protein A. For the LiChrospher, each method gave a coverage of approximately 10 mg of protein A/g silica. This represents about one-third of a monolayer, based on a Stoke's diameter for protein A of 100 Å (46).

The Nucleosil SI 50 also gave a high coupling yield, with a coverage of approximately 9 mg/g silica. This nearly quan-

Table I. Static properties of protein A supports

Immobilization method	Support	Batch	Protein A immobilized (mg/g silica)
CDI	LiChrospher SI 500	1 (pH 8)	9.0 ± 2.6
		2 (pH 6)	8.6 ± 1.8
		3 (pH 4)	10.2 ± 1.8
		Average	9.3 ± 1.9
EA	LiChrospher SI 500	1	11.3 ± 2.3
		2	8.2 ± 0.4
		Average	9.7 ± 2.2
SB	LiChrospher SI 500	1	9.6 ± 0.9
		2	10.7 ± 1.8
		3	----------
		Average	10.1 ± 1.4
	Nucleosil SI 50	1	9.0 ± 0.4

[a]Based on the manufacturer's value for the initial activity of the protein A. The initial activity of the protein A used in preparing the SB Nucleosil and CDI supports was given as being 12.5 mg IgG/mg protein A and that used for the EA and SB LiChrospher supports was given as being 13.1 mg IgG/mg protein A.

% Protein A immobilized	Static capacity (mg IgG/g silica)	Specific activity (mg IgG/mg protein A)	% Initial protein A activity[a]
90 ± 26	4.7 ± 1.4	0.5 ± 0.2	4.2
87 ± 18	5.1 ± 0.7	0.6 ± 0.1	4.8
102 ± 18	7.0 ± 2.5	0.7 ± 0.2	5.5
93 ± 19	5.7 ± 1.9	0.6 ± 0.2	4.8
97 ± 20	8.0 ± 1.0	0.7 ± 0.2	5.4
76 ± 4	9.7 ± 1.3	1.2 ± 0.2	9.0
86 ± 8	8.8 ± 1.3	0.9 ± 0.2	7.2
87 ± 8	21.5 ± 2.7	2.2 ± 0.3	17.1
89 ± 15	23.5 ± 1.7	2.2 ± 0.4	16.8
-------	15.7 ± 0.5	---------	----
88 ± 11	19.8 ± 4.2	2.2 ± 0.3	17.0
90 ± 4	5.1 ± 0.1	0.57 ± 0.03	4.5

titative binding of protein A to Nucleosil was unexpected since the Stoke's diameter of protein A is twice the nominal pore size of Nucleosil SI 50. This can be explained by the fact that roughly 25% of the pores in most commercial silicas have diameters greater than twice the nominal pore size (89). Combined with the ten-fold greater surface area of Nucleosil SI 50 vs. LiChrospher SI 500, this may have resulted in more area actually being available for protein attachment on the Nucleosil SI 50 than on the LiChrospher SI 500. Another contributing factor may have been the elongated shape of protein A (46,48), which could have permitted it to enter some of the pores of the Nucleosil along its long axis, again creating more surface area for protein A attachment.

Table I also gives the activity obtained for each protein A support. Of particular interest are the last two columns, which list the specific activity of the protein A and the percent of its initial activity remaining after immobilization. The latter is based on values given by the manufacturer for the binding of human IgG to protein A, which should represent a protein A binding capacity equivalent to that obtained with rabbit IgG (50). The data in Table I indicate that 83 to 96% of this initial activity was lost due to immobilization.

Losses of activity are common when macromolecules are immobilized (29,90). For protein A this probably occurs because native protein A is specifically attached to the bacterial cell wall through its cell wall binding region (48), while the relatively nonspecific immobilization methods used here can couple it via any accessible amine groups. This may have resulted in multiple points of attachment between protein A and the support, causing possible denaturation or improper orientation of protein A on the support, resulting in inactivation or steric hinderance of its binding site (11).

A comparison of the LiChrospher results in Table I shows that the SB method gave immobilized protein A with about twice the specific activity of that produced by the EA method and four times that given by the CDI method. Since each method introduced approximately the same number of active groups onto the support, this may reflect differences in the reactivity of these groups in binding free amines on the protein or may indicate differences in the microenvironment of the resulting immobilized ligand (29,90). Such differences are further indicated by the fact that the activities varied even when each technique was allowed to sample the same free amine groups on the protein A. This can be seen by comparing the SB-500, EA-500, and CDI-500-2 results, all

prepared using approximately the same pH and ionic strength conditions in the immobilization step.

Differences can also be observed in the activities of the SB-50 and SB-500 protein A, with the Nucleosil support having an activity only one-fourth of the corresponding LiChrospher phase. Since both supports were prepared by the same method, this may indicate differences in the relative amount of protein A on each support that was able to bind to IgG. For example, most of the protein A in the pores of the Nucleosil was probably unavailable for binding to IgG, due to the narrow pore size of the support or steric hindrance created by ligands present near the entrance of the pores. Either of these effects could have prevented IgG from reaching ligand sites further within the support.

Kinetic Properties of Immobilized Protein A

After the static properties of each support had been examined, their kinetic properties were also determined. This was accomplished by measuring the amount of nonretained IgG on each support as a function of flowrate. Some typical chromatograms obtained are given in Figure 5. In this figure, the two peaks characteristic of the split-peak effect can be seen, representing the nonretained and retained IgG fractions, respectively. Figure 5 also demonstrates how the relative

Figure 5. The split-peak effect for IgG on immobilized protein A. The chromatograms shown are for 10 μL of 2.2 mg/mL rabbit IgG applied to the EA-500 column at flowrates of 1.50 (a), 1.75 (b), 2.00 (c), and 2.25 (d) mL/min. The IgG was applied at the first arrow. The bound IgG was eluted by a pH step change applied at the second arrow. The small peak immediately following the second arrow represents a background shift due to the pH step change

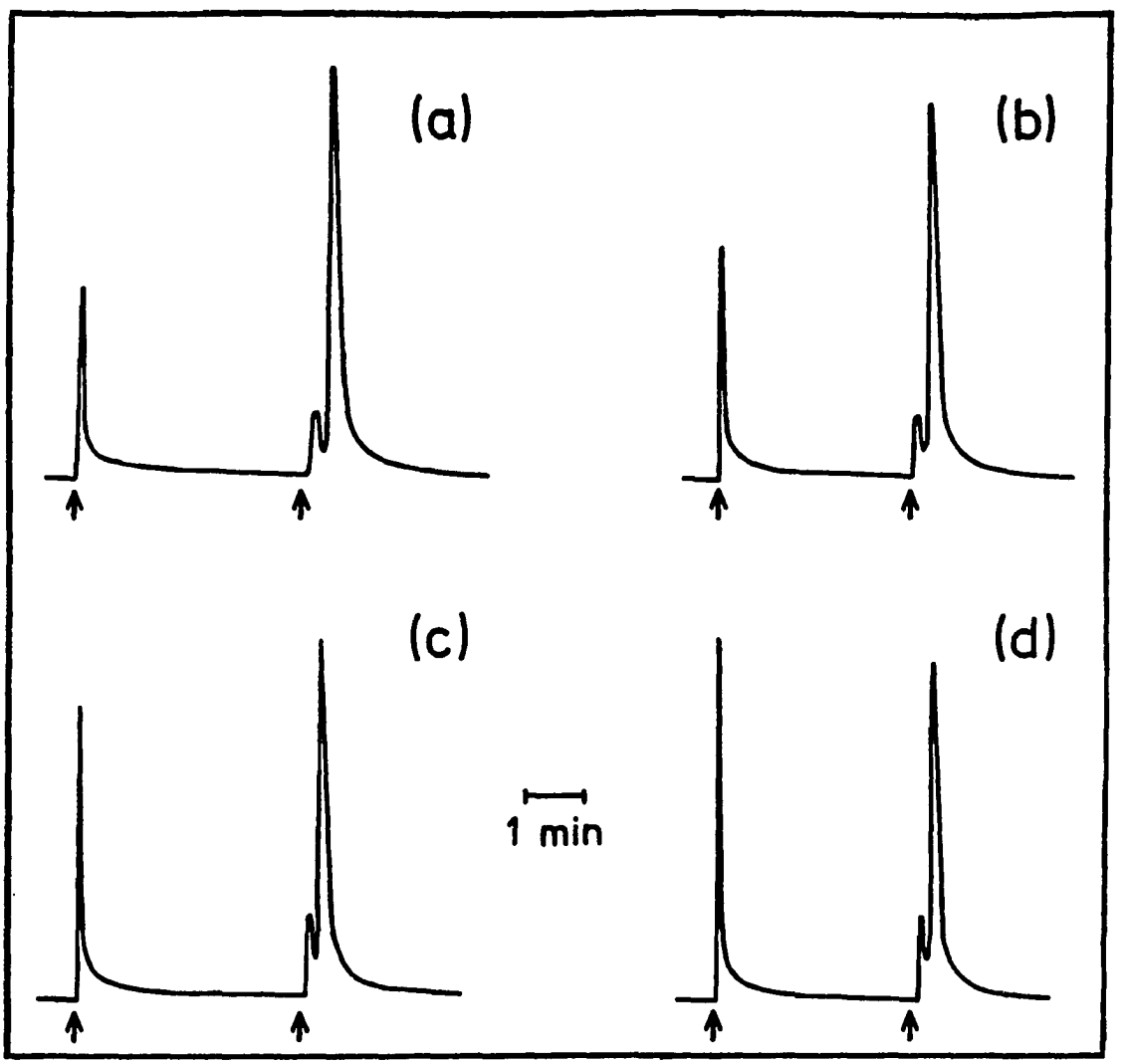
(a)
(b)
(c)
(d)
1 min

amount of bound and free IgG changes with flowrate, with the nonretained peak area increasing and the retained peak area decreasing as the flowrate is increased. By varying the flowrate in this experiment, it was possible to change the amount of nonretained IgG from a few percent at low flowrates to almost 50% when higher flow rates were used. During the course of these studies, the protein A columns were noted to be quite stable, as found previously (27), with both their kinetic and static behavior being reproducible throughout the course of the experiment.

Once the amounts of nonretained and retained IgG had been determined at various flowrates, the data were then plotted according to Equation 26. Examples of these plots are given in Figure 6. Each line shown is the linear least-squares fit through the origin for the corresponding data set. Except for the SB-500 22 μg results, all data in Figure 6 are for the next-to-smallest sample studied on each column, so that the scatter of these plots is representative of the entire data set. Note that for each plot the linear relationship predicted by Equation 26 was observed. This indicated that, for the purpose of quantitation, the model used here did give an adequate description of the split-peak effect.

In comparing these plots, it can be seen that different slopes were obtained with the various protein A supports under

Figure 6. Typical split-peak plots for IgG on protein A columns. The columns and samples sizes represented are as follows: SB-500, 22 µg IgG (○); SB-500, 11 µg IgG (●); SB-50, 15 µg IgG (▲); CDI-500, 2.7 µg (■); and EA-500, 8.2 µg (◆)

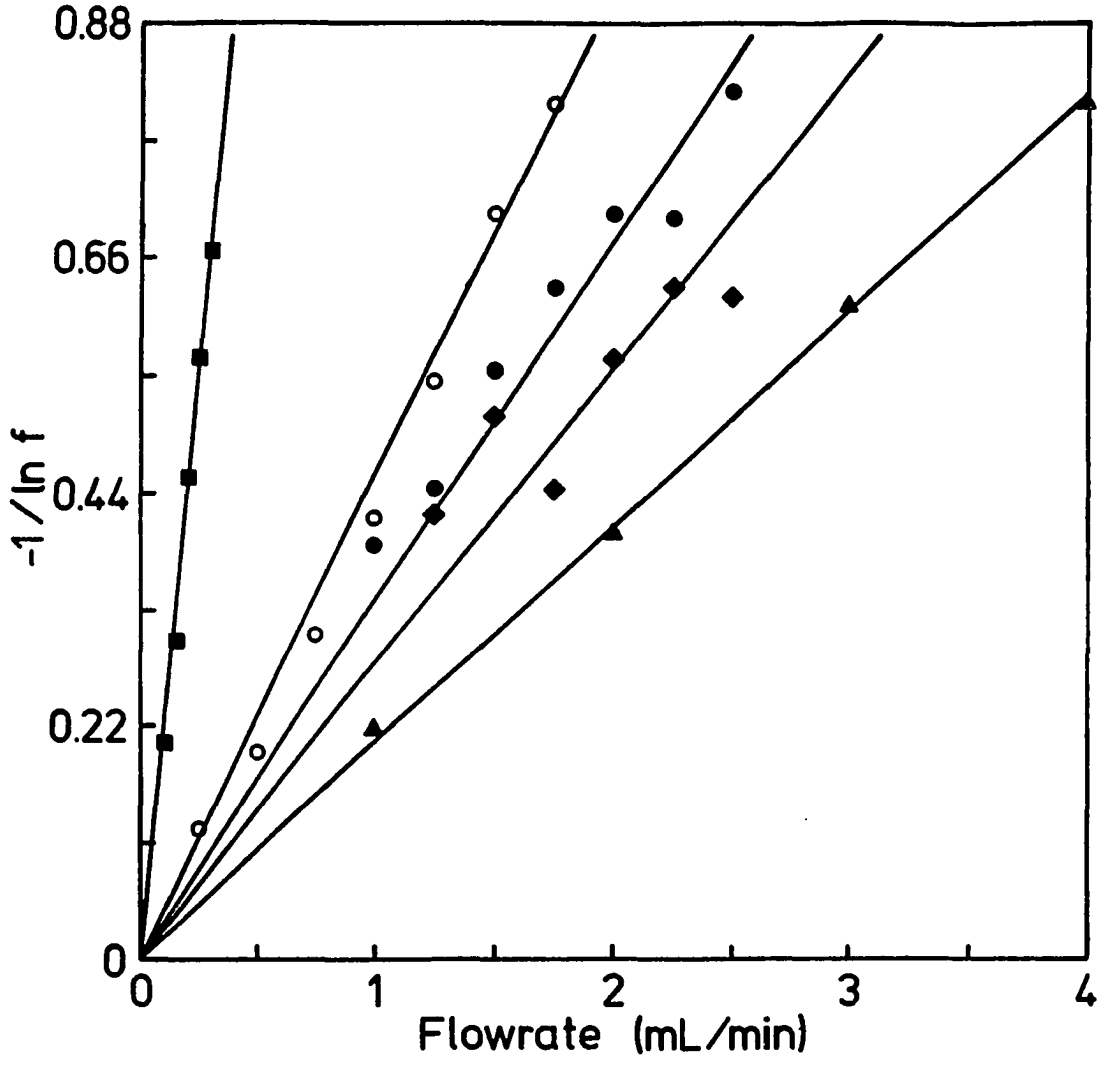
0.88
0.66
0.44
0.22
0
-1/ln f
0
1
2
3
4
Flowrate (mL/min)

similar operating conditions. Based on Equation 26, this can be used as an indication that the supports differed in their kinetic properties, with the slopes increasing as the rate of analyte adsorption decreased. It was determined qualitatively from these slopes that the CDI-500 support had the slowest adsorption kinetics, while the SB-50 support exhibited the fastest adsorption kinetics.

These differences were examined more quantitatively by evaluating the individual parameters in the slope obtained for each support. This required that slopes independent of sample size be used in order to fulfill the assumptions made in deriving Equation 26. To see if these values were independent of sample size, the split-peak slope of each support was measured at several different sample loads using the same type of least-squares fit as performed in Figure 6. These slopes were then plotted vs. sample size, as shown in Figure 7. It was found for each affinity support and sample load studied that the data gave the linear response predicted by Equation 26. However, it was also found that the slopes obtained with these supports increased with sample size. Since each data set gave an apparently linear relationship between the slope and sample load, a linear least-squares fit was used to extrapolate to the slope at zero sample size. The

Figure 7. The change in the split-peak slope with sample size for IgG on protein A columns. The columns represented are the CDI-500 (■), EA-500 (◆), SB-500 (●), and SB-50 (▲). The split-peak slopes for the CDI-500 column were ten-fold larger than shown

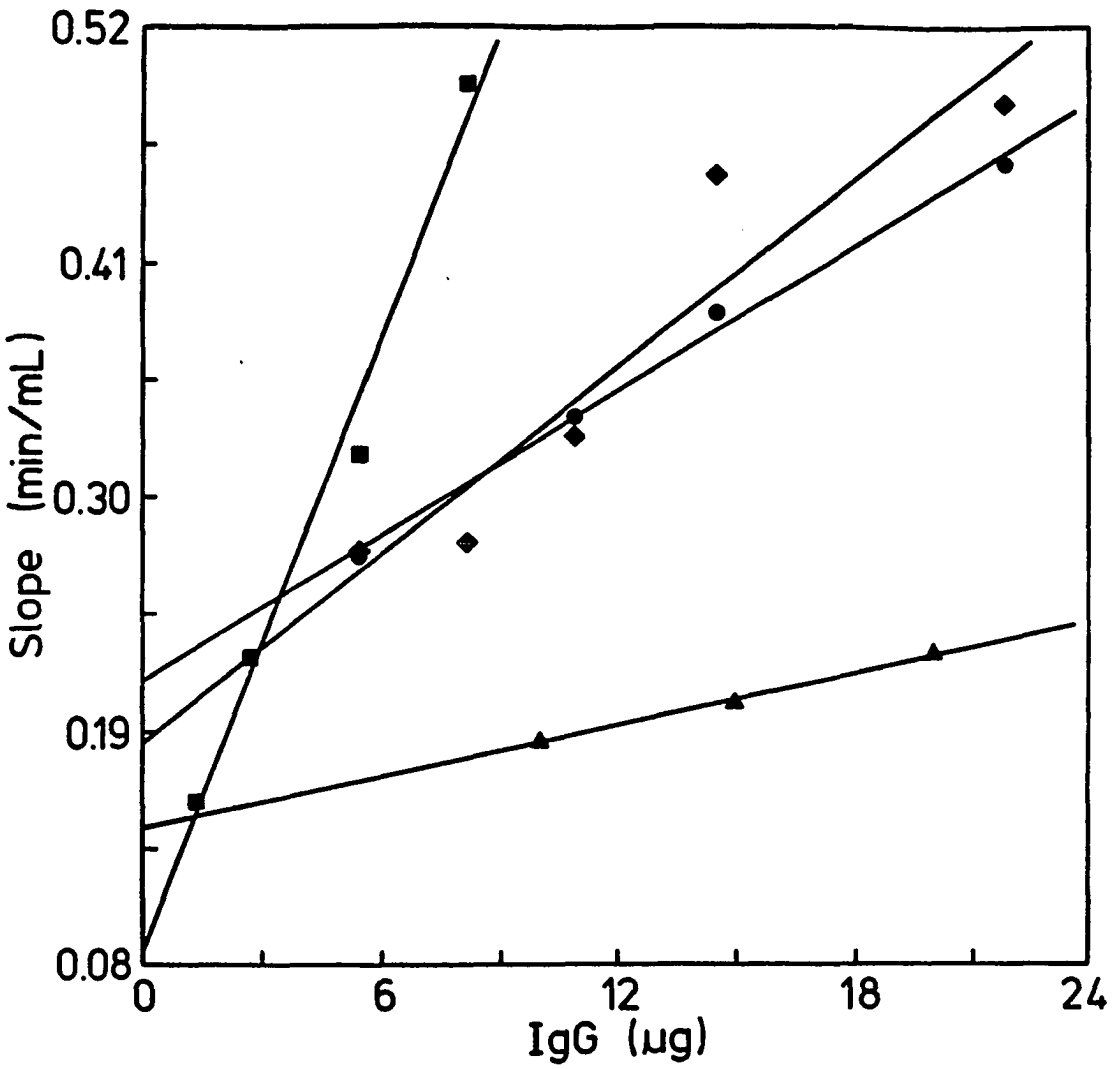
0.52
0.41
0.30
0.19
0.08
Slope (min/mL)
0
6
12
18
24
IgG (µg)

extraploted slopes obtained from this procedure are given in Table II.

These extrapolated slopes were used to calculate the value of k_3 for each of the affinity supports. This required that independent values of V_e, m_L, and k_1 also be known. V_e and m_L were determined as discussed previously, with the results given in Table II. Estimates of k_1 were obtained by using the two methods described earlier. In the first of these methods, the band-broadening of IgG under isocratic elution conditions was studied using 10 cm diol-bonded LiChrospher SI 500 and Nucleosil SI 50 columns. Plots of H vs. u were then made, as shown in Figure 8. In both cases, the linear relationship predicted by Equation 32 was observed. From the slope of these plots, k_1 was calculated to be 4.0 s^{-1} and 36 s^{-1} for the LiChrospher SI 500 and the Nucleosil SI 50, respectively. The larger k_1 value for the Nucleosil support indicates that it was a more efficient support (i.e., had faster mass transfer kinetics) than the LiChrospher. This was expected since it was found that IgG could enter approximately 96% of the LiChrospher pore volume, while on the Nucleosil it could only penetrate about 15% of the pores. This caused the Nucleosil to behave like a nonporous or pellicular support for the IgG, giving it faster mass transfer kinetics than the LiChrospher support.

Table II. Column parameters for kinetic studies

Column	Extrapolated slope (s/mL)	V_e[a] (μL)	m_L[b] (nmol)
CDI-500-3[c]	52 ± 14	27	1.4
EA-500-1	11.1 ± 2.4	27	1.6
SB-500-3	12.8 ± 0.5	27	3.2
SB-50-1	8.7 ± 0.3	22	1.0

[a]Estimated from the isocratic studies.

[b]Calculated from the IgG static capacity in Table I using an experimentally-determined packing density of 0.38 g/mL for the LiChrospher SI 500 and of 0.37 g/mL for the Nucleosil SI 50.

[c]Batch number from Table I.

Figure 8. Total plate height vs. linear velocity for IgG on diol-bonded silica columns. The supports used were diol-bonded LiChrospher SI 500 (●) and Nucleosil SI 50 (■)

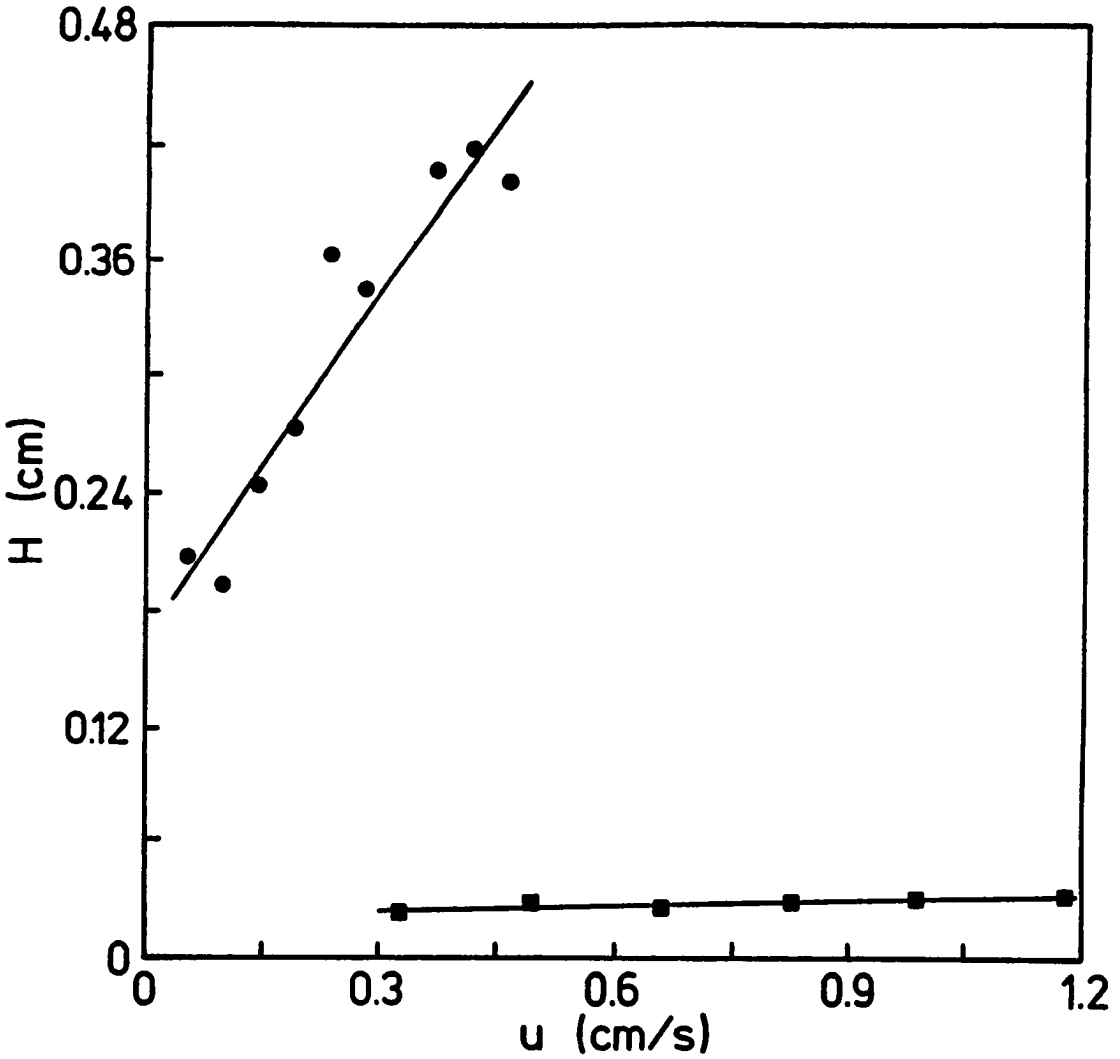
0.48
0.36
0.24
0.12
0
H (cm)
0
0.3
0.6
0.9
1.2
u (cm/s)

The second estimate of k_1 was obtained by performing split-peak experiments with IgG on short reversed-phase columns, with the assumption that diffusion was the rate-limiting step in protein adsorption. Figure 9 shows the results obtained when the data were plotted according to Equation 27. Like the affinity results in Figure 6, these results also showed the linear relationship predicted by the model. These plots did differ from those in Figure 6, however, in that no sample size dependence of the slope was noted over a two-fold range in IgG concentration. The reason for this difference between the two systems will be discussed in Section III. By performing the same type of linear fit to the data as used in Figure 6, values for k_1 of 8.6 s^{-1} and 149 s^{-1} were obtained for the LiChrospher and Nucleosil supports, respectively. The larger k_1 value for the Nucleosil SI 50 again indicates that it was a diffusionally more efficient support for IgG than the LiChrospher SI 500.

A comparison of the isocratic and split-peak values of k_1 reveals that the k_1 estimates of both supports were larger when the split-peak method was used. One way in which this can be explained is based on heterogeneity of the chromatographic system. All columns are somewhat heterogeneous due to variability in the particle size of the support, nonuniformity in the packing structure of the column, differences in the

Figure 9. Split-peak plots for IgG on reversed-phase columns. The two columns used contained LiChrospher SI 500 (●) and Nucleosil SI 50 (■) reversed-phase supports

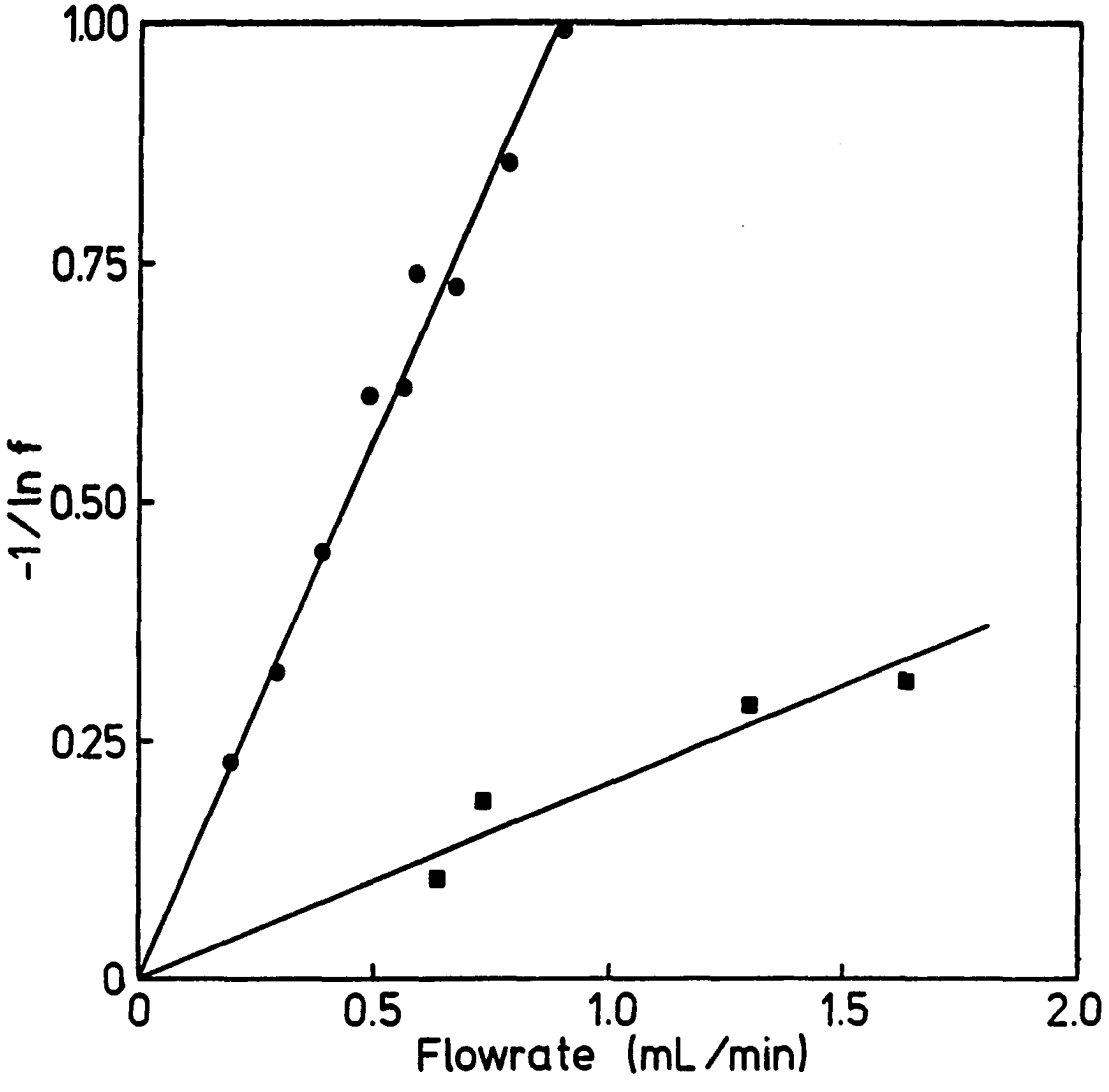
1.00
0.75
0.50
0.25
0
-1/ln f
0
0.5
1.0
1.5
2.0
Flowrate (mL/min)

binding strength of the adsorption sites, and other factors (31,66). The result is that a range of different kinetic processes are actually present, making the rate parameters used here apparent rate constants, or functions of these individual processes. This may have affected the results obtained if the two methods used to estimate k_1 responded differently to heterogeneity. For example, in the isocratic studies, band-broadending was used as the basis of the measurement. Since band-broadening is predominantly caused by the slowest kinetic processes in the column, the values of k_1 obtained would be expected to be weighted toward the smaller rate constants. In the split-peak studies, k_1 is measured based on retention of analyte via a single adsorption step. Since the majority of analyte is probably retained by the fastest adsorption processes, the k_1 values obtained here should be weighted toward the larger k_1 values. Therefore, it is reasonable that the k_1 values determined by the split-peak method were larger than those obtained by the isocratic method.

Regardless of whether or not such effects were present, it was possible to use these estimates of k_1 to more closely examine the kinetic properties of the protein A supports. The results obtained when this was done are summarized in Tables III and IV. By using these estimates of k_1 to calculate

Table III. Kinetic data from isocratic studies

Column	k_1 (s^{-1})	$1/k_1$ V_e (s/mL)[a]	k_3 (M^{-1} s^{-1})[b]
CDI-500-3[c]	4.0	9.2	$(1.7 \pm 0.8) \times 10^4$
EA-500-1	4.0	9.2	$\sim 3 \times 10^5$
SB-500-3	4.0	9.2	$\sim 8 \times 10^4$
SB-50-1	36.	1.3	$(1.3 \pm 0.4) \times 10^5$

[a]Calculated using the V_e values from Table II.

[b]Calculated using the extrapolated slopes from Table II.

[c]Batch number from Table I.

Table IV. Kinetic data from split-peak studies

Column	k_1 (s^{-1})	$1/k_1$ V_e (s/mL)[a]	k_3 (M^{-1} s^{-1})[b]
CDI-500-3[c]	8.6	4.3	$(1.5 \pm 0.7)_4 \times 10^4$
EA-500-1	8.6	4.3	$\sim 9 \times 10^4$
SB-500-3	8.6	4.3	$\sim 4 \times 10^4$
SB-50-1	149.	0.31	$(1.16 \pm 0.04) \times 10^5$

[a]Calculated using the V_e values from Table II.

[b]Calculated using the extrapolated slopes from Table II.

[c]Batch number from Table I.

$1/k_1 V_e$ and by comparing this to the extrapolated slope of each affinity column, it was found that two of the supports, the CDI-500 and SB-50, were primarily adsorption-limited, while the others had both diffusion and adsorption contributing significantly to the overall rate of retention. Thus, for the CDI-500 and SB-50 supports actual values of k_3 could be calculated, while for the other supports only rough estimates could be made. The k_3 values obtained for each support are also given in Tables III and IV.

In examining these values, it was found that the SB method, based on the SB-50 data, gave immobilized protein A with a k_3 value of approximately 1.2×10^5 M^{-1} s^{-1}. Similar results, although less precise, were obtained for the SB-500 and EA-500 supports. The CDI method, however, gave immobilized protein A with a k_3 value of only 1.6×10^4 M^{-1} s^{-1}. This clearly indicates that the immobilization method used in preparing protein A supports can significantly affect the kinetic properties of the protein A.

Note that by combining these results with the site heterogeneity argument presented earlier, it is possible to explain the sample size dependence of the split-peak slope observed in Figure 7. For example, if there are a range of adsorption rates present in a system, it would be expected that solute would tend to fill those sites with the fastest

rate of adsorption first. Thus, as sample size is increased, the kinetics should appear to become slower and the measured split-peak slope should increase. This is exactly what was observed in Figure 7. To carry this even further, one would expect that very heterogeneous columns would tend to be the most sensitive to such effects. For instance, if it is assumed that the ligand in the SB and EA columns was primarily homogeneous or native protein A, then the kinetically slower CDI column probably contained protein A in a more heterogeneous state, with a possible range of k_3 values all the way from that of native protein A to less than the value actually measured. The predicted result would be a larger change in slope with sample size for this support, as was seen in Figure 7.

Since no known literature values for the adsorption rate constant of protein A have been published, it is not possible to determine whether or not the k_3 value for the SB-50 data of 1.2×10^5 M^{-1} s^{-1} is the true adsorption rate constant for protein A. However, the binding of antibody with antigens, a similar set of reactions with which protein A competes for immunoglobulins, has typical adsorption rate constants in the range of 10^4 to 10^6 M^{-1} s^{-1} (91), so this result is certainly reasonable.

The equilibrium binding constant for Sephadex-immobilized protein A and rabbit IgG has been previously reported to be 4.1×10^8 M^{-1} (92). Assuming that this is also true for the system studied here and that the SB-50 value of k_3 is the true adsorption rate constant, then a value for k_{-3} of 2.9×10^{-4} s^{-1} is obtained. This value compares favorably with typical antibody-antigen dissociation constants of 10^{-5} to 10^{-2} s^{-1} (91), also indicating that the results obtained in this experiment are reasonable.

CONCLUSIONS

In this experiment, it was found that IgG adsorption on both affinity and reversed-phase columns gave the linear response between -1/ln f and flowrate predicted by the model. It was concluded from this that the model gave an adequate description of the split-peak effect, especially in terms of quantitating this phenomenon. This makes it useful for a number of applications, such as the evaluation and optimization of the performance of chromatographic supports. Supports can be evaluated or compared by simply measuring the split-peak slope for each under similar operating conditions. The support with the fastest rate of adsorption can then be determined by choosing that giving the smallest split-peak slope. This was illustrated with the protein A data in Figure 6, where it was found that the SB-50 gave the smallest slope and fastest kinetic properties of any of the protein A supports studied.

If estimates of k_1 and V_e are also known, even more information about the kinetics of the supports can be obtained. For example, k_1 and V_e can be used to determine the size of the diffusional term of the split-peak slope. This allows one to determine whether adsorption or diffusion is the rate-limiting step in analyte retention. By doing this with the protein A data, it was found that two of the supports

were adsorption-limited, while the others had both adsorption and diffusion contributing to the overall rate of retention. This type of information is useful in improving the performance of chromatographic supports. For example, if diffusion is found to be rate-limiting, it may be possible to increase the rate of analyte retention by using a support with a smaller particle diameter, increasing both k_1 and k_{-1} according to Equation 31. If adsorption is rate-limiting, it may be possible to use a higher ligand coverage (i.e., an increased value of m_L) to increase the rate of retention.

In this experiment, this approach was carried even further by using values of m_L, k_1, and V_e to determine the value of k_3 for each protein A support. From the results given in Tables III and IV, it was found that k_3 varied by up to ten-fold depending on which immobilization method was used in preparing the supports. This is significant since it indicates that the kinetic properties of an affinity ligand can be affected by the immobilization method used to prepare it. Thus, it is important to consider this in choosing a coupling method. The results presented suggest that the Schiff base technique is the immobilization method of choice for protein A, since it gave ligand with both superior static and kinetic properties vs. that obtained with either the EA or CDI methods.

This last set of studies also suggests that the split-peak method might be useful in the measurement of adsorption rate constants for macromolecular interactions. If this is the case, then this technique would offer several potential advantages over the present isocratic method. For example, since it is based on an area rather than a peak width measurement, it is not as susceptible to extracolumn band-broadening as the isocratic method. It should also be more precise, since peak areas can be much more precisely measured than peak widths or variances (69). A third potential advantage of this method is that techniques other than peak area measurements can be used to obtain the retained and non-retained fractions. This can be done by simply collecting these fractions as they elute from the column and later analyzing them with the desired technique.

Another advantage of this method is that it does not require the use of biospecific elution, a technique often needed with the isocratic method. Recall that in biospecific elution a species that competes for analyte or ligand binding sites is added to the mobile phase to elute analyte from the column. Although this is an easy way of isocratically eluting analyte, it can cause problems in analyte detection. As a result, the use of the isocratic method has been largely limited to systems which have competing species that are

significantly different from the analyte, such as the binding of enzymes with inhibitors or substrates (29,90). A similar detection problem can occur in other kinetic methods used in studying biological systems, such as stopped-flow analysis or perturbation techniques (93). This is not a problem with the method presented here, since the free and bound analyte are readily separated and nonspecific as well as biospecific elution techniques can be employed. This makes this technique potentially useful for studying a wide variety of macromolecular interactions, especially those involving similar interacting species. In order for this method to be useful for this, however, further work must first be done to determine how the rate constants obtained with this approach compare to the results of other techniques.

Further work is also needed to explain the sample size dependence of the split-peak slope. In some applications, such as the comparison of the overall adsorption kinetics of affinity supports, it may be possible to deal with this by careful standardization of the column size and sample load conditions. For the determination of rate constants, however, a better understanding of this effect is needed to allow the results to be minimized or corrected for it. Studies in this area will be presented in Section III. Also in Section III, the reason for the differences in the split-peak dependence of

affinity and reversed-phase columns will be examined. The effect of heterogeneity and other secondary effects on this dependence will also be further discussed.

SECTION II.

DESIGN AND OPTIMIZATION OF A DUAL-COLUMN AFFINITY CHROMATOGRAPHIC SYSTEM

INTRODUCTION

In the previous chapter, it was demonstrated how the split-peak effect can be used in comparing and evaluating the adsorption kinetics of chromatographic supports. This makes it useful in choosing or designing more efficient supports, allowing faster separations. However, the problem still remains as to how to deal with the split-peak effect when it appears on supports that have already been prepared or on columns already in use. For these cases, a technique is needed to determine what conditions must be used to give the desired degree of retention in the minimum amount of time. In this experiment, such a technique is presented which allows the evaluation of support adsorption kinetics through the use of a single rate parameter. The method is demonstrated by using it in the design and optimization of an HPAC analytical separation.

The separation developed in this work is one of clinical interest, the determination of two serum proteins. HPAC was chosen as the basis for this separation since its high selectivity enables it to be used for the determination of one or a few species in complex samples, such as serum or urine, with little interference from other components. This makes HPAC potentially useful in clinical chemistry, where such samples are commonly encountered. An example of the current

use of low-performance affinity chromatography in this field is the determination of glycosylated hemoglobins in blood (94). In this experiment, a method is developed for the determination of human serum albumin (HSA) and IgG in serum.

HSA is the most commonly determined of the serum proteins (95). It is the major protein component of serum, making up 50 to 65% of the total protein content, with typical concentrations of 35 to 52 g/L (96). Presently-used methods for determining albumin include spectrophotometry, electrophoresis, and single radial immunodiffusion (SRID) (95,96). Albumin is of interest clinically because its serum concentration is a general indicator of disease and the nutritional state of an individual. For example, decreases in HSA levels can occur due to protein loss (such as occurs in kidney damage, severe hemorrhages, and burns), decreases in protein synthesis or intake (as takes place in malnutrition, starvation, and liver cell damage), or overhydration (95-99).

The determination of immunoglobulin levels in serum is also of clinical interest. In humans, the immunoglobulins (or circulating antibodies) consist of five known classes: IgG, IgA, IgM, IgD, and IgE. Of these, IgG is the most abundant in serum, making up 75 to 80% of the immunoglobulin fraction. Normal levels of IgG vary from 7.0 to 16.8 g/L (96). IgA and IgM also occur at significant levels in serum with concen-

trations of 1.4 to 2.2 and 0.80 to 1.20 g/L, respectively, but IgD and IgE occur in only trace amounts (i.e., less than 0.2% of the total immunoglobulin fraction) (98). Immunoglobulin levels are commonly determined by electrophoresis, immunoelectrophoresis, SRID, nephelometry, and radioimmunoassay (RIA) (96,98,99). These levels are of interest since they are altered by many diseases and indicate the state of the humoral immune system (96,98). For example, increases in the serum IgG levels can be an indication of infection or liver disease. Abnormal levels of IgG can also be the result of disorders of the immune system such as occur in autoimmune or monoclonal diseases and acquired immunodeficiency syndromes (99).

Possible affinity ligands for these proteins include immobilized anti-HSA antibodies for HSA (24) and protein A for IgG (26,27). As discussed in the preceding chapter, the ability of protein A to bind to immunoglobulins has made it a useful ligand for isolating several types of IgG, including human IgG (26,27). Of the four subclasses of human IgG (i.e., IgG_1 through IgG_4), protein A binds all but IgG_3, which is not adsorbed or only slightly bound to protein A (50,100). IgG_3 represents 5 to 9% of the total IgG fraction (101).

In this work, these affinity ligands were used in a dual-column system to allow both HSA and IgG to be determined from a single serum sample. Such an approach has the advantage of

retaining the high selectivity of each affinity matrix while allowing vastly different components to be determined simultaneously. A general scheme is presented here for the design and optimization of such multi-analyte affinity systems based on the kinetic properties of the supports as well as their static properties and elution characteristics.

THEORY

The kinetic properties of the supports were determined using the split-peak method described in Section I. In the preceding section, the relationship between the flowrate and fraction of analyte eluting in the nonretained peak was given as

$$\frac{-1}{\ln f} = F\left(\frac{1}{k_1 V_e} + \frac{1}{k_3 m_L}\right) \tag{26}$$

where a plot of $-1/\ln f$ vs. F yields a straight line with an intercept of zero and a slope equal to $(1/k_1 V_e + 1/k_3 m_L)$.

It was pointed out earlier that each of the slope terms, $1/k_1 V_e$ and $1/k_3 m_L$, are inversely proportional to the column volume, V_{col}. This is a result of the fact that V_e and m_L are related to V_{col} by the equations

$$V_e = \varepsilon_e V_{col} \tag{33}$$

$$m_L = [L] \varepsilon_p V_{col} \tag{34}$$

where ε_e and ε_p are the interparticle and intraparticle porosities (i.e., V_e/V_{col} and V_p/V_{col}) and [L] is the ligand concentration in the pore volume, as defined previously.

Substituting Equations 33 and 34 into 26, an alternate form of the split-peak equation is obtained.

$$\frac{-1}{\ln f} = \frac{F}{V_{col}}\left(\frac{1}{k_1\,\varepsilon_e} + \frac{1}{k_3\,[L]\,\varepsilon_p}\right) \qquad (35)$$

Since all terms in the slope are now independent of column volume, these may be replaced by a single constant, C. Substituting this constant into Equation 35 yields

$$\frac{-1}{\ln f} = \frac{F\,C}{V_{col}} \qquad (36)$$

By using Equation 36, then, the adsorption kinetics of a support can be described by a single parameter independent of both flowrate and column volume. Experimentally, C may be determined by injecting pure analyte into a column of known volume, measuring the fraction eluted in the nonretained peak at various flowrates, and determining the slope that results from a plot of $-1/\ln f$ vs. F/V_{col}.

Note that Equation 36 is simply the integrated rate equation for a first-order reaction, where V_{col}/F is the reaction time and C is the inverse of the apparent adsorption rate constant. The result is that C can be used to determine the time and column volume-flowrate combination needed to adsorb a given fraction of analyte. This makes it useful in optimizing sample application conditions.

EXPERIMENTAL

Reagents

The protein A, HSA, human IgG, human IgA, rabbit IgG, and affinity-purified goat anti-human IgG, anti-human IgA, and anti-human IgM antibodies were from Sigma (St. Louis, MO). The human IgM and the rabbit anti-HSA antisera were from Dako (Santa Barbara, CA). All biochemicals used were of the purest grades available. Reagents for the bicinchoninic acid (BCA) protein assay were from Pierce (Rockford, IL). The Coomassie Brilliant Blue G-250 was from Kodak (Rochester, NY), the agarose was from MCB (Norwood, OH) and the poly(ethylene glycol) (PEG), MW 8000, was from Aldrich (Milwaukee, WI). The LiChrospher SI 4000 and SI 500 (10 μm particle diameter, 4000 Å and 500 Å pore sizes, respectively) were obtained from Rainin (Woburn, MA). The Serachem Clinical Chemistry Control sera were from Fisher (St. Louis, MO).

Instrumentation

The chromatographic and data acquisition systems used were the same as described in Section I, with the addition of a Rainin 7000 switching valve. This valve, placed after the anti-HSA column, contained the protein A column in place of a sample loop. This allowed the protein A column to be switched

off-line during part of the analysis. The detector was a Hitachi 100-10 (Tokyo, Japan) operated at 280 nm. The pH of each collected fraction was measured using an Orion 601-A pH/mV meter and a Bioprobe combination electrode from Fisher. A Bio-Rad 1420B power supply (Richmond, CA) was used for the electrophoresis and a Zeineh soft-laser scanning densitometer (LKB, Gaithersburg, MD) was used to analyze the gels.

Procedures

Preparation of protein A and anti-HSA supports

Diol-bonded LiChrospher SI 4000 and SI 500 were prepared as described previously (80). The diol contents of the SI 4000 and SI 500 prior to activation were 24 and 200 μmol/g silica, respectively, as determined by the periodate oxidation method (84,85).

The protein A and anti-HSA matrices were prepared using the Schiff base method (25) with the modifications described in Section I. This method was chosen due to the superior kinetic and static properties obtained with it for protein A in the previous study. The protein A was coupled to the SI 500 by using 10 mg protein A/g LiChrospher SI 500 in the immobilization step, and the anti-HSA was coupled by using 2.0 mL of anti-HSA antiserum/g LiChrospher SI 4000. The protein A had a specific activity of 12 mg human IgG/mg

protein A, as determined by SRID (102). The HSA antiserum had a specific activity of 38.3 µg HSA/mg protein, as determined by immunoprecipitation (103), and a protein content of 19.6 g/L. The activated silica was placed in 2 mL of pH 5.7 0.10 M phosphate buffer/g silica and was sonicated under vacuum for 15 min. The protein was then added and the mixture shaken at 4 °C for 6 days. After 6 days, 500 mg of sodium borohydride/g silica was added to reduce any remaining activated groups (25). The samples were then centrifuged, washed with 2 M sodium chloride and water, and stored at 4 °C in 0.1 M pH 7.0 phosphate buffer. Part of each sample was washed with water, vacuum-dried at room temperature, and assayed for protein content, using the BCA method (104) with protein A or IgG as the standard, and diol-bonded silica as the blank. The remaining protein A and anti-HSA silicas were then vacuum slurry-packed (83) into minicolumns of a published design (79).

Chromatography

The application buffer for both supports was 0.05 M phosphate 0.05 M citrate buffer (pH 7.0). The elution buffer was 0.05 M phosphate 0.05 M citrate (pH 3.0). The kinetic properties of both matrices were measured at 25 °C. All other chromatography was performed at room temperature.

The static adsorption capacity of each matrix was found by continuously applying 0.1 mg/mL human IgG or 0.01 mg/mL HSA to the appropriate matrices, packed in 6.4 mm x 4.1 mm I.D. columns. Both these and all other standard human IgG and HSA solutions were prepared in the pH 7.0 buffer. The breakthrough capacities were determined by integration of the curves (87) and were corrected for the void volume of the system.

The kinetic adsorption properties of both matrices were studied by the split-peak method described in Section I. The protein A kinetic studies were performed using rabbit IgG as the analyte under the same conditions as used earlier. For the anti-HSA matrix, a 12.8 mm x 4.6 mm I.D. column and a 50 µL loop were used over a flowrate range of 0.5 to 0.75 mL/min.

The elution of human IgG and HSA as a function of pH was studied using a 6.4 mm x 4.1 mm I.D. protein A column and a 12.8 mm x 4.6 mm I.D. anti-HSA column. The columns were first saturated with 0.25 mg/mL human IgG or 0.08 mg/mL HSA, respectively, at 0.50 mL/min. A series of step changes from 0 to 100% pH 3.0 buffer were then made in 5% or 10% increments (i.e., 0.2 or 0.4 pH units) at 15 minute intervals. The area of the peak eluted at each pH was determined by planimetry after subtraction of a background run. A fraction was collected at each step change, and the pH was measured.

Quantitation of serum samples was performed at a flowrate of 1.0 mL/min using anti-HSA and protein A columns, connected in series, and a 10 µL sample loop. The standards were 2.0 to 14.2 mg/mL HSA and 0.5 to 4.0 mg/mL human IgG. The serum samples were diluted 1:5 with the pH 7.0 buffer prior to injection. After the nonretained peak had been eluted from both columns, the anti-HSA column was eluted with pH 3.0 buffer, keeping the protein A column switched off-line. After the HSA had been eluted, the protein A column was switched on-line to elute the IgG. Samples of each retained and nonretained fraction from injections of normal serum were collected for later analysis.

Electrophoresis

Sodium dodecyl sulfate polyacrylamide gel electrophoresis (SDS-PAGE) was performed on 10% discontinuous vertical slab gels at pH 8.8, using a previously-published procedure (105). Samples of 50 to 150 µL were applied, using HSA and human IgG as the electrophoretic standards. The gels were stained with Coomassie Blue and analyzed with a scanning densitometer.

Radial immunodiffusion

SRID was performed as described earlier (106), using 1.5 mm gels and 2 mm sample wells. The gels contained 1% agarose in 0.01 M phosphate buffer (pH 7.4), along with 0.85% sodium

chloride, 0.02% sodium azide, and 2% PEG. The gels also contained 0.2 to 1.6 $\mu g/cm^2$ of affinity-purified goat antibodies against either human IgG, IgA, or IgM. The chromatographic fractions applied were preconcentrated 5- to 30-fold on Minicon B-15 clinical sample concentrators (Amicon, Danvers, MA). After development, the gels were stained with Coomassie Blue.

RESULTS AND DISCUSSION

Static Properties of Protein A and Anti-HSA Supports

The static properties obtained for the protein A and anti-HSA supports are given in Table V. The protein A SI 500 results were essentially the same as those given in Section I under the same immobilization conditions. The immobilization yield for protein A was 86 ± 8%, and the resulting specific activity was 17% of the initial value claimed by the manufacturer. This rather low specific activity also agrees with the findings presented in Section I. As discussed in the preceding section, this low activity may be due to such effects as denaturation or improper orientation of protein A on the matrix as a result of the immobilization process.

The anti-HSA support had an immobilization yield of 43%. This low yield was probably a result of the SI 4000 being saturated with immobilized protein, since the coverage was calculated to be approximately 1.0 monolayers based on a Stoke's diameter for IgG of 100 Å (107). This was also suggested by the fact that when the same immobilization conditions were used with a higher surface area support, such as LiChrospher SI 500, virtually 100% of the protein in the antiserum was immobilized.

Table V. Properties of protein A and anti-HSA supports

Support	Protein immobilized (mg/g silica)	Static capacity (mg/g silica)	Specific activity (mg/mg)	Split-peak constant[a] (s)
Protein A SI 500	8.6 ± 0.8	17.7 ± 0.5	2.1 ± 0.2	1.69
Anti-HSA SI 4000	16.5 ± 1.1	0.90 ± 0.08	(5.5 ± 0.6) x 10^{-2}	< 2.8

[a]The slopes given for the protein A and anti-HSA supports are for sample loads of 2 and 20% of the maximum static capacities, respectively.

The specific activity of the anti-HSA support, as determined by breakthrough analysis, was 72% of the initial value predicted by immunoprecipitation, assuming a maximum binding capacity of two HSA molecules per antibody. This indicated that relatively little anti-HSA activity was lost during the immobilization process.

Elution Profiles of IgG and HSA as a Function of pH

The conditions required for elution of human IgG and HSA from the affinity supports were determined for a pH elution scheme. The results are shown in Figure 10. For human IgG, all of the retained analyte was found to elute from the protein A SI 500 over a pH range of 7.0 to 3.6. This is in agreement with previous experimental results (50). Part of the reason for the broadness of this elution range was revealed by taking the derivative of the curve with respect to pH, giving the pH elution profile. When this was done, two major peaks were found to be present in the profile: the largest with a maximum in the elution profile at approximately pH 4.5, and a slightly smaller peak with a maximum at about pH 4.9. These results agree with those obtained by Ohlson for human IgG on protein A SI 4000 (100) and Duhamel et al. for human IgG on protein A Sepharose (108). In these earlier studies, the peak at the lower pH was identified as IgG_1 and

Figure 10. Total percent of human IgG eluted from protein A SI 500 (●) and HSA eluted from anti-HSA SI 4000 (■) as a function of pH

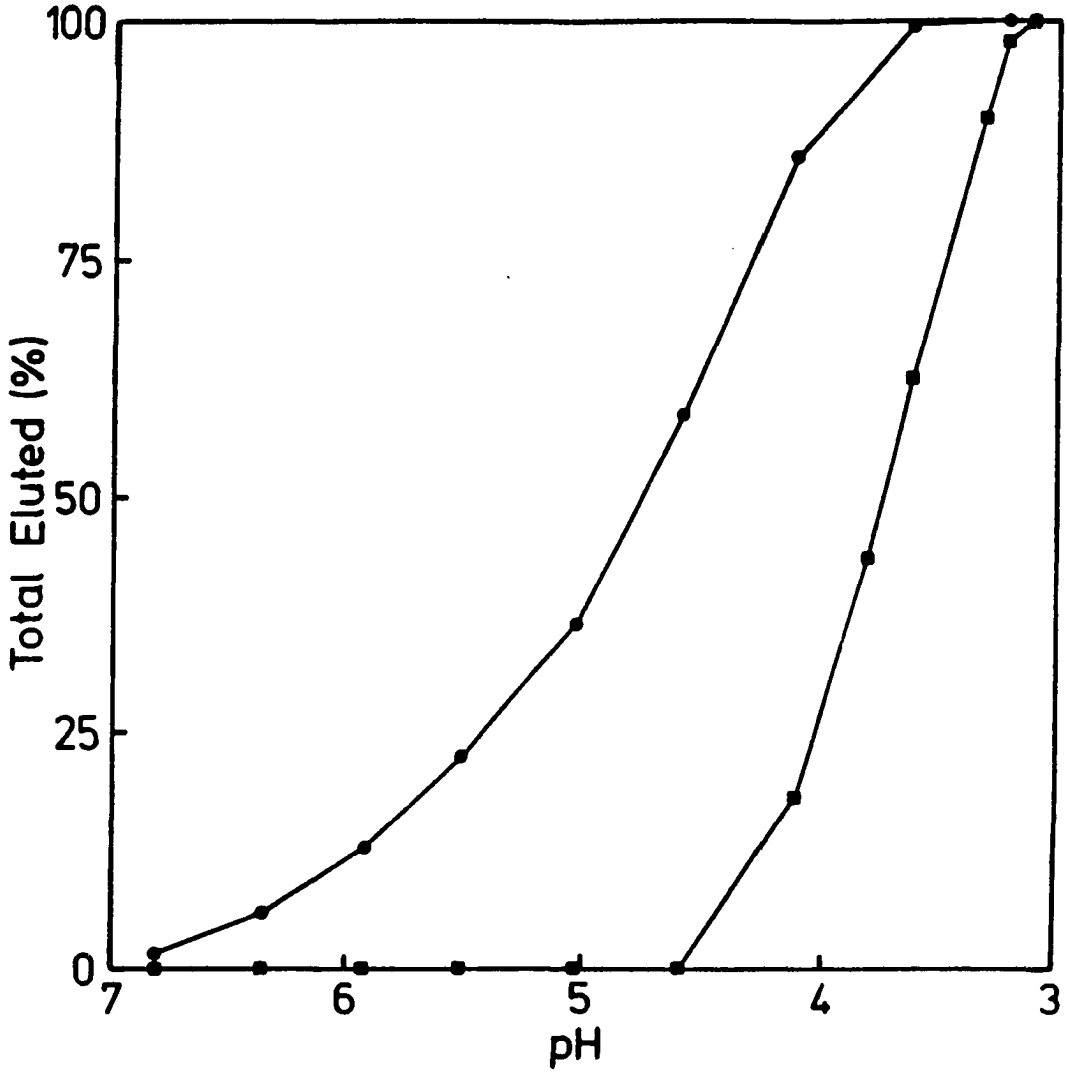
100
75
50
25
0
Total Eluted (%)
7
6
5
4
3
pH

the other as IgG_2 (100,108). Because there were at least two independently eluting species present, the result was that the pH range needed for total sample elution was broadened, as was seen in Figure 10. Another contributing factor to broadening of the pH elution range may have been heterogeneity of the immobilized protein A, as discussed in Section I.

A much narrower pH range was needed to elute HSA from the anti-HSA support. Figure 10 shows that all of the HSA was eluted from the anti-HSA SI 4000 between pH 4.5 and 3.0. The first derivative with respect to pH of the curve gave an elution profile consisting of one peak, which had a maximum between pH 3.8 and 3.6. The pH range of this profile is the same as that of the N-F transition of serum albumin, during which the protein undergoes a reversible conformational change (109). This suggests that such a transition might be the mechanism by which this analyte-ligand complex dissociates.

In comparing the human IgG and HSA curves in Figure 10, significant overlap of the two was found to occur, particularly in the pH range of 4.5 to 3.5. The maximum difference in the two curves was 68% at pH 4.1, where 18% of the HSA and 86% of the human IgG were eluted. Since the number of moles of HSA in serum is typically nine times greater than that of IgG, it was concluded that this difference was not sufficient to resolve these two components quantitatively on an anti-

HSA/protein A dual column system, especially if done only by means of either a series of pH step changes or a pH gradient.

Selection of Operating Conditions

Because a pH step change or pH gradient elution scheme alone was found to be insufficient to totally resolve IgG and HSA on this system, an alternative elution method had to be found. The technique used was based on a column-switching system, such as shown in Figure 11, allowing the IgG and HSA to be eluted independently from one another. In a typical analysis, this switching system was used by first injecting sample into the pH 7.0 application buffer with both columns on-line (a). This allowed the sample to pass through both columns and the HSA and IgG to be adsorbed. Once the non-retained peak was eluted, the protein A column was switched off-line (b) and pH 3.0 buffer was applied to elute the HSA. The protein A column was later switched back on-line to elute the IgG (a). Finally, pH 7.0 buffer was again applied and the cycle repeated. Using this system, it was possible to adjust the resolution between the IgG and HSA peaks to any desired value by changing the time at which the protein A column was brought back on-line.

An advantage of this system was that, by having the sample pass through the anti-HSA column first, it was possible

Figure 11. Column-switching system for the protein A/anti-HSA system. The diagram shows the system with both the anti-HSA and protein A columns on-line (a) and with only the anti-HSA column on-line (b)

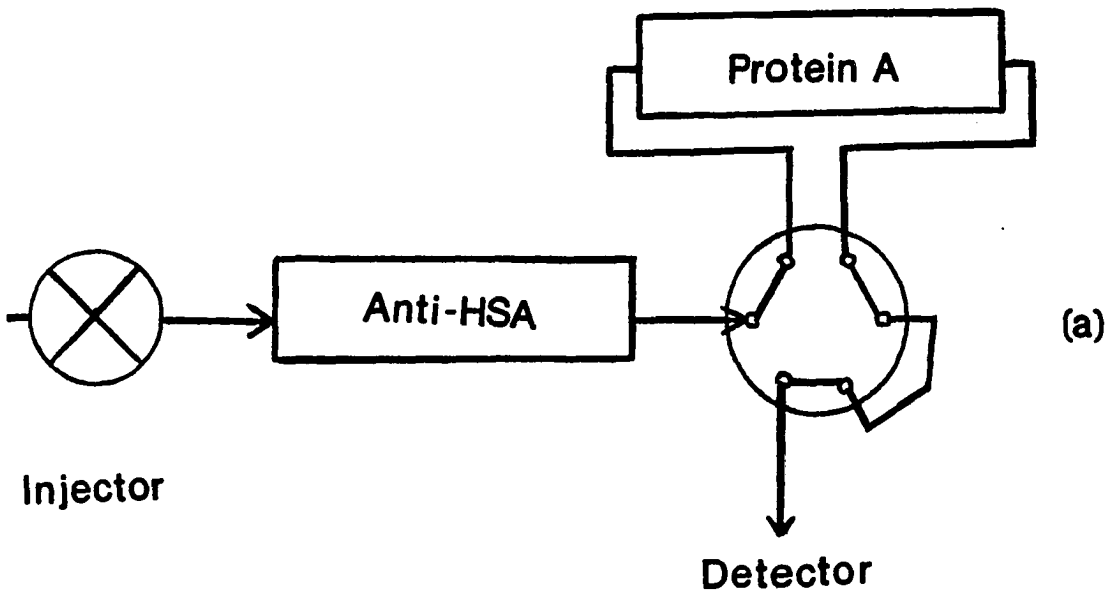
Protein A
Anti-HSA
Injector
Detector

(a)

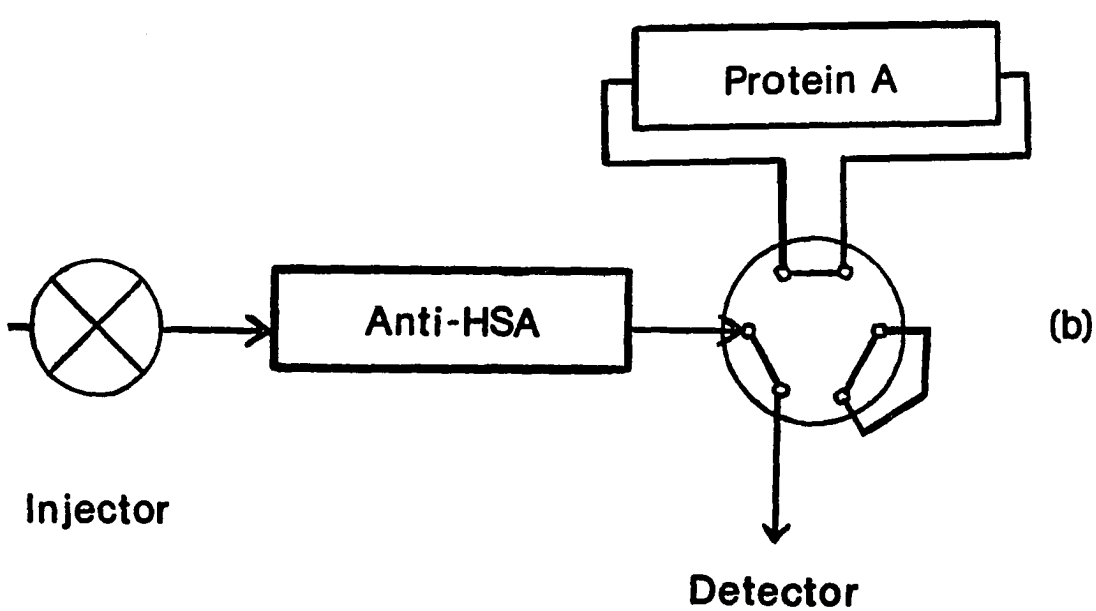
Protein A
Anti-HSA
Injector
Detector

(b)

to reduce interferences in the IgG determination due to HSA adsorption on protein A. This was of concern since in previous studies it was shown that protein A binds to porcine, canine, and feline albumin (110). To test for adsorption of human albumin on protein A, injections of normal serum were made into a 10 cm x 4.1 mm I.D. protein A SI 500 column, and the retained fractions collected. SDS-PAGE was then performed on these fractions. Three bands were seen in the retained sample. The two major bands corresponded to those for the H and L chains of an IgG standard and the third matched that produced by an HSA standard. Integration of the areas under each band with a scanning densitometer revealed that up to 9% of the total area was in the HSA band of the sample (55). This indicated that a significant amount of HSA had been adsorbed on the protein A column. By placing the anti-HSA column first in the dual-column system, an attempt was made to minimize this effect by removing any HSA present before the sample passed through the protein A column.

Once the elution scheme and column order had been decided, it was necessary to determine the column sizes needed to retain IgG and HSA quantitatively under normal operating conditions. Two parameters were considered in determining this: the binding capacity of the supports and their adsorption kinetics. The kinetic properties of the supports were

particularly of interest, since this has not only been shown to be a limiting factor in analyte retention for protein A, as demonstrated in Section I, but also for a number of immunoaffinity HPAC supports (28,34,37,39). This parameter was examined using the split-peak method. The values of the split-peak constant (C) obtained for these supports are given in Table V.

In determining the required column sizes, a flowrate of 1.0 mL/min and a sample size of 30 µg IgG and 100 µg HSA (i.e., a 10 µL injection of a 1:5 dilution of normal serum) were assumed to be typical operating conditions. The column volume needed to give a column capacity equal to the sample load was determined from the static capacity values in Table V. The minimum value of V_{col} required by the adsorption kinetics was calculated from Equation 36, using the values of C in Table V, the given flowrate, and assuming 99% retention (i.e., f = 0.01).

The results are summarized in Table VI. For the protein A matrix, the minimum value of V_{col} required to give a sufficient sample binding capacity was only 4.5 µL. However, the minimum value of V_{col} needed to kinetically adsorb the IgG was about 30 times this value, or 130 µL, making adsorption kinetics the limiting factor in determining column size for this matrix. For the anti-HSA support, the static capacity

Table VI. Column size requirements for anti-HSA and protein A supports

Support	Minimum column volume (µL)	
	Static requirement[a]	Kinetic requirement[b]
Protein A SI 500	4.5	130
Anti-HSA SI 4000	230	< 220

[a]Based on a sample composed of 30 µg IgG and 100 µg HSA. The results were calculated from the static capacity data in Table V using packing densities of 0.38 g/mL for SI 500 and 0.49 g/mL for SI 4000.

[b]Based on a flowrate of 1.0 mL/min, the split-peak kinetic data in Table V, and a minimum retention of 99%.

term was slightly larger than that estimated for the adsorption kinetics, making the binding capacity the limiting factor. In this case, a minimum column volume of 230 µL was calculated for the anti-HSA matrix. To allow for more concentrated samples than assumed here, such as might occur when abnormal serum is tested, column volumes of 160 µL for the protein A and 530 µL for the anti-HSA were actually used (i.e., column sizes of 12.4 mm x 4.1 mm I.D. and 40.4 mm x 4.1 mm I.D., respectively).

This system was tested, and the cycle time optimized, by injecting standards containing 80 µg HSA and/or 20 µg human IgG. Some typical chromatograms obtained are shown in Figure 12. Injection of HSA (a) gave a single retained peak which was eluted from the anti-HSA column, and injection of IgG (b) gave a single retained peak which eluted from the protein A column. A sample containing HSA and IgG (c) gave a chromatogram that was essentially the same as the sum of those obtained with the HSA and IgG standards. By using the elution times and peak widths obtained with these standards, as well as the void times for the system and the time required to switch from one buffer to another, a total cycle time of 6.0 min for the separation was obtained, using the event sequence given in Figure 12. Under these conditions, the resolution (Rs) between the HSA and IgG peaks was 1.0. By delaying the

Figure 12. Chromatograms obtained after injections of HSA (a), IgG (b), HSA plus IgG (c), and normal serum (d) into the dual-column system. The event sequence used was as follows: 0.00 min, switch from pH 3 to 7 buffer; 0.50 min, sample injection; 2.25 min, protein A column switched off-line, switch to pH 3 buffer; 4.00 min, protein A column switched on-line. The samples and chromatographic conditions used were the same as described in the text. The small peak at 1.4 min in (a-c) was due to the solvent change from pH 7 to 3 plus IgG_3 in (b-c)

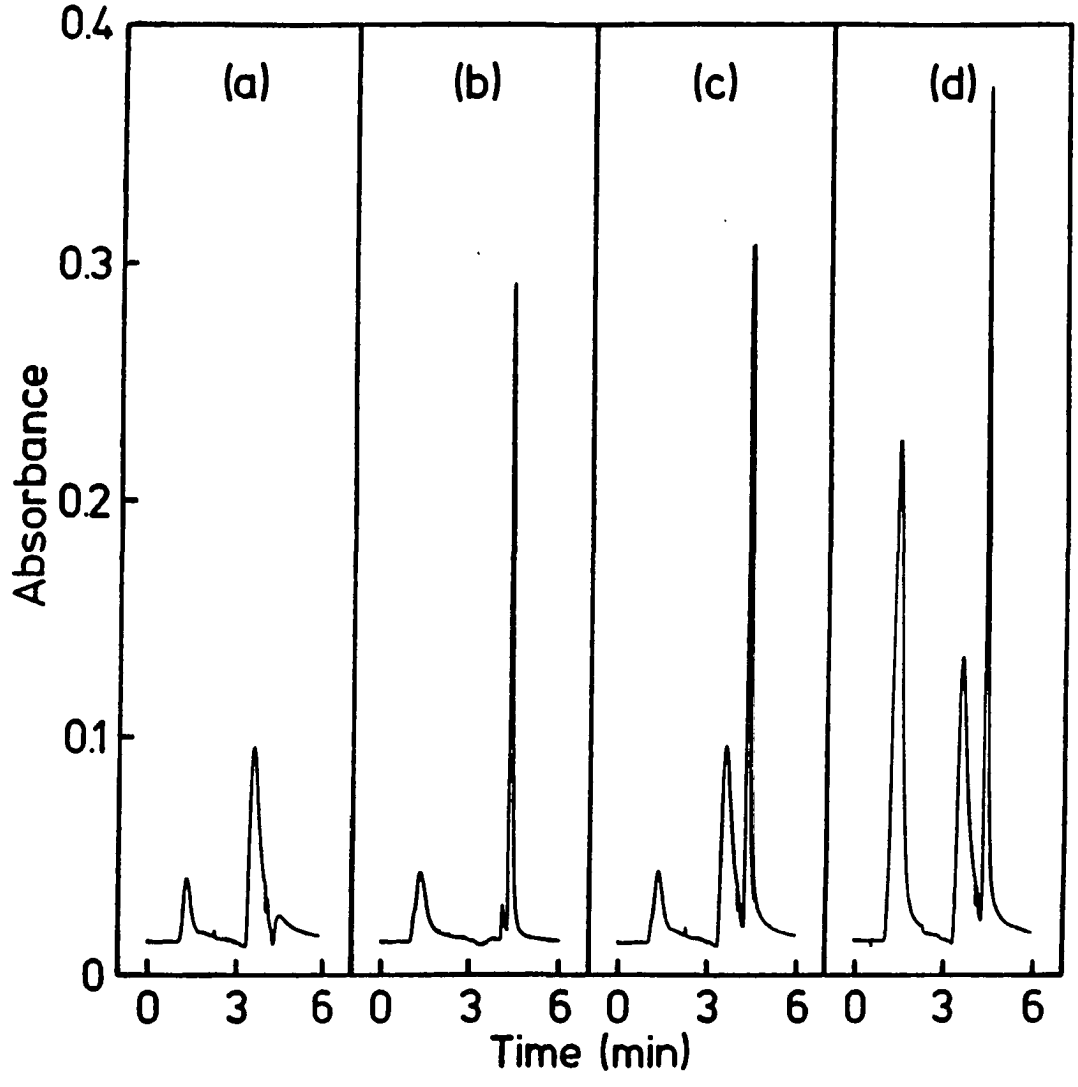
0.4
0.3
0.2
0.1
0
Absorbance
(a)
(b)
(c)
(d)
0 3 6 0 3 6 0 3 6 0 3 6
Time (min)

time at which the protein A column was brought back on-line, it was possible to obtain baseline resolution (i.e., Rs $\geq$ 1.5) in a cycle time of less than 7.0 min.

Using this elution scheme, the HSA peaks obtained were typically broader than those for IgG. An attempt was made to reduce the HSA peak width by using more acidic elution conditions. By going to pH 2.0, it was possible to decrease the HSA peak width by 50% and the IgG peak width by 20%. At this pH, however, the total cycle time actually increased, since at pH $\leq$ 2.6 the time required to regenerate the protein A column with pH 7.0 buffer became longer than the value of 30 seconds required at an elution pH of 3.0. Because of this effect, the elution pH was kept at 3.0 in order to minimize the cycle time while allowing both HSA and IgG to be quantitatively eluted.

Quantitation of HSA and IgG in Serum

Injections of a series of protein standards, containing 20 to 140 µg HSA or 5 to 40 µg of human IgG, were used to calibrate the system. These standards covered the expected range of 70 to 104 µg HSA and of 14 to 34 µg IgG for a 10 µL sample of a 1:5 dilution of normal serum. The event sequence used was chosen to give a value for Rs $\geq$ 1.5 between the HSA and IgG peaks so that both peak heights and areas could be determined. The responses were linear up to 100 µg for IgG

and 140 µg for HSA. Correlation coefficients of 0.996 to 0.997 over 7 to 9 points were obtained for all of the calibration curves. From these curves, the limit of detection for IgG at a signal-to-noise ratio (S/N) of 3 was estimated to be 0.68 µg when either peak height or peak area measurements were used. For a 1:5 dilution of a serum sample, this is equivalent to an initial serum concentration of 0.34 g/L. The limit of detection at a S/N of 3 for HSA was 2.6 µg using peak heights and 3.5 µg using peak areas, corresponding to initial serum concentrations of 1.3 to 1.8 g/L, respectively.

A series of injections of control sera, diluted 1:5 with pH 7.0 buffer was next made. A sample chromatogram is shown in Figure 12(d). The results are shown in Tables VII and VIII for serum samples containing normal and abnormal levels of IgG and HSA. The data given are the average of 7 to 8 serum injections for IgG and 3 to 5 injections for HSA. No significant difference was noted for either IgG or HSA when comparing the peak area and peak height results. As has been noted previously, the results obtained for IgG with this method agreed well with those of commercial SRID (27) and nephelometric assays. All experimental values were within one standard deviation of the range of control values given by the manufacturer. Similar agreement was found between the experimental values for HSA and the control values from commercially

Table VII. IgG results for control serum samples

Sample	IgG concentration (g/L)		
	Peak height results	Peak area results	Reference values[a]
Normal control serum	9.5 ± 0.6	9.7 ± 0.2	8.6 ± 0.3 to 9.3 ± 0.4
Abnormal control serum	5.6 ± 0.2	5.8 ± 0.5	5.4 ± 0.3 to 5.7 ± 0.4

[a]The reference values given are the low and high assay values provided by the manufacturer.

Table VIII. HSA results for control serum samples

Sample	HSA concentration (g/L)		
	Peak height results	Peak area results	Reference values[a]
Normal control serum	43 ± 1	47 ± 1	40 ± 3 to 44 ± 4
Abnormal control serum	26 ± 2	26 ± 2	21 ± 3 to 27 ± 2

[a]The reference values given are the low and high assay values provided by the manufacturer.

available spectrophotometric and colorimetric dye-binding assays. The precision of the HSA and IgG experimental results was also comparable to that of the control methods. For instance, the HSA peak height and peak area results gave average precisions of 4.7% and 4.6% (one relative standard deviation) for the two samples tested, while the commercial methods had a range of 1.8% to 6.3%. The IgG peak height and peak area results had average precisions of 4.5% and 5.1%, compared to values of 3.7% to 11.9% obtained with the other methods.

The reproducibility of the results obtained with this system was examined using a series of 45 injections of normal control serum. The heights and areas of the HSA peaks were found to vary by $\pm$ 4.0% and $\pm$ 3.4%, respectively, while the heights and areas of the IgG peaks varied by $\pm$ 2.6% and $\pm$ 3.6%, respectively.

A similar set of injections was used to determine the lifetime of the system. No signs of column deterioration (e.g., abnormally-shaped peaks, increasing/decreasing peak heights or peak areas) were observed in over 120 injections into the anti-HSA column. These injections included 60 standard samples and 60 serum samples. This is a much longer lifetime than the typical 20 to 25 column cycles reported for similar high-performance immunoaffinity matrices under acidic

elution conditions (54). This is probably a result of the fact that only a mildly acidic elution buffer of pH 3.0 was used here instead of a pH of 2.0 to 1.0, as commonly used with such matrices (54). The protein A column showed no signs of deterioration after more than 170 injections, including 60 standards and 110 serum samples. This indicates that the immobilized protein A was very stable, as has been noted previously (27).

The protein A and anti-HSA matrices, prior to packing, were also found to be quite stable. For example, when stored in pH 7.0 buffer at 4 ^{o}C, the protein A matrix showed no change in its characteristics over a period of at least 18 months and the anti-HSA matrix over a period of at least 6 months.

The purities of the IgG and HSA peaks were examined by SDS-PAGE. Using injections of normal serum, only one band was observed in the fraction eluted from the anti-HSA column. This was identical to that given by an HSA standard. The fraction eluted from the protein A column contained two bands. These matched the bands for the H and L chains of a human IgG standard. Analysis of the gels by scanning densitometry showed no detectable amount (i.e., less than 0.5% of the total area) of IgG in the HSA peak or HSA in the IgG peak. Also, no other bands in either fraction were detected, with more than

99% of the integrated densitometer scans being due to HSA in the HSA peak and the H and L bands in the IgG peak.

SDS-PAGE of the nonretained normal serum fraction showed that no detectable amount of HSA (i.e., less than 0.5% of the total HSA collected) was present. The relative amount of IgG in the nonretained peak was determined to be 8% by SRID. This agrees with the typical IgG_3 levels in normal serum of 5 to 9% (101).

The levels of IgM and IgA in the IgG and nonretained peaks were also determined by SRID. These were of interest since IgM and IgA have the ability to bind protein A (50), making them possible interferences in the determination of IgG. From the SRID results, more than 95% of both the IgM and IgA was found to be eluted in the nonretained peak. These levels agree with those obtained previously on a similar protein A HPAC system (100). However, these levels are much greater than would be predicted based on the IgM and IgA levels of 66% and 30%, respectively, that are capable of binding to protein A (50). A possible explanation for this difference is that IgA and IgM may have exhibited a split-peak effect on the protein A matrix, similar to that seen for IgG but with slower adsorption kinetics. This slower adsorption could be the result of the larger size (98) and slower diffusional properties of IgM and IgA compared to IgG, or the

fact that IgM and IgA may have a different mechanism of binding to protein A than IgG (50).

CONCLUSIONS

Several parameters were considered in the design of the HPAC system developed in this experiment. These included the static and kinetic properties of the supports as well as the elution conditions required for each analyte. The kinetic properties were evaluated using a modified version of Equation 26, which allowed the adsorption kinetics of each support to be described by a single constant. This constant was then used to calculate the column size required by each support to produce the desired degree of retention at a given flowrate. By considering this along with the binding capacity of each support, the minimum column size required to quantitatively retain analyte on each matrix was determined. For the protein A support, column size was limited by the rate of immunoglobulin adsorption, while the column size of the anti-HSA matrix was mainly limited by the static capacity. In considering both factors, a separation was obtained in which no significant amount of HSA or IgG, other than the expected level of IgG_3, was nonretained. This was demonstrated by electrophoresis and SRID.

The data presented show that this system was effective in selectively quantitating IgG and HSA in serum, giving results for both normal and abnormal samples comparable to those obtained with commercial methods. One potential advantage of

this method over other techniques is its speed of analysis, with the determination of both IgG and HSA being possible in only 6.0 min. In comparison, the time required for an equivalent analysis by electrophoresis or immunodiffusion is on the order of hours or days. Another advantage of this method is its small sample requirement, with only 2 μL of serum being needed per injection. The selectivity of the system also makes it subject to fewer interferences than are encountered with the usual electrophoretic and spectrophotometric techniques (97). Moreover, this method can be easily automated. This can be accomplished by using a system such as described in Reference 54 with the addition of an automatic valve for column selection. All of these characteristics suggest that this method should be useful for the rapid, routine analysis or screening of serum samples.

Another advantage of this method is that the ratio of HSA/IgG in a sample can be obtained without prior calibration of the system. This can be calculated by using the absorptivities of IgG and HSA at the detection wavelength along with their peak areas. This is analogous to the determination of the albumin/globulin ratio (98). Such ratios have the advantage of being more sensitive than absolute measurements in detecting diseases where the level of one component increases and another decreases. For example, the HSA/IgG ratio should

be especially useful in the diagnosis of liver disease and chronic infections, where HSA levels are typically decreased and IgG levels increased (98).

One possible limitation of this separation scheme is that, since IgG_3 appears to be nonretained, differences in the relative IgG_3 content of the samples and standards can give rise to slight errors in the IgG determination. This can be minimized by using IgG standards prepared from pooled human serum, such as has been recommended for use with other immunoglobulin assays (111), in order to obtain standards with average IgG_3 levels. Alternatively, anti-human IgG antibodies could be used in place of protein A as the affinity ligand.

The effect of several potential interferences for this method were examined. Two of these were IgM and IgA, possible contaminants in the IgG determination due to their ability to bind to protein A. However, they did not interfere in this method since more than 95% of both components were eluted in the nonretained peak, possibly as a result of slow adsorption kinetics. Another interference studied was HSA, also a contaminant in the IgG determination due to its adsorption on protein A columns. This interference was removed by placing the anti-HSA column first in the system, a method which was shown to remove all of the HSA before it reached the protein A column. This demonstrates the potential usefulness of

affinity columns in removing undesirable sample components, a technique referred to as negative affinity chromatography (112), in analytical applications of HPAC or HPLC.

As previously discussed, this dual-column system was not only effective in removing HSA as a contaminant, but was also useful in determining sample levels of both HSA and IgG. The use of such multicolumn or multidimensional systems has several potential advantages for chromatography in general (113). This technique is particularly promising for HPAC, since one of the disadvantages of affinity chromatography is that it can normally be used to detect only one or a few similar components at a time. The multicolumn approach given here is one way in which this limitation can be overcome, allowing several different analytes to be determined with the same system.

SECTION III.

NONLINEAR ELUTION EFFECTS IN SPLIT-PEAK CHROMATOGRAPHY

INTRODUCTION

The last two sections have demonstrated how the split-peak method can be used in a number of practical applications. Examples have included the optimization of the adsorption kinetics of affinity columns and the comparison of the kinetic properties of affinity matrices. In both studies, Equation 26 was used as the basis for examining the kinetics of adsorption. As mentioned previously, the derivation of this equation is based on a number of assumptions, one of which is that the split-peak measurements are made under linear elution conditions. In other words, it is assumed that the relative size of the nonretained and retained peaks are independent of sample size. However, it was found in Section I that this is not the case for the IgG-protein A system. To better understand the reasons for this, the goal of this study was to examine the effect of nonlinear elution conditions on the relative size of the nonretained peak and to determine ways in which this effect might be controlled.

In general, the effect of nonlinear elution conditions, or column overloading, has long been of interest in chromatography. This has been true in both analytical and preparative-scale work, since such conditions may not only result in changes in column capacity, but can also affect solute retention (114-117), band-broadening (114-116), and

resolution (118). A number of studies have been performed to better understand these effects and to develop methods by which they can be quantitated. Due to the complexity of the systems and calculations involved, computer simulations are often used in such studies (114,115,119,120).

Nonlinear effects in split-peak chromatography are typically seen as an increase in the relative size of the non-retained fraction with sample load. This has been observed with several affinity systems. These include not only the adsorption of IgG on protein A columns, but also the binding of IgG (34), insulin (34,39), and interferon (37) on immuno-affinity columns. However, this dependence has not been observed for IgG retention on reversed-phase columns, as shown in Section I.

It has already been mentioned that in some applications, such as the comparision of the split-peak slopes of affinity matrices or the optimization of column adsorption conditions, it may be possible to deal with these effects by standard-ization of the column size and load conditions. This was the approach used for these applications in the previous two studies. However, in more fundamental work, such as the determination of adsorption rate constants, this approach is no longer sufficient if accurate results are to be obtained. Instead, techniques and guidelines are needed to minimize

or eliminate nonlinear effects so that results independent of sample size can be obtained.

In this experiment, the effect of nonlinear elution conditions on split-peak measurements was studied using computer simulations. The two chromatographic cases examined were those in which the overall adsorption kinetics were either diffusion- or adsorption-limited. These are the two most useful cases for the determination of rate constants. Using simulations, guidelines were developed for minimizing nonlinear effects in both cases. The simulation results were then compared to data obtained for two experimental systems: the retention of IgG on protein A columns and the adsorption of hemoglobin on reversed-phase columns.

THEORY

Computer Model

The computer model used was the same as presented earlier (65). In this model, the column is divided into a large number of slices, each of which is further divided into three distinct regions: the flowing mobile phase, the stagnant mobile phase, and the stationary phase. All material injected on the column begins in the flowing mobile phase of the first slice. The simulation is performed by repeatedly carrying out two alternating operations. In the first, the material in each slice is distributed between the three phases according to the given set of kinetic equations and rate constants describing the system of interest. This is done for one unit of time, or one iteration. Once this has been done throughout the column, the material in the flowing mobile phase of each slice is shifted down the column one unit in order to simulate flow or convective mass transfer. At the same time, the amount of material leaving the last slice of the column is monitored, corresponding to detection of the chromatographic peak. This process is repeated until all but a given fraction of solute has eluted from the column, in this case all but 1 ppm of the remaining free analyte.

Two effects not directly considered by this model are extracolumn band-broadening prior to the column and band-broadening within the excluded volume of the column. One cause of the first is the use of large sample loops. This is an important consideration in split-peak chromatography, since in both this work and related studies (121) injection volumes approaching or exceeding the excluded volume of the column have been used. Although this is not a problem under linear elution conditions, as was shown in Section I, it can potentially affect split-peak measurements made under non-linear conditions. This effect can be studied in simulations by changing the number of iterations over which a given sample is applied.

Band-broadening within the excluded volume of the column can occur by such processes as eddy diffusion or longitudinal diffusion. Although such an effect is not easily studied with this model, its role is probably not large compared to extracolumn band-broadening or other effects, especially when considering the relatively short column residence time of the nonretained peak and the small columns that have thus far been used in split-peak measurements.

In order to compare the simulation results under non-linear elution conditions to those predicted under linear conditions, Equation 23 was used.

$$\frac{-1}{\ln f} = \frac{u_e}{h}\left(\frac{1}{k_1} + \frac{k_{-1}}{k_1 k_3 [L]}\right) \qquad (23)$$

As given earlier, u_e is the linear velocity of an excluded, nonretained solute, h is the column length, and [L] is the initial concentration of ligand in the column, m_L/V_p. Like Equation 26, the above expression predicts a linear relationship between -1/ln f and a term related to the column residence time of the analyte, u_e/h. Also as in Equation 26, the slope is comprised of two terms: the first, $1/k_1$, being related to the kinetics of mass transfer or diffusion, and the second, $(k_{-1}/k_1 k_3 [L])$, being a function of the system's adsorption kinetics. Using Equation 23, it is possible to calculate the theoretical value of -1/ln f under linear elution conditions given u_e/h, [L], and the rate constants of the system. This equation is particularly useful in simulations of the type done here since the total residence time of analyte in the column can be varied by changing the column length h (i.e., the number of slices in the column) while keeping u_e and the reaction time in each slice constant (i.e., an excluded linear velocity of one slice/iteration and a reaction time of one iteration).

Equations for Diffusion-Limited Kinetics

Two cases were considered in looking at nonlinear elution effects: mass transfer- or diffusion-limited kinetics, and adsorption-limited kinetics. The first case studied was that of simple diffusion-limited kinetics with irreversible adsorption. In this case, adsorption is assumed to be much faster than mass transfer, or $k_3 \gg k_{-1}$, such that any solute entering the stagnant mobile phase binds to free ligand rather than diffusing back to the flowing mobile phase. The effect on Equation 23 as adsorption becomes infinitely fast (i.e., k_3 approaches infinity) is that the second slope term, $(k_{-1}/k_1 k_3 [L])$, becomes much smaller than the first. This reduces Equation 23 to

$$\frac{-1}{\ln f} = \frac{u_e}{h} \left(\frac{1}{k_1}\right) \tag{37}$$

which is an expression equivalent to that given in Equation 27. Equation 37 predicts that for the diffusion-limited case under linear elution conditions, a plot of $-1/\ln f$ vs. $u_e/h\ k_1$ should yield a line with a slope of one and an intercept of zero.

The results for this case under nonlinear conditions can be obtained by representing the system by the following reactions:

$$E_e \underset{k_{-1}}{\overset{k_1}{\rightleftharpoons}} E_p \qquad (38)$$

$$E_p + L \xrightarrow{\text{Fast}} E_p\text{-}L \qquad (39)$$

As given previously, E_e and E_p represent the free analyte in the flowing and stagnant mobile phases, respectively, and L represents the free ligand remaining in the column. Unlike the system used previously, however, this system no longer considers [L] or m_L to be constant. In other words, linear elution conditions are no longer assumed to be present.

Note in these reactions for the diffusion-limited case that two situations may occur. The first takes place when free L is present in the stagnant mobile phase. In this situation, any E diffusing into the stagnant mobile phase immediately binds to ligand, preventing E from diffusing back to the flowing mobile phase. The net reaction of Equations 38 and 39 under these conditions can be written as

$$E_e \xrightarrow{k_1} E_p\text{-}L \qquad (40)$$

This can be described by the integrated rate expression for a simple first-order reaction (122)

$$m_{E_{es}} = m_{E_{eso}} e^{-k_1 t} \qquad (41)$$

where t is the time of reaction, and $m_{E_{es}}$ and $m_{E_{eso}}$ are the moles of E_e present at times t and 0. The subscript "s" is used here to refer to the fact that these parameters are those for the particular slice studied during a given iteration.

The second situation which can occur takes place when all free L in the slice has been depleted, so that E is no longer able to adsorb onto the stationary phase in that region. The result is that E can only undergo diffusion into and out of the pores of the support, making the net reaction

$$E_e \underset{k_{-1}}{\overset{k_1}{\rightleftharpoons}} E_p \qquad (42)$$

This reaction can be described by the integrated rate expression for a reversible first-order reaction (122)

$$m_{E_{es}} = m_{E_{es\infty}} + (m_{E_{eso}} - m_{E_{es\infty}})\, e^{-(k_1 + k_{-1})\, t} \qquad (43)$$

where $m_{E_{es\infty}}$ is the moles of E present at equilibrium in the flowing mobile phase of the slice of interest.

The point at which the system switches from the situation given in Equation 40 to that in Equation 42 occurs when enough solute has entered the stagnant mobile phase to totally bind any free ligand present. The reaction conditions required for this can be determined by using Equation 41 and the mass balance expressions for the system, giving the equation

$$m_{L_{so}} = m_{E_{eso}} (1 - e^{-k_1 t}) \quad (44)$$

which gives the time and mole conditions at which all free L is depleted. If the reaction conditions are such that $m_{L_{so}}$ is greater than or equal to the right-hand side of Equation 44, then the system can be described by Equation 41. If $m_{L_{so}}$ is less than this expression, Equation 41 is used until all ligand in the slice has been depleted and then Equation 43 is used to describe the system.

Equations for Adsorption-Limited Kinetics

The second case studied was that of simple, irreversible adsorption-limited kinetics. In this case, diffusion is assumed to be much faster than adsorption (i.e., k_1 and $k_{-1} >> k_3$) giving rise to an equilibrium in mass transfer of solute between the stagnant and flowing mobile phases. The effect on Equation 23 is that its diffusional slope term, $1/k_1$, becomes small vs. that for adsorption, reducing Equation 23 to

$$\frac{-1}{\ln f} = \frac{u_e}{h} \left(\frac{k_{-1}}{k_1 k_3 [L]}\right) \quad (45)$$

The expected result, then, for the adsorption-limited case under linear elution conditions is that a plot of -1/ln f vs.

$(u_e/h)(k_{-1}/k_1\ k_3\ [L])$ will give a line with a slope of one and an intercept of zero.

To calculate the results for this case under nonlinear conditions, the system is represented by the reactions

$$E_e \underset{}{\overset{K_1}{\rightleftharpoons}} E_p \tag{46}$$

$$E_p + L \xrightarrow{k_3} E_p\text{-}L \tag{47}$$

Integrated rate expressions describing this system can be derived using an approach similar to that given for a one phase, second-order reaction in Reference 122. This is done by first writing the rate law expression for the reaction in Equation 47.

$$\frac{-d\ [L]_s}{dt} = k_3\ [E_p]_s\ [L]_s \tag{48}$$

In this equation, $[E_p]_s$ and $[L]_s$ are the concentrations of E_p and L in the stagnant mobile phase of the slice studied and all other terms are as defined previously. Converting Equation 48 to an expression in terms of moles gives

$$\frac{-d\ m_{L_s}}{dt} = \frac{k3}{V_{ps}}\ m_{E_{ps}}\ m_{L_s} \tag{49}$$

where V_{ps} is the pore volume per slice, V_p/h. The mass balance expression for this system can next be obtained by using the reaction stoichiometry given in Equation 46 and 47.

$$(m_{E_{eso}} - m_{E_{es}}) + (m_{E_{pso}} - m_{E_{ps}}) = (m_{L_{so}} - m_{L_s}) \qquad (50)$$

Since it is given that diffusion for this system is much faster than adsorption, or that mass transfer is in equilibrium, the ratio V_{ps}/V_{es} may be substituted for $m_{E_{ps}}/m_{E_{es}}$ according to Equation 3. By using this in Equation 50 along with the fact that $V_{ps} + V_{es}$ is V_{ms}, the total slice void volume, the mass balance expression in terms of $m_{E_{ps}}$ can be written as

$$m_{E_{ps}} = (m_{E_{eso}} + m_{E_{pso}} - m_{L_{so}} + m_{L_s})\ (V_{ps}/V_{ms}) \qquad (51)$$

This equation may be simplified by replacing $(m_{E_{eso}} + m_{E_{pso}} - m_{L_{so}})$ with a single constant, x. Substituting this into Equation 51 and combining Equations 51 and 49 results in the following differential equation:

$$\frac{-d\ m_{L_s}}{m_{L_s}\ (x + m_{L_s})} = (k_3/V_{ms})\ dt \qquad (52)$$

Depending on the value of x, two different solutions to Equation 52 may be obtained. For $x \neq 0$, integration of Equation 52 between times 0 and t yields

$$\ln\left(\frac{m_{L_s}}{m_{E_{ps}}}\right) = \ln\left(\frac{m_{L_{so}}}{m_{E_{pso}}}\right) + \left(m_{L_{so}} - m_{E_{eso}} - m_{E_{pso}}\right)\left(k_3 / V_{ms}\right) t \quad (53)$$

For the case where x = 0, Equation 52 reduces to the following form:

$$\frac{-d\, m_{L_s}}{(m_{L_s})^2} = \left(k_3 / V_{ms}\right) dt \quad (54)$$

Integration of this expression between times 0 and t yields

$$\frac{1}{m_{L_s}} = \frac{1}{m_{L_{so}}} + \left(\frac{k_3}{V_{ms}}\right) t \quad (55)$$

Thus, if the initial conditions in a slice during a given iteration are such that $(m_{E_{eso}} + m_{E_{pso}} - m_{L_{so}})$ is zero, Equation 55 is used to describe the system. If $(m_{E_{eso}} + m_{E_{pso}} - m_{L_{so}})$ is not zero, then Equation 53 is used.

EXPERIMENTAL

Reagents

The protein A, rabbit IgG, and bovine hemoglobin were from Sigma (St. Louis, MO) and were the purest grades available. The morpholine and CDI were from Aldrich (Milwaukee, WI). The n-octyldimethylchlorosilane was from Petrarch (Bristol, PA). The LiChrospher SI 500 (10 μm particle diameter, 500 Å pore size) was obtained from Alltech (Deerfield, IL).

Instrumentation

The chromatographic and data acquisition systems were the same as described in Section I. The detector used for the IgG studies was a Hitachi 100-10 (Tokyo, Japan) operated at 280 nm. For the hemoglobin studies, the detector was a Kratos 757 (Ramsey, NJ) operated at 414 nm. Computer simulations were performed on a National Advanced Systems 9160 computer (Mountain View, CA).

Procedures

Computer simulations

All simulations were performed in Fortran G using double-precision logic. Listings of the programs used are given in

the Appendix. The simulations were initiated by placing the desired amount of material in the flowing mobile phase portion of the first slice and were ended when all but 1 ppm of the remaining nonadsorbed material had eluted off the column.

Programs were tested for convergence by performing a series of equivalent simulations in which columns were divided into increasingly larger numbers of slices while the rate constants for the system were proportionately decreased. All values reported are within 20 ppm of the estimated value for a column divided into an infinite number of slices, as determined in this manner.

Preparation of protein A and reversed-phase supports

The LiChrospher reversed-phase support was prepared according to published procedures (83,86) using 5.0 g n-octyldimethylchlorosilane/g silica and 50 g of carbon tetrachloride/g silica.

The diol-bonded LiChrospher was also prepared as described previously (80). The diol coverage of the LiChrospher prior to activation was 200 μmol/g silica as determined by the periodate oxidation method (84,85).

Protein A was immobilized onto the diol-bonded LiChrospher using the CDI method (81) described in Section I. Immobilization was performed at pH 4.0 using 10 mg protein A/g

silica. As determined in Section I, the immobilization yield of protein A under these conditions is approximately 100%.

Chromatography

The weak mobile phase for the reversed-phase matrix was 0.02 M ammonium phosphate, 0.01% morpholine (v/v), (pH 7.0). All hemoglobin solutions were prepared in this buffer. The strong mobile phase was 2-propanol containing 0.01% morpholine. Protein retained on the reversed-phase support was eluted by using a linear 20 min gradient from 0 to 100% 2-propanol at a flowrate of 0.25 mL/min.

The application buffer for the protein A matrix was 0.10 M potassium phosphate buffer (pH 7.0) and the elution buffer was 0.10 M potassium phosphate (pH 3.0). All IgG solutions were prepared in the pH 7.0 phosphate buffer. Elution of IgG adsorbed on the protein A was done by a step change in pH.

Both the reversed-phase and protein A matrices were placed into their respective weak mobile phases and vacuum-slurry packed (83) into columns of a previously-published design (79).

Kinetic studies on these columns were performed at 25 ^{o}C. All other chromatography was performed at room temperature.

Prior to the kinetic studies, both the protein A and reversed-phase columns were pretreated several times with either excess IgG or hemoglobin to remove any residual active

groups or irreversible adsorption sites. To test for the removal of such sites, the static capacity of each matrix was measured by integration of the resulting breakthrough curves (87) and correcting for the void volume of the system. The capacities were found to be 8.6 ± 0.4 mg IgG/g silica for the protein A matrix and 47.1 ± 0.4 mg hemoglobin/g silica for the reversed-phase matrix. The static capacities of the matrices were estimated to decrease by less than 5% over the course of the kinetic studies.

The split-peak behavior of the matrices was studied using the method described in Section I. For the protein A, split-peaks were obtained by injecting 10 μL of 0.14 to 0.55 mg/mL IgG on a 6.35 mm x 4.1 mm I.D. column at flowrates of 0.02 to 0.5 mL/min. The areas of both the nonretained and retained peaks were determined by computer integration, normalized vs. flowrate, and corrected for any sample impurities (0.8% of the total IgG area) or background shifts present. The total corrected IgG area was found to be a linear function of sample size over the entire concentration range studied. These corrected areas were used to calculate the free fraction f as described in Section I.

For the reversed-phase columns, split-peaks were observed by injecting 3 μL of 0.5 to 2.0 mg/mL hemoglobin on a 6.35 mm x 1.0 mm I.D. column at flowrates of 0.06 to 0.63 mL/min. The

nonretained peak area was found as described above, normalized vs. flowrate, and corrected for the solvent background. No corrections for sample impurities, which were less than 0.2% of the total area, were made. The corrected area was found by injecting sample through an open tube and correcting for the solvent background. This total corrected area was found to vary linearly with sample size over the entire sample range studied. The free fraction was calculated by dividing the nonretained area by this total corrected area.

RESULTS AND DISCUSSION

Simulations for Diffusion-Limited Kinetics

In the first simulation study, the effect of nonlinear elution conditions in split-peak chromatography was examined for systems with diffusion-limited kinetics and irreversible adsorption. This was done by monitoring the relative size of the nonretained peak as a function of solute residence time and column load. In this and in all following studies, the column load was defined as $m_{E_{total}}/m_L$, or the ratio of the total moles of solute applied to the column to the moles of free ligand initially present. Also, reduced velocity parameters, such as $u_e/h\ k_1$ and $(u_e/h)(k_{-1}/k_1\ k_3\ [L])$, were used in all simulation studies to give results independent of the absolute values of the system rate constants.

The normalized split-peak plots for this case are given in Figure 13 for loads of 16 to 128% of the column capacity. Each plot in Figure 13 is the best-fit curve through 27 data points distributed over the entire $u_e/h\ k_1$ range shown. By plotting the data for this case as a function of the reduced velocity parameter $u_e/h\ k_1$, the results were found to not only be independent of the absolute value of k_1, but were also independent of the porosity term V_p/V_e (i.e., k_1/k_{-1}) over the range in V_p/V_e of 0.1 to 2.0. These V_p/V_e values include

Figure 13. Normalized split-peak plots at various column loads for the case of diffusion-limited kinetics with irreversible adsorption. The plots given are for column loads of 16 to 128%, in intervals of 16%. The line shown is the response predicted under linear elution conditions by Equation 37

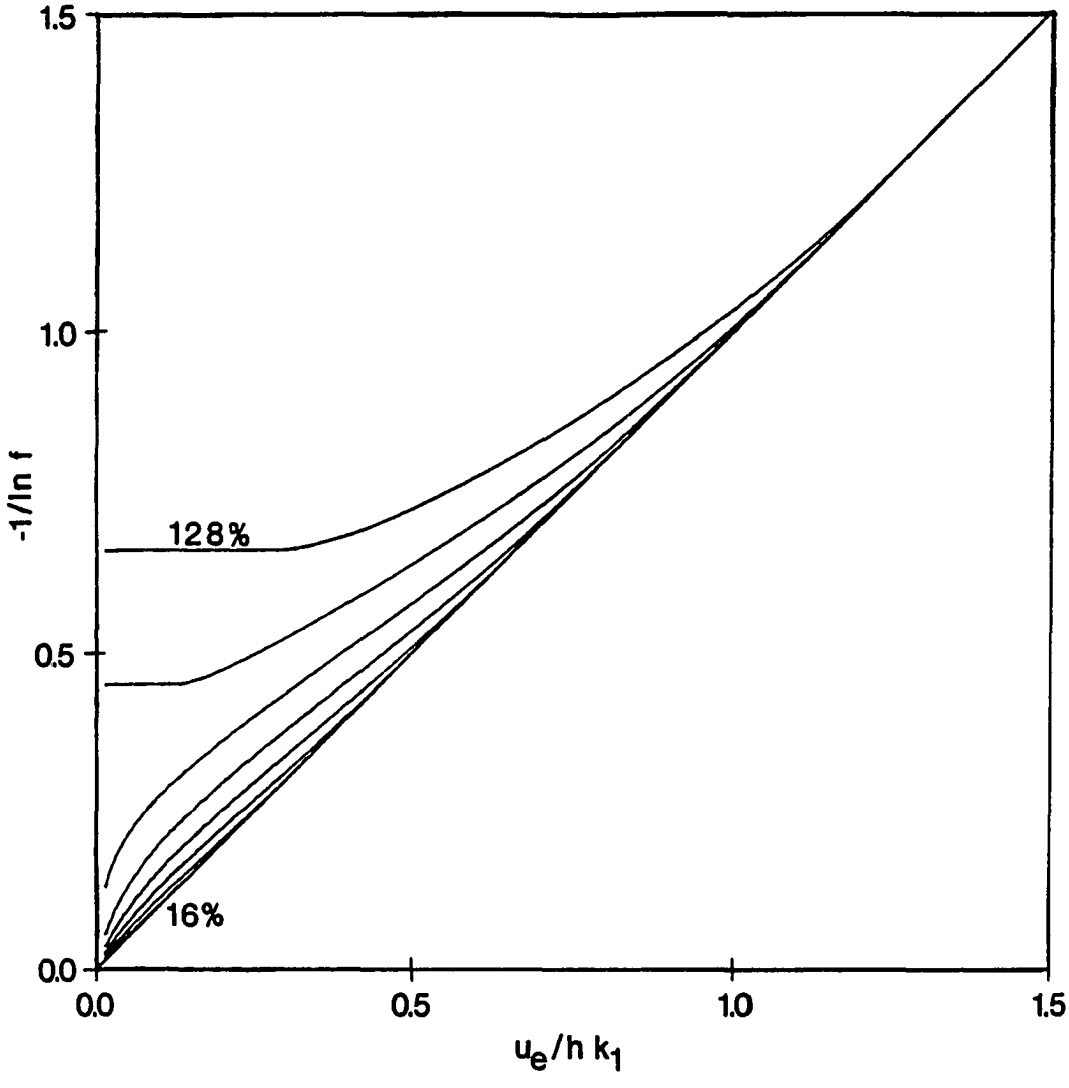
1.5
1.0
0.5
0.0
-1/ln f
128%
16%
0.0
0.5
1.0
1.5
$u_e/h\ k_1$

those found with common chromatographic matrices (123,124). In testing for extracolumn effects, it was found that the data in Figure 13 were also independent of the injection volume over the load range of 1.6 to 128% and $u_e/h\ k_1$ values of at least 0.06 to 1.28, since no change in -1/ln f was noted under these conditions in going from an application volume of one slice to twice the excluded volume of the column.

Under linear elution conditions, the plots in Figure 13 would be expected to give the linear relationship predicted by Equation 37. Under the nonlinear conditions used to generate the data, however, deviations from the ideal response were found to occur at all loads studied. In general, the simulation values of -1/ln f were larger than or equal to those predicted, with the extent of the deviations increasing with column load. These deviations typically occurred when the value of $u_e/h\ k_1$ was small, or the residence time large, but disappeared as $u_e/h\ k_1$ increased. Also, the range of $u_e/h\ k_1$ values over which deviations occurred increased in proportion to the column load applied. For instance, a load of 64% gave deviations up to a $u_e/h\ k_1$ value of approximately 0.64 while a load of 128% gave deviations up to a value of about 1.28.

It was further observed in Figure 13 that plots for loads of less than 100% appeared to have a zero intercept, while

those for loads of greater than 100% had an intercept greater than zero. This is due to the fact that as $u_e/h\ k_1$ approaches zero, or the solute residence time becomes infinitely long, the amount of sample adsorbed reaches its maximum value. When the sample applied is less than or equal to the column capacity, all would be expected to adsorb, causing -1/ln f to approach zero. If the load is larger than the column capacity, then the amount adsorbed approaches this capacity, leaving some free solute behind and giving -1/ln f a value greater than zero.

As stated in Section I, an experimental system believed to exhibit diffusion-limited kinetics is the adsorption of some proteins on reversed-phase columns. One protein thought to show such behavior is hemoglobin (121). To compare this system to the simulation results presented, split-peak plots were made for injections of hemoglobin on a C8 reversed-phase column at known loads. The results are given in Figure 14 for loads of 1.7 and 6.8%.

In order to compare the experimental results in Figure 14 to the simulation data in Figure 13, it was necessary to determine what range of reduced velocities was represented by the data in Figure 14. This was done by making use of the linear region of the 0.50 mg/mL data, which occurred at flowrates of approximately 0.25 mL/min or greater. Since

Figure 14. Split-peak plots for hemoglobin on a reversed-phase column. The plots shown are for 3 µL injections of 0.50 mg/mL (●) and 2.00 mg/mL (■) bovine hemoglobin. The chromatographic conditions were the same as described in the text. The line shown is the linear fit for the 0.50 mg/mL data over a flowrate range of 0.25 to 0.63 mL/min

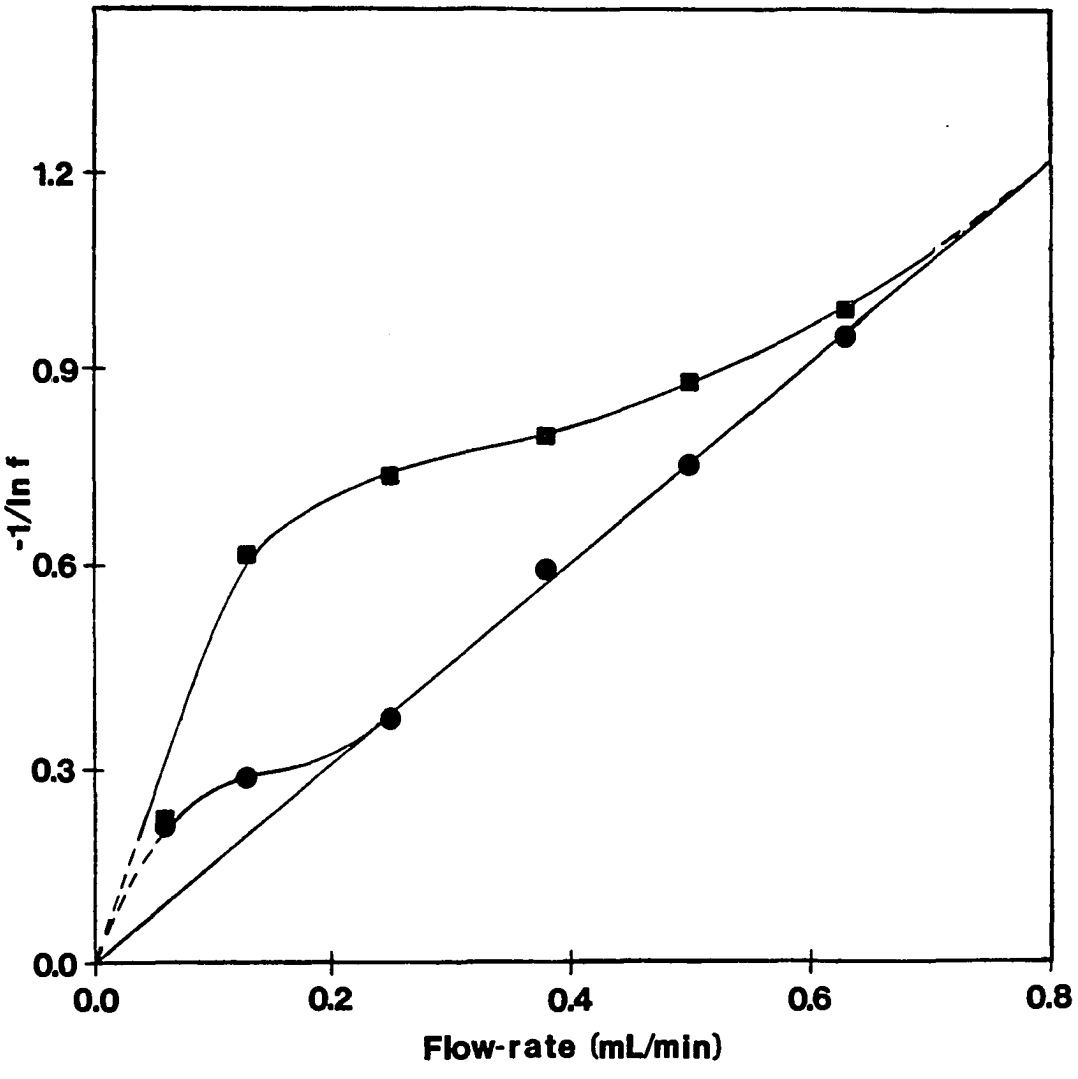
1.2
0.9
0.6
0.3
0.0
-1/ln f
0.0
0.2
0.4
0.6
0.8
Flow-rate (mL/min)

this region followed the relationship between residence time and -1/ln f predicted by Equation 37, it was used to represent the theoretical response of the system under linear elution conditions. A linear least-squares fit to the data in this range gave a slope of 1.48 $\pm$ 0.06 min/mL and an intercept of 0.01 $\pm$ 0.03. By multiplying each flowrate in Figure 14 by this slope, it was determined that the experimental data shown represented a $u_e/h\ k_1$ range of 0.09 to 0.93.

Several similarities can be seen in Figures 13 and 14. For example, the data in Figure 14 show the same deviation patterns seen in Figure 13 in that the obtained values of -1/ln f are larger than predicted at long residence times, or slow flowrates, but approach the expected response for linear elution conditions as flowrate increases. Also, in both figures the size of the deviations and the flowrate range over which they occur increase with the load. Furthermore, this flowrate range again appears to increase roughly in proportion to the load, with the 0.50 mg/mL data showing nonideal effects up to a flowrate slightly over 0.2 mL/min and the 2.0 mg/mL data showing deviations up to a flowrate of approximately 0.8 mL/min.

Figures 13 and 14 differ in that the deviations in -1/ln f seen experimentally were larger than those predicted from the simulations. This can be due to a number of

secondary effects not taken into account by the kinetic model used. Such effects may include site heterogeneity, as discussed in Section I, and reversible binding (125). Site heterogeneity can be important for the diffusion-limited case if ligands with different mass transfer properties are present, such as those located at different depths within the matrix or on particles of different diameters. Under linear elution conditions, this results in k_1 becoming an apparent rate constant, or a function of the individual mass transfer rates present. This also occurs under nonlinear conditions but with the additional possibility that some types of sites may saturate before others. The result is a change in k_1 and $-1/\ln f$ with sample load, giving greater deviations than would be expected for a simple homogeneous matrix. This can be illustrated by using the results given in Section I. In this previous chapter, it was found that the apparent k_1 measured for IgG on reversed-phase supports of the same diameter decreased by 17-fold in going from a matrix resembling the simple homogeneous case, such as C8 Nucleosil SI 50 on which IgG could only access ligands near the surface of the particles, to a more heterogeneous support, such as C8 LiChrospher SI 500 on which IgG could also sample ligands within the pores. This type of behavior makes site hetero-

geneity a likely explanation for the differences noted between Figures 13 and 14.

Reversible binding may be an important factor in split-peak measurements if weakly-retained solute elutes near the nonretained peak, increasing the apparent free fraction and value of -1/ln f measured. In previous simulation studies, it was shown for linear elution conditions that this is a significant problem only for systems with k' values of 10 or less (125). Although deviations due to reversible binding may increase under nonlinear conditions, the fact that hemoglobin was estimated to have a k' over 1500 in this experiment suggests that this was not a major effect.

Regardless of which secondary effects were present, the data in Figures 13 and 14 clearly show that nonlinear effects in split-peak chromatography under diffusion-limited conditions can be minimized or even eliminated by choosing the proper load and/or flowrate. This helps explain why such effects were not seen earlier in work examining retention of IgG on reversed-phase columns, as presented in Section I. In this previous study, it was found that IgG adsorption on C8 Nucleosil SI 50, which should have behaved similarly to the homogeneous case in Figure 13, gave no nonlinear effects over loads of 7.3 to 14.5% and a $u_e/h\ k_1$ range of 0.13 to 0.36. A comparison of these values with those in Figure 13 shows that

no observable deviations would have been expected under these conditions. A similar study on C8 LiChrospher SI 500, performed under the same chromatographic conditions used for the heterogeneous case in Figure 14, gave no nonlinear effects for loads of 2.4 to 4.0% and a $u_e/h\ k_1$ range of 0.24 to 0.94. Assuming IgG and hemoglobin behaved similarly on this matrix, a comparision of these values with those in Figure 14 indicates that no significant deviations would have been expected for the data at 2.4% load or over the majority of this range for the 4.0% load data. The results in Figure 14 do predict some observable deviations at the lower $u_e/h\ k_1$ values for the 4.0% load, but the fact that these were not observed may be a result of differences in the response of IgG and hemoglobin to secondary effects. For example, IgG may have been less susceptible than hemoglobin to site heterogeneity due to its larger size, a Stoke's diameter of 104 Å for IgG vs. 62 Å for hemoglobin (45,126), preventing it from sampling as many diffusionally-distinct ligands within the pores.

The disappearance of deviations for the diffusion-limited case at small residence times or column loads was examined further by performing a second series of simulations in which the effect of increasing loads on -1/ln f was measured at constant values of $u_e/h\ k_1$. This corresponds to an experiment

in which -1/ln f is determined at a constant flowrate while the sample load is varied. Figure 15 shows the results obtained at several $u_e/h\ k_1$ values. In Figure 15, the load is normalized vs. $u_e/h\ k_1$ to illustrate its relationship to this parameter as deviations begin to occur. The y-axis is also normalized vs. $u_e/h\ k_1$, but this is done only for ease of presentation.

For each value of $u_e/h\ k_1$ monitored, the resulting plot showed no deviations from the expected response under linear conditions at small values of Load/($u_e/h\ k_1$) (i.e., small sample loads). But when this term exceeded 1.0, deviations in -1/ln f began to occur. It was also noted that the relative size of these deviations increased with the value of $u_e/h\ k_1$ monitored.

Based on the simulation and kinetic models used, an equation was derived to explain why the deviations in Figure 15 began to occur at such a well-defined point. To do this, it was assumed that all deviations began in the first slice of the column during the first iteration, when the amount of free analyte was largest vs. that of free ligand. Under these conditions, the initial amount of free ligand present in the slice, $m_{L_{so}}$, is equal to $N_s\ m_L/h$, where m_L/h is the original amount of ligand per slice and N_s is the number of slices examined. Since only the first slice is considered in this

Figure 15. The effect of increasing load on -1/ln f at a constant value of $u_e/h\ k_1$. The plots shown are for $u_e/h\ k_1$ values of 0.16 (●), 0.32 (◆), 0.64 (▲), and 1.28 (■). The horizontal line is the response predicted under linear elution conditions by Equation 37

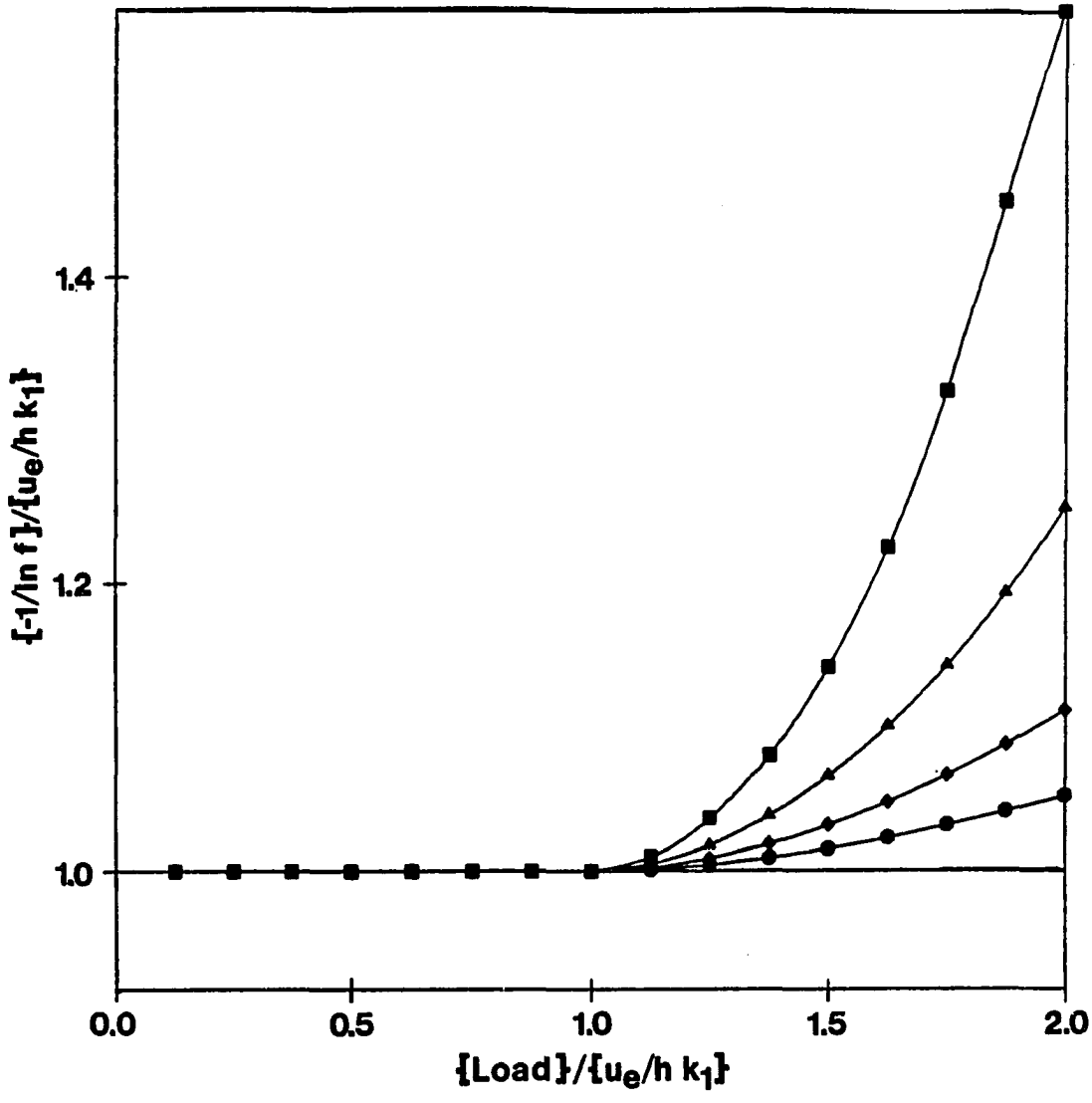
1.4
1.2
1.0
{-1/ln f}/{ue/h k1}
0.0
0.5
1.0
1.5
2.0
{Load}/{ue/h k1}

case, N_s is equal to one slice. Also under these conditions, the initial amount of free analyte in the slice, $m_{E_{eso}}$, is equal to the total amount of analyte applied, or (Load)(m_L), using the definition of load given earlier. Furthermore, it is possible from the simulation model to replace the slice reaction time t by the quantity N_s/u_e. Using these expressions along with Equation 44 gives the following relationship:

$$\text{Load} \leq [h\ (1 - e^{-k_1\ N_s/u_e})/N_s]^{-1} \qquad (56)$$

This equation gives the range of loads that can be used at a given value of $u_e/h\ k_1$ before deviations begin to occur in a system composed of a finite number of slices.

The equivalent expression for a real system, or one approaching an infinite number of slices, can be obtained by finding the limit of Equation 56 at a constant value of $u_e/h\ k_1$ by simultaneously increasing the number of slices in the column and decreasing the amount of time per slice or increasing u_e to keep the total residence time constant. As this is done, the exponential term of Equation 56, $e^{-k_1\ N_s/u_e}$, approaches zero and may be replaced by $(1 - k_1\ N_s/u_e)$, the first- and zeroth-order terms of its Taylor series expansion (127). Substitution of this into Equation 56 gives

$$\text{Load}/(u_e/h\ k_1) \leq 1 \qquad (57)$$

which is the same relationship noted empirically in Figure 15. This expression shows that either a small load or large value of $u_e/h\ k_1$ minimizes deviations because both cause the ratio in Equation 57 to decrease. Equation 57 also explains why the range over which deviations appear is directly proportional to the load applied. This occurs since as larger loads are used, a proportionately larger value of $u_e/h\ k_1$ is needed to bring the ratio in Equation 57 back to a value of 1.0 or less.

By combining Equation 57 with Equation 37, an alternate relationship is obtained for predicting when deviations occur even when the kinetic parameters of the system or the value of $u_e/h\ k_1$ is not known.

$$\text{Load}/(-1/\ln f) \leq 1 \qquad (58)$$

Thus, by measuring $-1/\ln f$ for a known sample load at the flowrate of interest and computing the above ratio, an estimate of whether or not nonlinear effects are occurring can be made for diffusion-limited systems following the model used here. If the ratio is greater than 1.0, deviations would be expected to occur. As the ratio becomes less than or equal to 1.0, the chance of deviations occurring would be expected to greatly decrease.

The hemoglobin data suggests that this ratio might also be useful in the study of more complex diffusion-limited

systems. This is indicated in Figure 14 by the fact that the flowrate at which deviations begin to occur appears to increase proportionately with the load. Based on the relationship between flowrate and -1/ln f given in Equation 27, this is equivalent to saying that deviations start to appear at a constant value of Load/(-1/ln f), in this case a ratio of 0.05. Though this value is much less than that predicted by Equation 58, probably as a result of the presence of secondary effects in the hemoglobin studies, the fact that it appears to be constant still makes it useful in minimizing nonlinear effects. For example, if the exact ratio at which deviations start to occur is known, as it is here, then the flowrate conditions required to eliminate nonlinear effects at any size load can be determined. Even if this particular value is not known, the ratio Load/(-1/ln f) is useful in indicating whether nonlinear effects may be present, since nonlinear effects are less likely to occur as Load/(-1/ln f) decreases. In general, it is known from Equation 58 that conditions giving a ratio of less than or equal to 1.0 should always be used to avoid nonlinear effects, while the hemoglobin results further indicate that for complex diffusion-limited systems, such as those using porous supports, conditions giving a ratio even as low as 0.05 or less may be desirable.

Simulations for Adsorption-Limited Kinetics

The second set of simulation studies examined nonlinear effects in split-peak chromatography for systems with irreversible adsorption-limited kinetics. The first series of simulations performed looked at the change in -1/ln f with increasing loads as a function of a reduced velocity parameter, $(u_e/h)(k_{-1}/k_1\ k_3\ [L])$.

The normalized split-peak plots obtained are shown in Figure 16 over the same range of reduced residence times and column loads as used in Figure 13. Each plot given is the best-fit curve through 13 to 16 data points distributed throughout the entire range shown. These plots were again found to be independent of V_p/V_e over the range of 0.1 to 2.0. It was also found based on the simulation model that varying the injection volume or extracolumn dispersion did affect the results slightly, with -1/ln f decreasing as the application volume increased. This was seen for each load studied, a range of 1.6 to 128%, over injection volumes ranging from one slice to twice the column excluded volume and a $(u_e/h)(k_{-1}/k_1\ k_3\ [L])$ range of 0.06 to 1.28. However, this effect was not a major problem in this study since this decrease was negligible vs. the overall deviations seen in Figure 16, with the largest observed decrease being only 0.3 ppt of the total deviation measured and with the extent of the decrease

Figure 16. Normalized split-peak plots at various column loads for the case of irreversible adsorption-limited kinetics. The plots given are for column loads of 16 to 128%, in intervals of 16%. The line shown is the response predicted under linear elution conditions by Equation 45

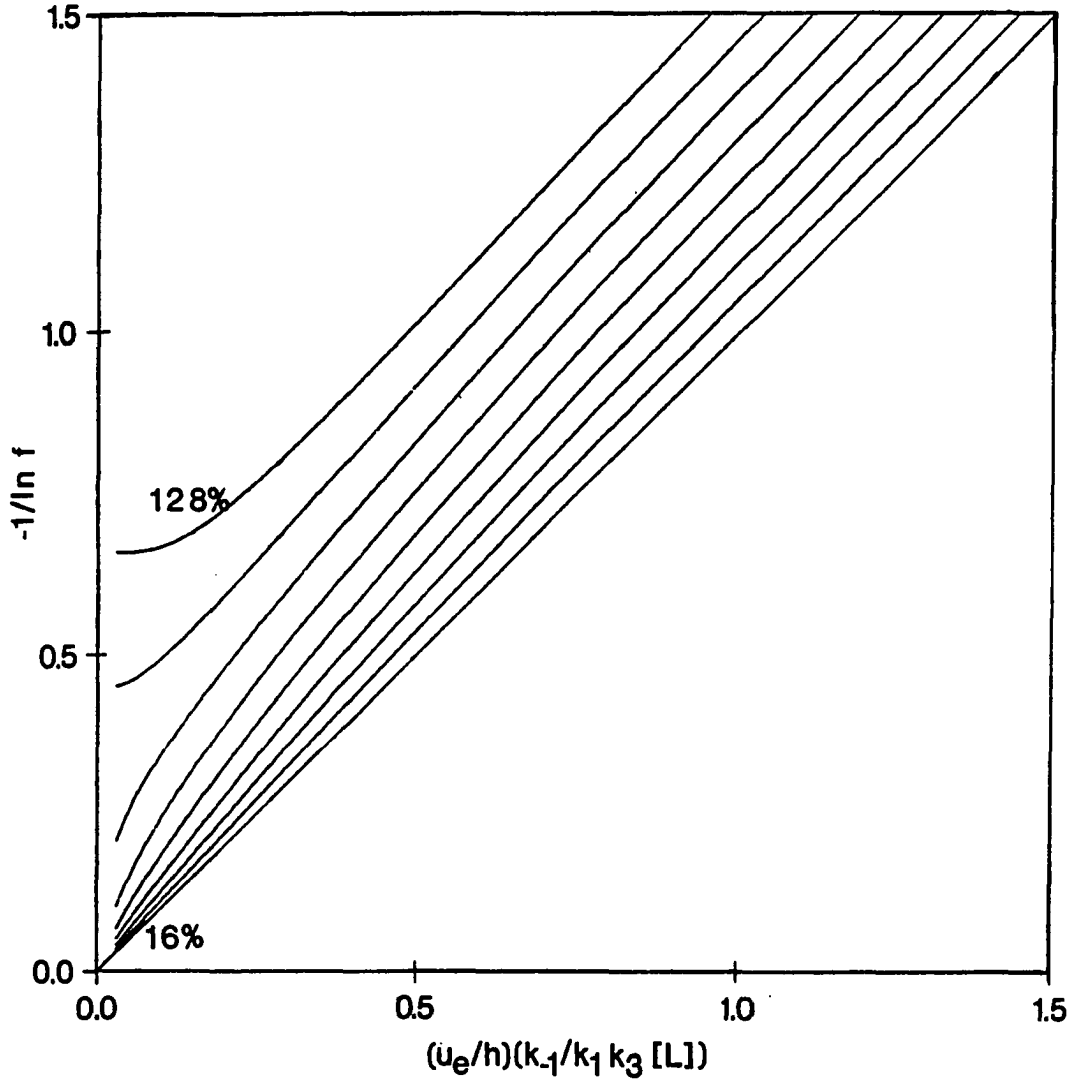
1.5
1.0
0.5
0.0
-1/ln f
128%
16%
0.0
0.5
1.0
1.5
(ue/h)(k-1/k1 k3 [L])

becoming smaller as the simulated columns were divided into an increasing number of slices.

In comparing the data in Figure 16 to the results predicted by Equation 45 under linear elution conditons, deviations were again seen for all loads studied. As noted in Figure 13, the simulations gave -1/ln f values larger than those predicted, with deviations increasing as load increased. It was also again seen that plots for loads of less than 100% appeared to have zero intercepts while those for loads above 100% gave nonzero intercepts. This occurred for the same reasons as discussed previously.

Despite the similarities between Figures 13 and 16, there were also significant differences. For example, the values of -1/ln f for the adsorption-limited case were typically greater than those for the diffusion-limited case under the same load and reduced residence time conditions. The two cases also differed in that the results in Figure 16 did not converge with the response predicted under linear elution conditions. Instead, no apparent decrease in absolute deviations was noted as $(u_e/h)(k_{-1}/k_1\ k_3\ [L])$ increased. This occurred for all loads studied and over a $(u_e/h)(k_{-1}/k_1\ k_3\ [L])$ range of at least 0.03 to 20 (i.e., an expected free fraction range under linear elution conditions of 3×10^{-13}% to 95%). It was further noted in Figure 16 that small loads, such as 16 and

32%, gave an almost linear increase in -1/ln f with (u_e/h) (k_{-1}/k_1 k_3 [L]), behavior not noted in the diffusion-limited results.

Differences in the adsorption- and diffusion-limited cases were also apparent when comparing their responses to increasing load at a constant residence time. The results for the adsorption-limited case, shown in Figure 17, differ from those under equivalent conditions for the diffusion-limited case in Figure 15 in that deviations were present at all loads and residence times studied while in the diffusion-limited case they occurred only once a certain load level had been reached. Also, it was again noted that the relative size of the deviations in the adsorption-limited case were larger than those for diffusion-limited systems under equivalent conditions.

Such differences can be explained based on the two kinetic models used. In the case of diffusion-limited kinetics, the system is represented by a series of first-order reactions and, under linear elution conditions, the split-peak slope is independent of the number of ligand sites. The result, as shown earlier, is that deviations occur only after all ligand in the first segment of the column has been depleted. This produces the behavior seen in Figures 13 and and 15, where certain load and residence time conditions must

Figure 17. The effect of increasing load on $-1/\ln f$ at a constant value of $(u_e/h)(k_{-1}/k_1\ k_3\ [L])$. The plots shown are for $(u_e/h)\ (k_{-1}/k_1\ k_3\ [L])$ values of 0.16 (●), 0.32 (◆), 0.64 (▲), and 1.28 (■). The horizontal line is the response predicted under linear elution conditions by Equation 45

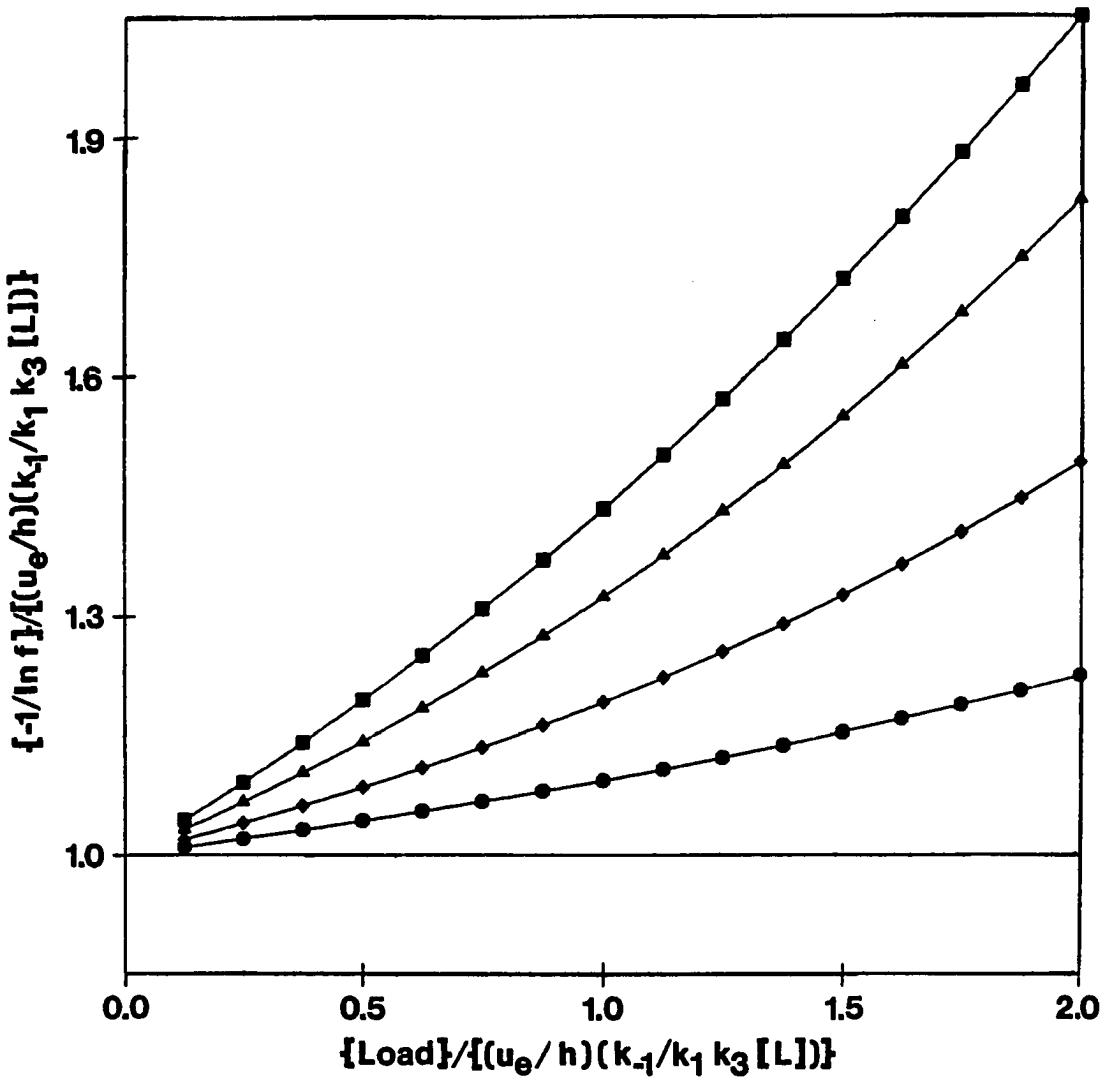
1.9
1.6
1.3
1.0
0.0
0.5
1.0
1.5
2.0
{-1/ln f}/{(u_e/h)(k_-1/k_1 k_3 [L])}
{Load}/{(u_e/ h)(k_-1/k_1 k_3 [L])}

be met to produce nonlinear effects. In the adsorption-limited case, however, the model used is second-order in nature and the split-peak slope is a function of 1/[L]. This means that any depletion of free ligand will cause the apparent rate constant k_3 [L] to decrease and the split-peak slope to increase. As a result, the adsorption-limited case would be expected to be more susceptible to deviations than the diffusion-limited case at any given load, with deviations occurring as long as finite sample loads are used.

In Section I it was shown that one experimental system exhibiting adsorption-limited kinetics is the binding of IgG to CDI-immobilized protein A affinity columns. Typical split-peak plots for this system are given in Figure 18 for loads of 0.9 to 3.7%. These plots are similar to the simulation results in Figure 16 in several ways. First, each data set in Figure 18 gave an apparent linear relationship between -1/ln f and flowrate, as seen for loads of 32% or less in Figure 16. Secondly, the IgG data at different loads did not converge to a single response at high flowrates, as was also seen with the simulation results, but continued to increase with flowrate over the entire range studied.

Because of this last factor, eliminating or even minimizing nonlinear effects for such a system can prove difficult if done by only adjusting the flowrate and/or load

Figure 18. Split-peak plots for IgG on a CDI-immobilized protein A column. The plots shown are for 10 μL injections of 0.14 (●), 0.27 (▲), and 0.55 (■) mg/mL rabbit IgG. The chromatographic conditions were the same as described in the text. The line given for each data set is its linear fit through the origin

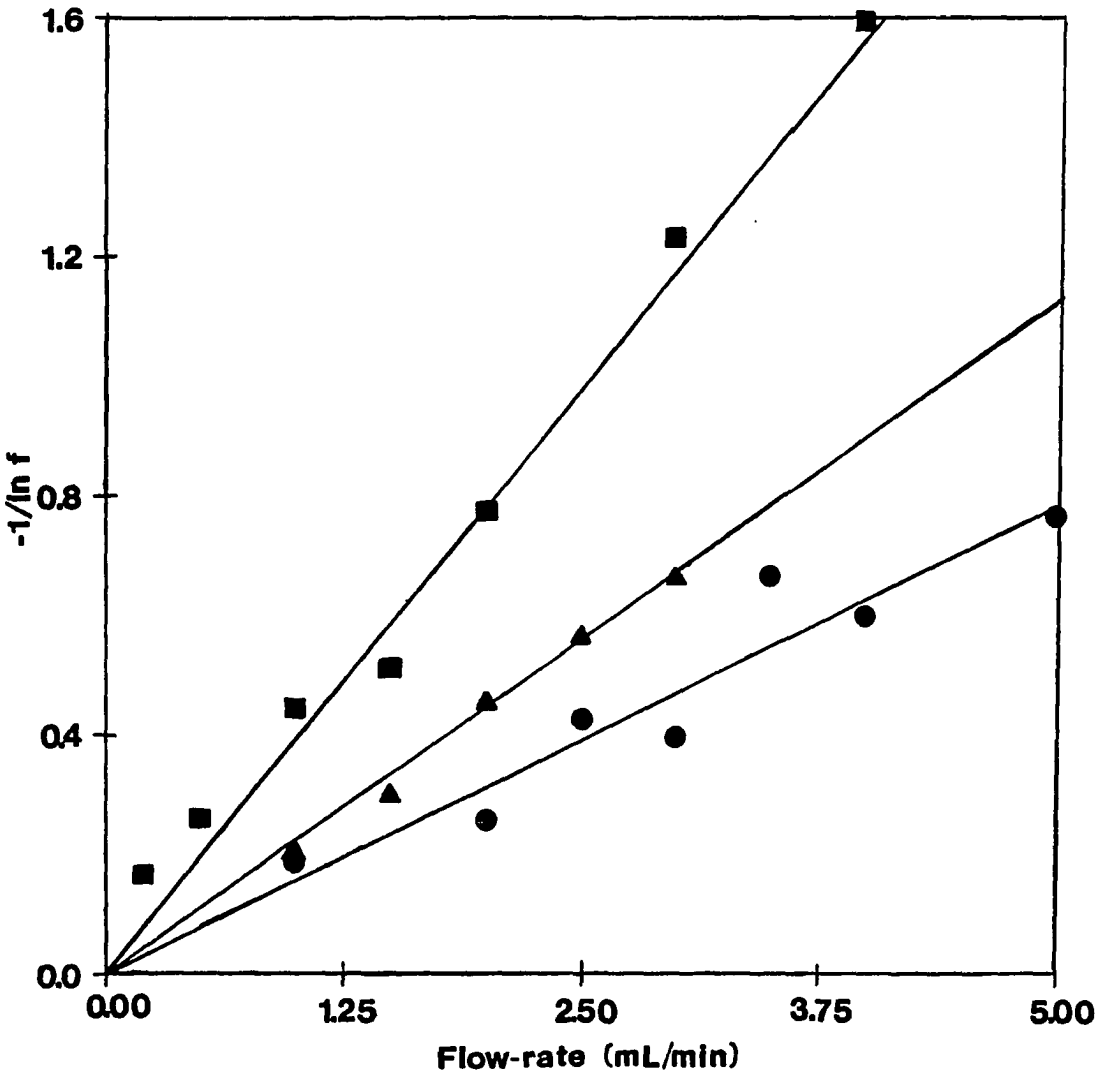
1.6
1.2
0.8
0.4
0.0
-1/ln f
0.00
1.25
2.50
3.75
5.00
Flow-rate (mL/min)

conditions. Instead, a technique is required to extrapolate the results under linear elution conditions from those obtained under nonlinear conditions. A third set of simulation studies were performed to determine what extrapolation methods could be effectively used. The technique tested was one using linear extrapolation, since in Section I it was shown that the split-peak slope of such protein A columns appeared to increase linearly with sample load.

These studies were done by using the simulation model to generate split-peak plots at various loads under adsorption-limited conditions. The slope of each plot was then measured using a linear least-squares fit through the origin, the same technique used in the previous study. Each slope was measured using 14 points over $(u_e/h)(k_{-1}/k_1\ k_3\ [L])$ values of 0.063 to 1.24. This range corresponds to free fractions of 10^{-5} to 45% under linear elution conditions. The slopes obtained were then plotted vs. load, as shown in Figure 19. The resulting curve showed an essentially linear increase in the measured slope for loads of 24% or less but with some curvature beginning to appear as the load increased further.

The data in Figure 19 were used to test the extrapolation procedure by performing linear least-square fits over various load regions of the plot. The intercept obtained (i.e., the extrapolated value of the slope at 0% load) was then compared

Figure 19. The effect of increasing load on the measured split-peak slope for a system with irreversible adsorption-limited kinetics. The slope values were determined as described in the text. The line shown is the linear fit to the data over the load range of 4 to 16%

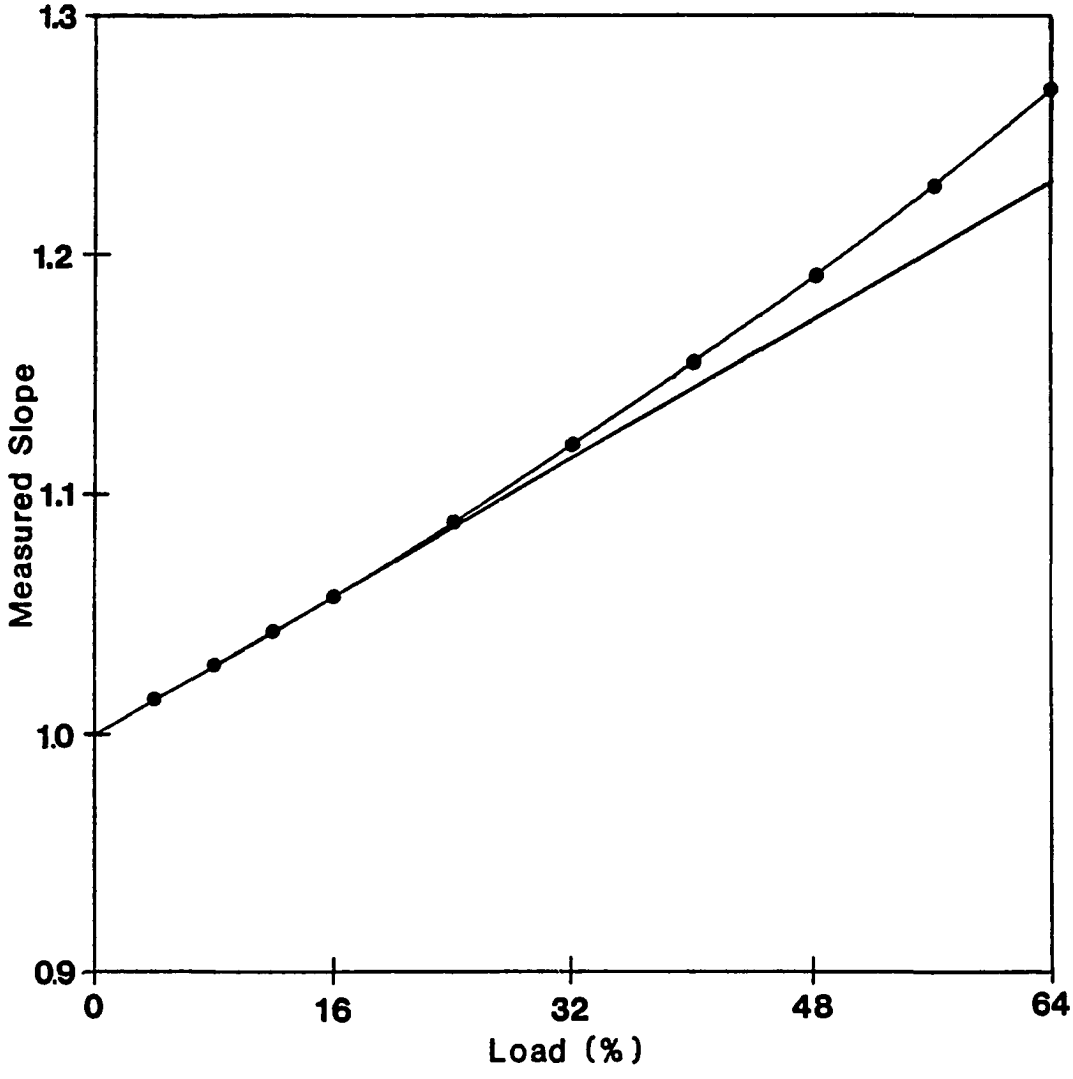
1.3
1.2
1.1
1.0
0.9
Measured Slope
0
16
32
48
64
Load (%)

to the value predicted under linear conditions, a true split-peak slope of 1.0000 according to Equation 45. The results obtained are summarized in Table IX. In general, the use of small loads in the extrapolation gave more accurate results than when larger loads were used, with an error of only 0.9 ppt being obtained with loads of 4 to 16%. However, even with the largest load range studied, 16 to 64%, the error was still less than the best experimental precision obtained with such measurements in the previous chapter, a value of $\pm$ 3.4%.

Figure 20 shows plots obtained when this extrapolation method was applied to various protein A columns using data from Figure 7, taken under approximately the same free fraction conditions used to generate the simulation results. The plots given represent the two matrixes shown earlier to be adsorption-limited, the CDI-500 and SB-50 protein A columns, and one in which both adsorption and diffusion contributed to the overall rate of IgG retention, the SB-500 protein A. Also shown are the simulation results for the load range of 4 to 16%.

In Figure 20, each protein A support gave the same linear response between the measured slope and load seen with the simulation results. This demonstrates the apparent applicability of this extrapolation method to complex as well as simple adsorption-controlled systems and, in the case of

Table IX. Error of linear extrapolation vs. load range for a system with irreversible adsorption-limited kinetics

Load range[a]	Linear least-squares fit parameters		% Error[b]
	Slope x 10^3	Intercept	
4 to 16%	3.62 ± 0.03	0.9991 ± 0.0003	-0.09
8 to 32%	3.87 ± 0.06	0.996 ± 0.001	-0.4
16 to 64%	4.43 ± 0.15	0.983 ± 0.007	-1.7

[a]The results for each data set are for 4 points distributed evenly throughout the load range studied.

[b]Calculated using the intercepts and an expected value under linear conditions of 1.0000.

Figure 20. The effect of varying load on the measured split-peak slopes for IgG on various protein A matrices. The protein A data are from Figure 7. The plots shown are for the SB-50 (▲), SB-500 (◆), and CDI-500 (●) matrices described earlier and the simulation results for the load range of 4 to 16% (■) from Figure 19

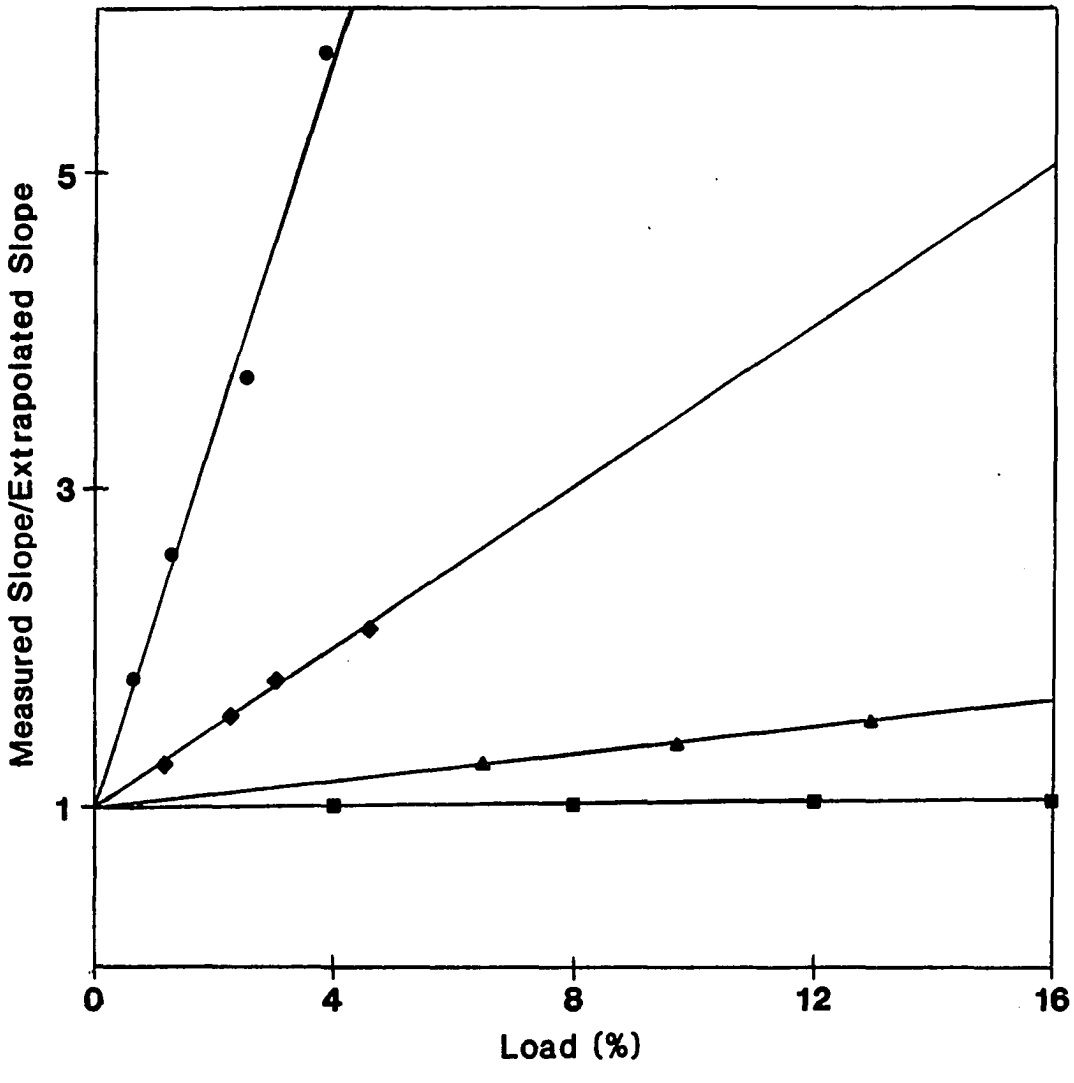
Measured Slope/Extrapolated Slope
5
3
1
0
4
8
12
16
Load (%)

the SB-500, even to those systems with some diffusional contribution to their kinetics. Although the reason for the linearity of the SB-500 response is not totally clear, it may indicate that as the transition from a simple diffusion-limited system to an adsorption-limited systems occurs, the increased sensitivity of the intermediate systems vs. the diffusion-limited case to column overloading may give them a response more closely resembling that of an adsorption-limited system.

Another observation made in Figure 20 was that the experimental data showed a much larger relative increase in slope with load than predicted from the computer modeling. For example, the slope of such a plot predicted from the simulations was 3.62×10^{-3} for the given loads while experimentally this value ranged from 0.043 to 1.18. This may, again, be a sign that secondary effects such as site heterogeneity or reversible binding were present.

Of these, site heterogeneity may have been particularly important. For adsorption-limited kinetics, this may be a result of both diffusional, or mass transfer, heterogeneity and heterogeneity of the ligand. The differences in mass transfer heterogeneity for the two matrix materials used in Figure 20 has already been discussed. The possible presence of ligand heterogeneity in these systems was also suggested

earlier in that the Schiff base and CDI coupling methods were shown in Section I to give immobilized protein A with different apparent adsorption rate constants, with the Schiff base protein A having a k_3 value ten times that produced by the CDI method. One possible interpretation given for this was that the CDI method denatured the protein to a greater extent, producing a more heterogeneous population of ligand and lowering the apparent value of k_3.

Based on both types of site heterogeneity, it is possible to predict the same order of deviations as seen in Figure 20. For example, the SB-50 support, with the largest adsorption rate constant and the smallest amount of mass transfer heterogeneity, would have been expected to most closely resemble the simple adsorption-limited case. The SB-500 data, obtained using the same type of protein A but on a more porous matrix, would have been predicted to give larger deviations. Lastly, the CDI-500 results, acquired on the same matrix material as the SB-500 but with possibly more heterogeneous protein A, would have been expected to give the largest deviations.

CONCLUSIONS

The simulation results presented show that nonlinear elution effects in split-peak chromatography can be minimized by using the proper separation conditions or extrapolation techniques. For the diffusion-limited case, it was found that these effects could be reduced or even eliminated by using small sample loads and/or fast flowrates. An expression was derived to calculate the flowrate and load conditions needed to produce nonlinear effects for the simple kinetic system studied. Although such a calculation is accurate for an experimental system only if its kinetics follow the model used here, this expression should still be useful for more complex diffusion-limited systems as a guideline in determining the approximate range of load or flowrate conditions that can be used without producing nonlinear effects.

For the adsorption-limited case, simulations demonstrated that nonlinear effects can not be totally eliminated by changing the flowrate or load. However, the data did show that such effects can be minimized by using extrapolation techniques. This was done by making a plot of the measured split-peak slope vs. sample load and performing a linear fit to determine the slope at zero sample load. When using loads less than 16%, the extrapolated slope obtained for the case studied varied by less than 1 ppt from that expected under

linear elution conditions. Although the error increased with the loads used, even over a load range of 16 to 64% its level was still acceptable, having a value of less than 2%.

The difference in nonlinear effects seen with the split-peak plots obtained for these two cases suggests that such plots may be useful tools in determining the rate-limiting step for solute retention in chromatographic systems. For example, the split-peak plots for hemoglobin on a C8 reversed-phase column showed the same nonlinear effects as the diffusion-limited case, while a similar study for IgG on a CDI protein A column gave results resembling those obtained for the adsorption-limited case. These results confirmed those of earlier experiments suggesting that the hemoglobin and IgG systems studied were diffusion- and adsorption-limited, respectively. Thus, by making split-peak plots at various loads and comparing the resulting curves to the simulation results presented here, it may be possible to determine the rate-limiting step in adsorption for a given matrix. This should not only be useful in obtaining kinetic data but also in the optimization of chromatographic separations.

Although the hemoglobin and IgG studies showed the same general responses predicted by the simulations, they also gave larger deviations than expected from the computer modeling.

It was proposed that this was due to the presence of secondary effects such as site heterogeneity or reversible binding. Of these, site heterogeneity may be particularly important since the relative size of deviations seen with various protein A columns was noted to follow the order predicted based on only their ligand and mass transfer heterogeneities. Mass transfer heterogeneity was also implicated in the hemoglobin study. Further computer modeling needs to be done to better determine the influence of this and other such phenomenon on the non-linear elution effects seen in split-peak chromatography.

GENERAL SUMMARY AND CONCLUSION

Summary of Experimental Results and Conclusions

Throughout this work, a number of different aspects of the split-peak effect have been considered. First, previous observations of this phenomenon were discussed as well as the relative importance of this effect in affinity separations. Equations were then derived to describe the split-peak effect in terms of the kinetic processes occurring within the column. These processes included diffusion of the analyte between the flowing and stagnant mobile phases and binding of the analyte with the immobilized ligand. Following this, it was demonstrated how these equations agreed qualitatively with previous experimental observations.

To quantitatively test the equations developed, the adsorption of IgG on protein A affinity columns was used. The results of this study were presented in Section I. For each column tested, the linear relationship predicted by the model was noted. The data from these plots were used to measure kinetic parameters for the binding of IgG to immobilized protein A. By comparing protein A columns prepared using different immobilization methods and support materials, it was found that diffusion was rate-limiting in some cases while adsorption was rate-limiting in others. It was also found

that the apparent adsorption rate constant for the IgG-protein A system varied by an order of magnitude depending on which immobilization method was used. This indicated that the kinetic properties of immobilized protein A could be affected by the coupling method used to prepare it.

The same model was used in Section II to optimize analyte adsorption in a high-performance affinity chromatographic system. This system consisted of two columns in series: the first containing immobilized anti-albumin antibodies and the second containing immobilized protein A. These were used for the analysis of HSA and IgG, respectively. In optimizing analyte adsorption at a given flowrate, the column size required by the antibody column was found to be limited by its binding capacity for HSA, while the protein A column was limited by the rate of immunoglobulin adsorption. Based on this and other information about the supports, a method was developed for the determination of both HSA and IgG in serum. This technique gave results in good agreement with those obtained with commercially available methods, while requiring only 2 μL of serum and 6.0 min per cycle. It was shown that both HSA and IgG were selectively retained by the system, with little interference from other serum components.

The last study examined the effect of nonlinear elution conditions on the relative size of the nonretained peak.

This was of interest since it was noted in the previous studies that the relative size of the nonretained peak varied with sample size for IgG adsorption on protein A columns. This was studied using computer simulations. Two different cases were examined: those in which either diffusion or adsorption was the rate-limiting step in analyte retention. The simulation data were compared to results obtained for the adsorption of hemoglobin on reversed-phase columns and the binding of immunoglobulin G to protein A columns. The hemoglobin results were similar to those obtained with simulations for the diffusion-limited case, while the IgG results resembled those seen with the adsorption-limited case. From the simulations, guidelines were developed for minimizing or eliminating nonlinear elution effects for both of the cases studied. For the diffusion-limited case, it was found that these effects could be reduced or even eliminated through the use of high flowrates and/or small sample loads. In the adsorption-limited case, it was shown that nonlinear effects could not be totally eliminated by merely adjusting the experimental conditions. However, it was also found that these effects could be minimized through the use of extrapolation techniques. The particular technique tested was one in which plots of the split-peak slope vs. sample size were made

and linear regression was used to extrapolate to the split-peak slope at zero sample size.

Over the course of these studies, a number of potential applications were discussed regarding the equations developed. One was the evaluation of the adsorption kinetics of affinity chromatographic supports. This was illustrated in Section I, where plots were prepared for various protein A supports according to Equation 26 and the slopes of these plots determined. Since the slope of this equation is related to the rate constants of the system, this parameter was used to compare the kinetic properties of the supports. Under given operating conditions, it was found that the SB-50 support gave the smallest slope and the fastest rate of analyte adsorption. The CDI-500 support, with the largest slope, had the slowest rate of adsorption.

This type of information is useful in choosing which affinity support to use for a particular separation. Although the kinetic properties of a support are not normally examined in the design and use of affinity systems, the results presented here suggest this can be an important consideration. This is especially true for protein A supports, which were shown to vary in their kinetic properties depending on the immobilization method and packing material used to prepare them. The method presented here is a potentially fast and

easy approach for evaluating such properties, allowing supports to be compared simply on the basis of the size of their split-peak slopes.

An application closely related to this is the optimization of analyte adsorption. This was discussed in Section II, where it was used in the design of a dual-column system for the determination of HSA and IgG in serum. In this case, a modified version of Equation 26 was used. This described the kinetic properties of a support in terms of a single constant independent of both the flowrate and column volume. Using data obtained with the protein A and anti-HSA supports, it was demonstrated how this constant could be used to calculate the minimum column residence time required to produce a given degree of analyte adsorption.

This method differs from that presented by Roy et al. (37) in that it is a fundamental approach, relating analyte adsorption directly to the kinetic processes within the column, whereas the earlier technique was entirely empirical in nature. This not only gives this method a better theoretical basis but also makes it more convenient to use. This is true since this technique makes use of a single constant to characterize a system rather than a series of graphs, as used in the earlier method. Also, once this constant has been determined for a support, it can be used to calculate the

flowrate conditions needed on any size column or the column size needed at any particular flowrate to give the desired degree of retention. The technique developed by Roy et al., on the other hand, requires that a series of separate retention studies be done for each column size and flowrate used.

The expressions developed in this work should also be useful in studying the kinetics of chromatographic interactions. One aspect of this was discussed in Section I, where it was suggested that they might be used to improve the performance of chromatographic supports. For example, if k_1 and V_e for a system are known in addition to its split-peak slope, then it can be determined whether adsorption or diffusion is the rate-limiting step in retention. This was illustrated with the protein A supports in Section I. Once the rate-limiting step is known, it is possible to take steps to improve the kinetics of the system. If diffusion is found to be rate-limiting, it was suggested that this might be done by using a packing material with a smaller particle diameter, increasing k_1 and k_{-1} and providing faster mass transfer. This can also be accomplished by going from porous supports to pellicular or nonporous supports, as indicated by the reversed-phase results in Section I. If adsorption is rate-limiting, it was suggested that the kinetics might be improved by using a higher ligand coverage.

The use of this model in studying chromatographic interactions is also of interest from a fundamental point-of-view. One example of this was given in Section I. In this experiment, the split-peak slopes of the protein A supports were combined with other chromatographic parameters to determine the value of k_3 for each support. This provided a means of studying the effect of using different immobilization methods on the kinetic properties of the resulting ligand. The equations developed in this work have also been used to examine the retention of proteins on reversed-phase columns (121). In this case, the experimental change in k_1 with the particle diameter and the diffusion coefficient was found to be the same as that predicted by Equation 31, indicating the system was indeed diffusion-limited (121). Both examples demonstrate the potential usefulness of this approach in examining the kinetics of analyte-ligand interactions and other chromatographic processes.

Suggestions for Further Research

All of the applications dealt with in the preceding discussion involved using the equations and model developed to study the kinetic properties of chromatographic systems. These applications included comparing the kinetic properties of affinity supports, designing more efficient chromatographic

supports, and optimizing analyte adsorption on affinity columns or matrices. Another area in which these equations might be useful is in the determination of rate constants for macromolecular interactions. Possible advantages of using split-peak measurements for this were discussed in Section I.

To use this approach for such determinations, it is first necessary to determine how the values of k_3 obtained with this method compare to those measured with other techniques. This requires that some model system be tested for which rate constants and equilibrium data are already available. Two systems that have already been proposed for such studies are the binding of dinitrophenyl (DNP) haptens with immobilized MOPC 315 antibodies and the binding of p-nitrophenyl α-D-mannopyranoside (PNPM) with immobilized concanavalin A (125). Both are well-characterized systems with known equilibrium and rate constants. For example, the interation of DNP-NH-CH_3 haptens with MOPC 315 has an adsorption rate constant of 5.2×10^8 M^{-1} s^{-1} and an equilibrium binding constant of 9.6×10^5 M^{-1} (128). The binding of PNPM with concanavalin A has a value for k_3 of 5.4×10^4 M^{-1} s^{-1} and a value for K_3 of 8.7×10^3 M^{-1} (129).

In preliminary calculations, it was shown that neither of these systems is suitable for the split-peak determination of adsorption rate constants (125). This was discovered when the

various experimental factors needed to obtain sufficient separation of the nonretained and retained peak (i.e., a $k' \geq 10$) and adsorption-limited conditions (i.e., $1/k_3 \, m_L > 1/k_1 \, V_e$) were considered. For the DNP-antibody system, it was shown that adsorption is too fast to allow k_3 to be accurately measured under reasonable operating conditions. In the PNPM-concanavalin A system, it was found that adsorption-limited conditions were more easily achieved, however, the column size required for this was too small to be experimentally useful. Other calculations showed that all necessary experimental requirements might best be met by using reactions with rate and equilibrium constants similar to those of the IgG-protein A system (125). One general class of reactions that fits this description is the binding of macromolecular antigens with antibodies.

A review of the literature reveals that there at least two such systems available for study. One is the binding of staphylococcal nuclease with anti-nuclease antibodies (130) and the other is the binding of hemoglobin S with anti-hemoglobin S antibodies (131). The first has been reported to have an adsorption rate constant of 4.1×10^5 M^{-1} s^{-1} and a equilibrium binding constant of 8.3×10^8 M^{-1} (130). The second system has been reported to have a k_3 of 5.8×10^5 M^{-1} s^{-1} and a K_3 of 2.1×10^{10} M^{-1} (131). Note that both systems

have rate and equilibrium constants comparable to those believed to describe the IgG-protein A system.

Another system which might be used is the interaction of various steroids with glucocorticoid receptors. In this case, the rate and equilibrium constants are available for the binding of at least 7 different steroids to the hormone receptor. For this series of reactions, k_3 has been shown to have values ranging from 2.3×10^3 to 2.6×10^4 M^{-1} s^{-1} and K_3 has been found to have typical values of 1.2×10^7 to 3.2×10^9 M^{-1} (132). Again, these are approximately the same order of magnitude as the constants believed to be present in the IgG-protein A system.

In using these systems for split-peak measurements, it is first necessary to prepare a support containing a ligand representing one of the molecules in the reaction of interest. This support can be prepared by using the immobilization methods already discussed or through a number of related techniques (5,29). As in the case of protein A, the kinetic properties of the ligand may be susceptible to the immobilization method used. Thus, steps should be taken to allow for this. One way in which this might be done is by comparing the rate constants obtained on supports prepared by different immobilization methods. This is the same technique used in Section I. Another approach would be to compare the

results obtained on a set of columns using different molecules from the system of interest as the affinity ligand. It is particularly important to take such precautions with the antibody-antigen systems described, due to the relative susceptability of proteins to immobilization effects (29,90). This may be less of a problem when using the glucocorticoid receptor system, since in this case a steroid can be used as the affinity ligand.

Once the support has been prepared and the conditions required to adsorb and elute analyte are known, split-peak measurements can be made. It should be possible to do this by using standard chromatographic detectors, monitoring absorbance at 280 or 254 nm. The adsorption rate for the system can be obtained by making making split-peak measurements at various flowrates and plotting the data according to Equation 26. From the slope of these plots and independent estimates of m_L, k_1, and V_e, it is possible to calculate k_3. In performing this experiment, it is advised that an estimate of the diffusional term of the slope first be obtained, using the methods described in Section I. This is to insure that adsorption-limited conditions are present when these measurements are made. It is also necessary to correct the results for nonlinear elution effects. This can be done by using the extrapolation technique described in Section III.

To properly correct for nonlinear elution conditions in such studies, further work needs to be done in examining the role of secondary effects on split-peak measurements. Of these effects, heterogeneity is particularly of interest. One reason for this is that heterogeneity was implicated in both the reversed-phase and affinity studies in Section III as a major reason for the differences between the experimental and simulation results. Heterogeneity is also of interest since it was noted in the protein A studies that the sample-size dependence of the split-peak slope appeared to be directly related to this effect. If this is true, then the split-peak effect might be useful in evaluating the heterogeneity of affinity columns.

To examine the role of heterogeneity more closely, a series of simulations can be performed similar to those presented in Section III. The models used for this must consider the effect of having at least two types of kinetically distinct ligands present along with either adsorption- or diffusion-limited kinetics. For the diffusion-limited case, such a system may be represented by the following reactions:

$$E_e \underset{k_{-1}}{\overset{k_1}{\rightleftharpoons}} E_p \qquad (59)$$

$$E_e \underset{k'_{-1}}{\overset{k'_1}{\rightleftharpoons}} E'_p \qquad (60)$$

$$E_p + L \xrightarrow{\text{Fast}} E_p\text{-}L \qquad (61)$$

$$E'_p + L' \xrightarrow{\text{Fast}} E'_p\text{-}L' \qquad (62)$$

These reactions describe mass transfer of E from the flowing mobile phase to two diffusionally-distinct regions in the column. These regions can be thought of as representing the surface of particles with different diameters or different parts of the same support, such as the area within its pores and on its surface. Mass transfer of analyte to these regions is described by the rate constants k_1/k_{-1} and k'_1/k'_{-1}, respectively. The ligands located at each type of site are referred to as L and L'. Although these ligands are both assumed to have infinitely fast adsorption kinetics, they are distinguished from each other since the relative amount of ligand occuring in each region may vary.

Simulations may be performed for this system by using the computer model presented in Section III and a series of equations describing the change in E_e, E_p, E'_p, L, and L' as a function of time. Such equations can be developed based on the work of Rakowski (133), allowing the effect of varying k_1/k_{-1}, k'_1/k'_{-1}, and m_L/m'_L to be determined.

The effect of heterogeneity in diffusion-limited systems may be studied experimentally by using the adsorption of hemoglobin on reversed-phase columns, the same system used in Section III. To examine this effect, it is proposed that split-peak measurements for hemoglobin be made on at least two columns, each containing a nonporous support of a different diameter. Assuming the supports have fairly uniform particle diameters, these columns should represent reasonably homogeneous systems. From split-peak measurements on these columns and independent estimates of V_e, the value of k_1 for each support can be determined. Since supports with different diameters are used, Equation 31 predicts that different values of k_1 should be obtained for each column.

Following these measurements, it is suggested that a series of split-peak studies on mixed-bed columns also be done. These columns can be prepared by combining any two of the previously studied supports. The result should be a controlled heterogeneous system. By varying the relative amount of each support added, the amounts of L and L' can be changed. The value of k_1/k_{-1} and k_1'/k_{-1}' can be adjusted by varying the particle diameter of the supports. A series of hemoglobin split-peak studies on such columns, then, should be useful in generating experimental data to compare to the simulation results.

A similar set of studies can be performed examining the effect of heterogeneity in the adsorption-limited case. The model proposed for these studies is represented by the following reactions:

$$E_e \overset{K_1}{\rightleftharpoons} E_p \tag{63}$$

$$E_p + L \xrightarrow{k_3} E_p\text{-}L \tag{64}$$

$$E_p + L' \xrightarrow{k_3'} E_p\text{-}L' \tag{65}$$

As in the simple adsorption-limited model used in Section III, these reactions assume that the free analyte is in equilibrium between the flowing and stagnant mobile phases. Unlike the model in Section III, however, the analyte can bind with two types of ligand sites in the stagnant mobile phase, each with its own kinetic properties.

Equations can also be developed to allow this system to be studied with the computer model. This can be done based on an approach similar to that used in Section III for the simple adsorption-limited case, giving expressions which describe analyte retention as a function of time and such parameters as K_1, k_3, k_3', the porosities of the support, and the relative amount of each ligand present. By using these equations with the computer model, simulations can be per-

formed to examine the effect of changing each of these variables on the relative size of the nonretained peak.

This system can be studied experimentally by examining the retention of glucocorticoid receptor on immobilized steroid columns. In these studies, it is proposed that split-peak measurements for the hormone receptor be made on at least two different steroid columns. These columns should contain nonporous supports made up of identical packing material but different immobilized steroids. Nonporous supports are used to minimize diffusional heterogeneity and to help produce adsorption-limited conditions. Using split-peak studies on these supports, the value of k_3 for each support can be determined. By using different steroids as the ligands, different values of k_3 should be obtained, a possible range of 2.3×10^3 to 2.6×10^4 M^{-1} s^{-1} (132).

Following these measurements, a series of split-peak measurements on mixed-bed columns can also be done. These columns can be prepared as described earlier by combining various amounts of the previously studied supports. The amount of L and L' in these columns can be varied by changing the relative amount of each support added. The values of k_3 and k_3' can be altered by using supports with different immobilized steroids. Again, the result is a controlled heterogeneous system. By adjusting these various parameters

and making split-peak measurements with the glucocorticoid receptor, experimental data can be obtained to compare to the simulation results.

In addition to these experiments, a number of other studies are also possible. These include an examination of the effect of reversible binding on split-peak measurements under nonlinear elution conditions, determination of the reasons behind the immobilization-dependence of protein A kinetics, and the use of the split-peak effect in the optimization or study of other affinity systems. Regardless of the work which remains, it is clear from the results presented that the split-peak effect can be a useful chromatographic tool. Because of this, it is predicted that the future will bring an increased use of this effect in the study and design of biomacromolecular separations.

LITERATURE CITED

1. "Gel Electrophoresis of Proteins"; Hames, B. D.; Rickwood, D., Eds.; IRL Press: Washington, D. C., 1981.

2. "Gel Electrophoresis of Nucleic Acids"; Rickwood, D.; Hames, B. D., Eds.; IRL Press: Washington, D. C., 1982.

3. "Gel Permeation and Ion-Exchange Chromatography of Proteins and Peptides"; Parvez, H.; Kato, H.; Parvez, S., Eds.; VNU Science Press: Utrecht, the Netherlands, 1985.

4. Parikh, I.; Cuatrecasas, P. Chem. Eng. News 1985, 63, 17.

5. Scouten, W. H. "Affinity Chromatography"; John Wiley and Sons: New York, 1981.

6. Chase, H. A. J. Biotech. 1984, 1, 67.

7. Easterday, R. L.; Easterday, J. M. In "Immobilized Biochemicals and Affinity Chromatography"; Dunlap, R. B., Ed.; Plenum Press: New York, 1974; p. 123.

8. Porath, J. J. Chromatogr. 1978, 159, 13.

9. Brocklehurst, K.; Carlsson, J.; Kierstan, M. P. J.; Crook, E. M. Biochem. J. 1973, 133, 573.

10. Yon, R. J. Biochem. J. 1972, 126, 765.

11. Walters, R. R. Anal. Chem. 1985, 57, 1099A.

12. Starkenstein, E. Biochem. Z. 1910, 24, 210.

13. Engelhardt, W. A.; Kisselev, L. L.; Nezlin, R. S. Monatsh. Chem. 1970, 101, 1510.

14. Campbell, D. H.; Luescher, E.; Lerman, L. S. Proc. Nat. Acad. Sci. USA 1951, 37, 575.

15. Lerman, L. S. Proc. Nat. Acad. Sci. USA 1953, 39, 232.

16. Arsenis, C.; McCormick, D. B. J. Biol. Chem. 1964, 239, 3093.

17. McCormick, D. B. Anal. Biochem. 1965, 13, 194.

18. Hjerten, S. Arch. Biochem. Biophys. 1962, 99, 446.

19. Axen, R.; Porath, J.; Ernback, S. Nature (London) 1967, 214, 1302.

20. Cuatrecasas, P.; Wilchek, M.; Anfinsen, C. B. Proc. Nat. Acad. Sci. USA 1968, 61, 636.

21. Walters, R. R. Trends Anal. Chem. 1983, 2, 282.

22. Regnier, F. E.; Noel, R. J. Chromatogr. Sci. 1976, 14, 316.

23. Messing, R. A. J. Am. Chem. Soc. 1969, 91, 2370.

24. Ohlson, S.; Hansson, L.; Larsson, P. -O.; Mosbach, K. FEBS Lett. 1978, 93, 5.

25. Larsson, P. -O.; Glad, M.; Hansson, L.; Mansson, M. O.; Ohlson, S.; Mosbach, K. Adv. Chromatogr. 1983, 21, 41.

26. Phillips, T. M.; More, N. S.; Queen, W. D.; T. V. Holohan; Kramer, N. C.; Thompson, A. M. J. Chromatogr. 1984, 317, 173.

27. Crowley, S. C.; Walters, R. R. J. Chromatogr. 1983, 266, 157.

28. de Alwis, W. U.; Wilson, G. S. Anal. Chem. 1985, 57, 2754.

29. Turkova, J. "Affinity Chromatography"; Elsevier Scientific Publishing Co.: Amsterdam, 1978.

30. Giddings, J. C.; Eyring, H. J. Phys. Chem. 1955, 59, 416.

31. DeLisi, C.; Hethcote, H. W.; Brettler, J. W. J. Chromatogr. 1982, 240, 283.

32. Lowe, C. R.; Harvey, M. J.; Dean, P. D. G. Eur. J. Biochem. 1974, 41, 341.

33. Mohr, P.; Pommerening, K. "Affinity Chromatography"; Marcel Dekker: New York, 1985; Chapter 6.

34. Sportsman, J. R.; Wilson, G. S. Anal. Chem. 1980, 52, 2013.

35. Kasche, V.; Buchholz, K.; Galunsky, B. J. Chromatogr. 1981, 216, 169.

36. Hearn, M. T. W. J. Chromatogr. 1986, 376, 245.

37. Roy, S. K.; Weber, D. V.; McGregor, W. C. J. Chromatogr. 1984, 303, 225.

38. Hollis, D.; Cooke, N. presented at the 24th Eastern Analytical Symposium, New York, Nov. 1985.

39. Sportsman, J. R.; Liddil, J. D.; Wilson, G. S. Anal. Chem. 1983, 55, 771.

40. DeLisi, C.; Hethcote, H. W. In "Affinity Chromatography and Related Techniques"; Gribnau, T. C. J.; Visser, J.; Nivard, R. J. F., Eds.; Elsevier Scientific Publishing Co.: Amsterdam, 1982; pp. 63-78.

41. Hethcote, H. W.; DeLisi, C. J. Chromatogr. 1982, 240, 269.

42. Hethcote, H. W.; DeLisi, C. J. Chromatogr. 1982, 248, 183.

43. Hethcote, H. W.; DeLisi, C. In "Affinity Chromatography and Biological Recognition"; Chaiken, I. M.; Wilchek, M.; Parikh, I., Eds.; Academic Press: Orlando, FL, 1983; pp. 119-134.

44. Landgrebe, M. E.; Wu, D.; Walters, R. R. Anal. Chem. 1986, 58, 1607.

45. Cantor, C. R.; Schimmel, P. R. "Biophysical Chemistry, Part II"; Freeman: San Francisco, 1980; Chapter 10.

46. Bjork, I.; Petersson, B. -A.; Sjoquist, A. Eur. J. Biochem. 1972, 29, 579.

47. Sjoquist, J.; Meloun, B.; Hjelm, H. Eur. J. Biochem. 1972, 29, 572.

48. Sjodahl, J. Eur. J. Biochem. 1977, 73, 343.

49. Kimball, J. W. "Introduction to Immunology"; Macmillan: New York, 1983; pp. 20-25, 233-237.

50. Lindmark, R.; Thoren-Tolling, K.; Sjoquist, J. J. Immunol. Methods 1983, 62, 1.

51. Verwey, E. F. J. Exp. Med. 1940, 71, 635.

52. Richman, D. D. In "New Developments in Diagnostic Virology"; Bachmann, P. A., Ed.; Springer-Verlag: New York, 1983; pp. 159-176.

53. Goding, J. W. J. Immunol. Methods 1978, 20, 241.

54. Phillips, T. M. LC Magazine 1985, 3, 962.

55. Crowley, S. C., Dept. of Chemistry, Iowa State University, Ames, IA; unpublished results.

56. Warr, G. W.; Hart, I. R. Am. J. Vet. Res. 1979, 40, 922.

57. Andrews, P.; Kitchen, B. J.; Winzor, D. J. Biochem. J. 1973, 135, 897.

58. Dunn, B. M. Applied Biochem. Biotechnol. 1984, 9, 261.

59. Chaiken, I. M. Anal. Biochem. 1979, 97, 1.

60. Veronese, F. M.; Bevilacqua, R.; Chaiken, I. M. Mol. Pharmacol. 1979, 115, 313.

61. Liu, Y. C.; Ledger, R.; Bryant, C.; Stellwagen, E. In "Affinity Chromatography and Biological Recognition"; Chaiken, I. M.; Wilchek, M.; Parikh, I., Eds.; Academic Press: Orlando, FL, 1983; pp. 135-142.

62. Eilat, D.; Chaiken, I. M. Biochemistry 1979, 18, 790.

63. Nilsson, K.; Larsson, P. -O. Anal. Biochem. 1983, 134, 60.

64. Muller, A. J.; Carr, P. W. J. Chromatogr. 1984, 284, 33.

65. Anderson, D. J.; Walters, R. R. J. Chromatogr. 1986, 376, 69.

66. Giddings, J. C. "Dynamics of Chroatography"; Marcel Dekker: New York, 1965.

67. Horvath, C.; Lin, H. -J. J. Chromatogr. 1978, 149, 43.

68. Denizot, F. C.; Delaage, M. A. Proc. Natl. Acad. Sci. USA 1975, 72, 4840.

69. Anderson, D. J.; Walters, R. R. J. Chromatogr. Sci. 1984, 22, 353.

70. Katz, E.; Ogan, K. L.; Scott, R. P. W. J. Chromatogr. 1983, 270, 51.

71. Stout, R. W.; DeStefano, J. J.; Snyder, L. R. J. Chromatogr. 1983, 282, 263.

72. Nilsson, R.; Myhre, E.; Kronvall, G.; Sjogren, H. O. J. Immunol. Methods 1983, 62, 241.

73. Hancock, W. S.; Sparrow, J. T. In "High-Performance Liquid Chromatography"; Horvath, C., Ed.; Academic Press: New York, 1983; Vol. 3, pp. 51-54, 60-63.

74. Karger, B. L.; Snyder, L. R.; Horvath, C. "An Introduction to Separation Science"; John Wiley and Sons: New York, 1973; Chapter 5.

75. Anderson, D. A. Ph.D. Dissertation, Iowa State University, Ames, IA, 1986.

76. van Deemter, J. J.; Zuiderweg, F. J.; Klinkenberg, A. Chem. Eng. Sci. 1956, 5, 271.

77. Kennedy, G. J.; Knox, J. H. J. Chromatogr. Sci. 1972, 10, 549.

78. Chen, J. -C., Weber, S. G. Anal. Chem. 1983, 55, 127.

79. Walters, R. R. Anal. Chem. 1983, 55, 591.

80. Walters, R. R. J. Chromatogr. 1982, 249, 19.

81. Crowley, S. C.; Chan, K. C.; Walters, R. R. J. Chromatogr. 1986, 359, 359.

82. Lowry, O. H.; Rosebrough, N. J.; Farr, A. L.; Randall, R. J. J. Biol. Chem. 1951, 193, 265.

83. Moore, R. M.; Walters, R. R. J. Chromatogr. 1984, 317, 119.

84. Siggia, S.; Hanna, J. G. "Quantitative Organic Analysis"; John Wiley and Sons: New York, 1979; pp. 42-43.

85. Woolf, A. A. Anal. Chem. 1982, 54, 2134.

86. Pearson, J. D.; Lin, N. T.; Regnier, F. E. Anal. Biochem. 1982, 124, 217.

87. Lund, U. J. Liq. Chromatogr. 1981, 4, 1933.

88. Walters, R. R. Anal. Chem. 1983, 55, 1395.

89. Warren, F. V.; Bidlingmeyer, B. A. Anal. Chem. 1984, 56, 950.

90. Zaborsky, O. R. "Immobilized Enzymes"; CRC Press: Cleveland, OH, 1973; Chapter 3.

91. Pecht, I.; Lancet, D. Mol. Biol., Biochem. Biophys. 1977, 24, 306.

92. Lindmark, R.; Biriell, C.; Sjoquist, J. Scand. J. Immunol. 1981, 14, 409.

93. Dunford, H. B. In "Fast Methods in Physical Biochemistry and Cell Biology"; Sha'afi, R. I.; Fernandez, S. M., Eds.; Elsevier Scientific Publishing Co.: Amsterdam, 1983; Chapter 2.

94. Mallia, A. K.; Hermanson, G. T.; Krohn, R. I.; Fujimoto, E. K.; Smith, P. K. Anal. Lett. 1981, 14, 649.

95. Peters, T., Jr.; Biamonte G. T.; Doumas, B. T. Sel. Methods Clin. Chem. 1982, 9, 317.

96. Kaplan, A.; Szabo, L. L. "Clinical Chemistry"; Lea and Febiger: Philadelphia, 1979; Chapter 5.

97. Peters, T., Jr. In "Advances in Clinical Chemistry"; Bodansky, O.; Stewart, C. P., Eds.; Academic Press: New York, 1970; Vol. 13, pp. 37-109.

98. Blick, K. E.; Liles, S. M. "Principles of Clinical Chemistry"; John Wiley and Sons: New York, 1985; Chapter 6.

99. Cochrum, K. R. In "Review of Physiological Chemistry"; Harper, H. A.; Rodwell, V. W.; Mayes, P. A., Eds.; Lange: Los Altos, CA, 1977; pp. 596-608.

100. Ohlson, S. In "Affinity Chromatography and Biological Recognition"; Chaiken, I. M.; Wilchek, M.; Pakikh, I., Eds.; Academic Press: New York, 1983; pp. 255-256.

101. Papadea, C.; Check, I. J.; Reimer C. B. Clin. Chem. 1985, 31, 1940.

102. Becker, W. Immunochemistry 1969, 6, 539.

103. Harboe, N. M. G.; Ingild, A. Scand. J. Immunol. 1983, 17, Suppl. 10, 345.

104. Smith, P. K.; Krohn, R. I.; Hermanson, G. T.; Mallia, A. K.; Gartner, F. H.; Provenzano, M. D.; Fujimoto, E. K.; Goeke, N. M.; Olson B. J.; Klenk, D. C. Anal. Biochem. 1985, 150, 76.

105. Laemmli, U. K. Nature (London) 1970, 227, 680.

106. Mancini, G.; Carbonara, A. O.; Heremans, J. F. Immunochemistry 1965, 2, 235.

107. Walters, R. R.; Graham, J. F.; Moore, R. M.; Anderson, D. J. Anal. Biochem. 1984, 140, 190.

108. Duhamel, R. C.; Schur, P. H.; Brendel K.; Meezan, E. J. Immunol. Methods 1979, 31, 211.

109. Habeeb, A. F. S. A. In "Immunochemistry of Proteins"; Atassi, M. Z., Ed.; Plenum Press: New York, 1979; Vol. 3, pp. 223-229.

110. Yamamoto, S.; Uesugi, R.; Omura, M.; Hirata, H. Bull. Azabu Univ., Vet. Med. 1982, 3, 203.

111. Curtius, H. C.; Roth, M. "Clinical Biochemistry"; de Gruyter: New York, 1974; Vol. 2, pp. 1499-1500.

112. Van der Loo, W.; Hamers, R. Protides Biol. Fluids 1976, 23, 603.

113. Raglione, T. V.; Sagliano, N., Jr.; Floyd, T. R.; Hartwick, R. A. LC Magazine 1986, 4, 328.

114. Wade, J. L.; Bergold, A. F.; Carr P. W. Anal. Chem. 1987, 59, in press.

115. Kalinchev, A. I.; Pronin, A. Y.; Zolotarev, P. P.; Goryacheva, N. A.; Chmutov, K. V.; Filimonov, V. Y. J. Chromatogr. 1976, 120, 249.

116. Yamaoka, K.; Nakagawa, T. J. Chromatogr. 1975, 103, 221.

117. Lenoir, J. -Y.; Rojey, A. Separat. Sci. 1972, 7, 13.

118. Buys, T. S.; DeClerk, K. J. Chromatogr. 1972, 69, 87.

119. Elbe, J. E.; Antle, P. E.; Grob, R. L.; Snyder, L. R. J. Chromatogr. 1987, 384, 25.

120. Elbe, J. E.; Antle, P. E.; Grob, R. L.; Snyder, L. R. J. Chromatogr. 1987, 384, 45.

121. Larew, L. A.; Walters, R. R. submitted to Anal. Biochem.

122. Espenson, J. H. "Chemical Kinetics and Reaction Mechanisms"; McGraw-Hill: New York, 1981; Chapters 2-3.

123. Englelhardt, H.; Mathes, D. J. Chromatogr. 1979, 185, 305.

124. Pfannkoch, E.; Lu, K. C.; Regnier, F. E.; Barth, H. G. J. Chromatogr. Sci. 1980, 18, 430.

125. Walters, R. R. In "Analytical Affinity Chromatography"; Chaiken, I. M., Ed.; CRC Uniscience: Boca Raton, FL, in press.

126. Cammack, K. A. Nature 1962, 194, 754.

127. Dwight, H. B. "Tables of Integrals and Other Mathematical Data", 4th Ed.; Macmillan: New York, 1961; p. 132.

128. Haselkorn, D. Ph.D. Dissertation, Feinberg Graduate School, Weizmann Inst. Sci., Rehovot, Isreal, 1975.

129. Clegg, R. M.; Loontiens, F. G.; van Landschoot, A.; Jovin, T. M. Biochemistry 1981, 20, 4687.

130. Sachs, D. H.; Schechter, A. N.; Eastlake, A.; Anfinsen, C. B. Biochemistry 1972, 11, 4268.

131. Noble, R. W.; Reichlin, M.; Schreiber, R. D. Biochemistry 1972, 11, 3326.

132. Jones, T. R.; Bell, P. A. Biochem. J. 1982, 204, 721.

133. Rakowski, A. Z. Phys. Chem. 1906, 57, 321.

ACKNOWLEDGEMENTS

I would like to take this opportunity to thank the many individuals who made contributions to this work. The first is my wife Jill. Without her love and support, this dissertation would not have been possible. Second, I would like to express my appreciation to Dr. Rodney Walters and Dr. Dennis Johnson, my major and co-major professors, for their help and guidance throughout my graduate career. I am also grateful to Dr. Herbert Hethcote for his theoretical contributions to this work and to Dr. James Espenson for his help in testing part of the simulation programs. The financial support of the Proctor and Gamble Company and the National Science Foundation was also greatly appreciated.

Thanks also goes to the various members of the Walters' research group: Dave Anderson, Bob Moore, Sam Crowley, John Graham, Danlin Wu, Larry Larew, Jackie Anhalt, King Chan, Mary Landgrebe, and Steve Gilles. Of these, I would like to particularly thank Mary and Sam for the preparation of the EA and CDI supports, Jackie and Larry for proofreading parts of this work, and Danlin for his help in preparing this manuscript.

In addition to these, I would like to thank God, who has given me the opportunity to come to Ames and learn about Him and His creation through my graduate studies. It is to Him that I would like to dedicate this work.

APPENDIX

The following pages contain listings of the programs used in the simulations presented in Section III. The first program is that which was used to examine the diffusion-limited case. The second is that which was used in the adsorption-limited studies. Both are similar in their overall design. Definitions of the variables used in these programs are included in the listings as well as simple explanations of how the programs operate.

```
C     ****************************************************************
C     *                                                              *
C     *             SIMULATION PROGRAM FOR THE CASE OF               *
C     *               DIFFUSION-LIMITED KINETICS WITH                *
C     *                   IRREVERSIBLE ADSORPTION                    *
C     *                                                              *
C     ****************************************************************
C
C
C     ******************PARAMETER INITIALIZATION**********************
C
C          C(X,Y) = THE SIMULATED COLUMN WHERE X IS THE SLICE
C                   NUMBER AND Y IS THE PHASE (Y = 1, 2, AND 3
C                   FOR THE FLOWING MOBILE PHASE, STAGNANT
C                   MOBILE PHASE, AND STATIONARY PHASE)
C          A(X,Y) = A STORAGE ARRAY TO ALLOW THE ANALYTE
C                   ELUTING FROM THE COLUMN DURING ANY
C                   ITERATION TO BE DISPLAYED, WHERE X = THE
C                   ITERATION NUMBER AND Y IS THE PHASE, AS
C                   ABOVE
C            LNGTH = THE TOTAL COLUMN LENGTH + 1
C         MONTR(X) = THE SLICE ON THE COLUMN MONITORED FOR
C                   ANALYTE ELUTION
C         INCRM(X) = THE ITERATION STEP SIZE AT WHICH THE
C                   ANALYTE ELUTION DATA IS TO BE PRINTED
C                   OUT FOR THE MONITORED SLICE MONTR(X)
C          RK1,RK2 = K1 AND K-1
C            VE,VP = VE AND VP
C            G1,G2 = VE/VM AND VP/VM
C           E1,EQ1 = e-(K1 + K-1) AND 1 - e(-K1)
C               NM = THE NUMBER OF SLICES MONITORED
C               E3 = THE TOTAL AMOUNT OF ANALYTE APPLIED
C               E2 = THE TOTAL FRACTION OF FREE ANALYTE ELUTED
C                   WHEN THE PROGRAM IS TERMINATED
C             IMAX = THE MAXIMUM NUMBER OF ITERATIONS ALLOWED
C
C            THE REMAINDER OF THE VARIABLES ARE TEMPORARY STORAGE OR
C            CALCULATION BUFFERS
C
C     ****************************************************************
C
      DIMENSION INCRM(8),MONTR(8)
      REAL*8 C(2562,3),A(20000,5),CT,D,RK1,RK2,VE,VP,G1,G2,E1,E2,E3,
     XEQ1,TF,SUM,SMF,CA,FF,D2
      LNGTH=401
      VE=1.
      VP=1.0
      RK1=0.050
      RK2=RK1*VE/VP
      G1=VE/(VE+VP)
      G2=VP/(VE+VP)
      E1=DEXP(-RK1-RK2)
      EQ1=1.-DEXP(-RK1)
      NM=4
```

```
      MONTR(1)=(LNGTH-1)
      MONTR(2)=(LNGTH-1)/2
      MONTR(3)=(LNGTH-1)/4
      MONTR(4)=MONTR(3)+20
      MONTR(5)=MONTR(3)-20
      MONTR(6)=(LNGTH-1)/32
      MONTR(7)=(LNGTH-1)/64
      MONTR(8)=(LNGTH-1)/128
      INCRM(1)=100
      INCRM(2)=100
      INCRM(3)=100
      INCRM(4)=100
      INCRM(5)=100
      INCRM(6)=100
      INCRM(7)=50
      INCRM(8)=50
      WRITE (9,10)
10    FORMAT (/,/,/,/,/,/,5X,
     X'CASE = DIFFUSION-LIMITED/SINGLE SITE-SINGLE ANALYTE')
C
C     ********************SIMULATION PROCEDURES*********************
C
C          THE SIMULATION IS CARRIED OUT WITHIN THREE NESTED LOOPS
C          ORGANIZED AS FOLLOWS:
C
C               LDCNT LOOP (VARIES LOAD APPLIED)
C
C                    IL LOOP (VARIES TIME SINCE INJECTION)
C
C                         K LOOP (VARIES SLICE EXAMINED)
C
C                              KINETIC EQUATIONS FOR THE CASE
C                              STUDIED FOR ANALYTE DISTIBUTION
C
C                         CONTINUE K LOOP (LINE 60)
C
C                    CONTINUE IL LOOP (LINE 150)
C
C               CONTINUE LDCNT LOOP (LINE 400)
C
C      ************************************************************
C
      DO 400 LDCNT=1,1
      C(1,1)=0.24*FLOAT(LNGTH-1)/(2.**FLOAT(LDCNT-1))
      E2=0.999999
      E3=C(1,1)
      C(1,2)=0.
      C(1,3)=0.
      FF=0.
      SUM=0.
      IMAX=20000
```

```
      DO 20 K=2,LNGTH
      DO 20 J=1,3
20    C(K,J)=0.
      KS=1
      KL=1
      DO 150 IL=1,IMAX
      IF (IL.LT.LNGTH) GO TO 30
      D2=FF/(FF+SUM)
      IF (D2.GE.E2) GO TO 160
30    SUM=0.
      DO 60 K=KS,KL
      IF (C(K,3).LT.1.) GO TO 40
      D=C(K,1)+C(K,2)
      IF (D.EQ.0.) GO TO 60
      C(K,1)=D*G1+(C(K,1)*G2-C(K,2)*G1)*E1
      C(K,2)=D-C(K,1)
      GO TO 60
40    D=C(K,3)+EQ1*C(K,1)
      IF (D.GT.1.) GO TO 50
      C(K,3)=D
      C(K,1)=C(K,1)*(1.-EQ1)
      GO TO 60
50    TF=-DLOG((C(K,3)+C(K,1)-1.)/C(K,1))/RK1
      C(K,1)=C(K,1)-1.+C(K,3)
      C(K,3)=1.
      D=C(K,1)+C(K,2)
      IF (D.EQ.0.) GO TO 60
      C(K,1)=D*G1+(C(K,1)*G2-C(K,2)*G1)*DEXP((TF-1.)*(RK1+RK2))
      C(K,2)=D-C(K,1)
60    CONTINUE
      K=KL
70    C(K+1,1)=C(K,1)
      IF (K.LT.LNGTH) SUM=SUM+C(K+1,1)+C(K+1,2)
      K=K-1
      IF (K.GE.KS) GO TO 70
      C(KS,1)=0.
      SUM=SUM+C(KS,2)
      KL=KL+1
      IF (KL.GT.LNGTH) KL=LNGTH
      D=C(KS,1)+C(KS,2)
      IF (D.EQ.0.) KS=KS+1
      DO 80 MQ=1,NM
80    A(IL,MQ)=C(MONTR(MQ)+1,1)
      FF=FF+A(IL,1)
150   CONTINUE
160   IMAX=IL
      DO 300 MQ=1,NM
      CT=A(MONTR(MQ),MQ)
      IMIN=MONTR(MQ)+1
      DO 170 I=IMIN,IMAX
170   CT=CT+A(I,MQ)
      IF (MQ.NE.1) GO TO 220
```

```
      D=0.
      TF=0.
      CT=CT/E3
      KZ=LNGTH-1
      DO 180 K=1,KZ
      D=D+C(K,3)/E3
180   TF=TF+(C(K,1)+C(K,2))/E3
      SUM=D+TF+CT
      SMF=CT/(CT+TF)
C
C     ****************PRINT OUT OF SIMULATION RESULTS**************
C
      WRITE (9,190)
190   FORMAT (/,/,
     X'*****************************************************************
     X/,/,14X,'ANALYTE FRACTIONAL DISTRIBUTION')
      WRITE (9,200) D,TF,CT,SUM,SMF
200   FORMAT (/,2X,'ADSORBED',2X,'FREE ON COL',2X,'ELUTED',2X,
     X'TOTAL RECOVERED',2X,'FRAC FR ELUTED',/,1X,D10.5,1X,
     XD10.5,1X,D10.5,2X,D12.7,4X,D12.7)
      CA=FLOAT(IMAX)/FLOAT(MONTR(1))
      WRITE (9,210) IMAX,MONTR(1),CA
210   FORMAT (/,20X,'ITERATION STATISTICS',/,/,11X,'ITERATIONS',2X,
     X'MAX LENGTH',2X,'ITER/MAX LENGTH',/,
     X13X,I5,7X,I5,7X,D10.5)
220   WRITE (9,230) RK1,RK2,VE,VP,MONTR(MQ)
230   FORMAT (/,/,/,/,/,/,12X,'K1',9X,'K2',6X,'VE',4X,'VP',4X,
     X'UE',2X,'LENGTH',/,8X,D9.4,2X,D9.4,2X,F4.2,2X,F4.2,2X,
     X'1.0',3X,I4)
      D=1./FLOAT(MONTR(MQ))
      TF=D/RK1
      SUM=E3/FLOAT(MONTR(MQ))
      E2=100.*((RK1/EQ1)-1.)
      WRITE (9,240) D,TF,SUM,E2
240   FORMAT (/,7X,'UE/L',7X,'UE/LK1',7X,'LOAD',6X,
     X'% SIMULATION ERROR',/,4X,F10.8,2X,F10.7,1X,F10.6,6X,F10.6)
      D=DEXP(-1./TF)
      IF (MQ.NE.1) CT=CT/E3
      E2=100.*CT/D
      WRITE (9,250) D,CT,E2
250   FORMAT (/,18X,'IDEAL',6X,'MEASURED',10X,'% OF IDEAL',/,3X,
     X' FREE AREA',3X,D10.5,2X,D10.5,5X,F16.8)
      D=-1./DLOG(CT)
      E2=100.*D/TF
      WRITE (9,260) TF,D,E2
260   FORMAT (3X,' -1/LN F',4X,F10.6,2X,F10.6,5X,F16.8)
      WRITE (9,270)
270   FORMAT (/,18X,'TIME',11X,'RESPONSE',/)
      INC=INCRM(MQ)
```

```
      IMIN=IMIN-1
      DO 280 I=IMIN,IMAX,INC
      IF (A(I,MQ).LT..000000001) GO TO 280
      WRITE (9,290) I,A(I,MQ)
280   CONTINUE
290   FORMAT (12X,I10,7X,F14.10)
300   CONTINUE
400   CONTINUE
500   STOP
      END
```

```
C     ******************************************************************
C     *                                                                *
C     *              SIMULATION PROGRAM FOR THE CASE OF                *
C     *            IRREVERSIBLE ADSORPTION-LIMITED KINETICS            *
C     *                                                                *
C     ******************************************************************
C
C
C     ********************PARAMETER INITIALIZATION*********************
C
C          C(X,Y) = THE SIMULATED COLUMN WHERE X IS THE SLICE
C                   NUMBER AND Y IS THE PHASE (Y = 1, 2, AND 3
C                   FOR THE FLOWING MOBILE PHASE, STAGNANT
C                   MOBILE PHASE, AND STATIONARY PHASE)
C          A(X,Y) = A STORAGE ARRAY TO ALLOW THE ANALYTE
C                   ELUTING FROM THE COLUMN DURINNG ANY
C                   ITERATION TO BE DISPLAYED, WHERE X = THE
C                   ITERATION NUMBER AND Y IS THE PHASE, AS
C                   ABOVE
C            LNGTH = THE TOTAL COLUMN LENGTH + 1
C         MONTR(X) = THE SLICE ON THE COLUMN MONITORED FOR
C         INCRM(X) = THE ITERATION STEP SIZE AT WHICH THE
C                   ANALYTE ELUTION DATA IS TO BE PRINTED
C                   OUT FOR THE MONITORED SLICE MONTR(X)
C            VE,VP = VE AND VP
C               G2 = VE/VP
C            G3,G6 = VP/VM AND VE/VM
C               R1 = K3/VM
C               G1 = K3 L/VM
C               NM = THE NUMBER OF SLICES MONITORED
C               E3 = THE TOTAL AMOUNT OF ANALYTE APPLIED
C               E2 = THE TOTAL FRACTION OF FREE ANALYTE ELUTED
C                   WHEN THE PROGRAM IS TERMINATED
C             IMAX = THE MAXIMUM NUMBER OF ITERATIONS ALLOWED
C               G5 = OVERFLOW MONITOR FOR LOG CALCULATIONS
C            G8,G9 = MONITORS TO COMPARE mLso TO (mEpso + mEeso)
C
C     ******************************************************************
C
      DIMENSION INCRM(11),MONTR(11)
      REAL*8 C(2562,3),A(5000,11),CT,D,VE,VP,G1,G2,G3,G4,G5,G6,E2,E3
     XG7,G8,G9,CC0,CC1,X1,X2,TF,SUM,SMF,CA,FF,D2,T,TM,R1
      LNGTH=257
      VE=1.
      VP=1.0
      R1=(1./2.)/(64.**2)
      G1=R1*DFLOAT(LNGTH-1)
      G2=VE/VP
      G3=VP/(VE+VP)
      G6=VE/(VE+VP)
      G5=87.498233534
      G8=0.999999999
      G9=2.000000000-G8
      NM=1
```

```
      MONTR(1)=(LNGTH-1)
      MONTR(2)=(LNGTH-1)/2
      MONTR(3)=(LNGTH-1)/4
      MONTR(4)=(LNGTH-1)/8
      MONTR(5)=(LNGTH-1)/16
      MONTR(6)=(LNGTH-1)/32
      MONTR(7)=(MONTR(2))+128
      MONTR(8)=(MONTR(3)+64)
      MONTR(9)=MONTR(4)+32
      MONTR(10)=MONTR(5)+16
      MONTR(11)=MONTR(6)+8
      INCRM(1)=100
      INCRM(2)=100
      INCRM(3)=100
      INCRM(4)=100
      INCRM(5)=100
      INCRM(6)=100
      INCRM(7)=100
      INCRM(8)=100
      INCRM(9)=100
      INCRM(10)=100
      INCRM(11)=100
      WRITE (9,10)
10    FORMAT (/,/,/,/,/,/,5X,
     X'CASE = ADSORPTION-LIMITED/SINGLE SITE-SINGLE ANALYTE')
C
C     ********************SIMULATION PROCEDURES**********************
C
C          THE SIMULATION IS CARRIED OUT WITHIN THREE NESTED LOOPS
C          ORGANIZED AS FOLLOWS:
C
C               LDNCT LOOP (VARIES LOAD APPLIED)
C
C                    IL LOOP (VARIES TIME SINCE INJECTION)
C
C                         K LOOP (VARIES SLICE EXAMINED)
C
C                              KINETICS EQUATIONS FOR THE CASE
C                              STUDIED FOR ANALYTE DISTRIBUTION
C
C                         CONTINUE K LOOP (LINE 120)
C
C                    CONTINUE IL LOOP (LINE 150)
C
C               CONTINUE LDCNT LOOP (LIE 400)
C
C     ****************************************************************
C
      DO 400 LDCNT=1,1
      C(1,1)=0.16*DFLOAT(LNGTH-1)*(1+DFLOAT(LDCNT-1)*2)
      E2=0.999999
```

```
      E3=C(1,1)
      C(1,2)=0.
      C(1,3)=0.
      FF=0.
      SUM=0.
      IMAX=20000
      DO 20 K=2,LNGTH
      DO 20 J=1,3
20    C(K,J)=0.
      KS=1
      KL=1
      DO 150 IL=1,IMAX
      IF (IL.LT.LNGTH) GO TO 30
      D2=FF/(FF+SUM)
      IF (D2.GE.E2) GO TO 160
30    SUM=0.
      DO 120 K=KS,KL
40    CC0=1.-C(K,3)
      X2=C(K,1)+C(K,2)
      X1=X2-CC0
      IF (CC0.GT.0.) GO TO 50
      CC1=0.
      GO TO 100
50    G7=CC0*G8
      IF (X2.LT.G7) GO TO 60
      G7=CC0*G9
      IF (X2.GT.G7) GO TO 60
      GO TO 70
60    G4=X1*G1
      IF (G4.LT.G5) GO TO 80
      CC1=0.
      GO TO 90
70    CC1=1/((1/CC0)+G1)
      C(K,2)=CC1*G3
      C(K,3)=C(K,3)+CC0-CC1
      GO TO 110
80    CC1=(CC0*X1)/((DEXP(X1*G1))*X2-CC0)
90    C(K,3)=C(K,3)+CC0-CC1
100   C(K,2)=(X1+CC1)*G3
110   C(K,1)=C(K,2)*G2
120   CONTINUE
      K=KL
130   C(K+1,1)=C(K,1)
      IF (K.LT.LNGTH) SUM=SUM+C(K+1,1)+C(K+1,2)
      K=K-1
      IF (K.GE.KS) GO TO 130
      C(KS,1)=0.
      SUM=SUM+C(KS,2)
      KL=KL+1
      IF (KL.GT.LNGTH) KL=LNGTH
      D=C(KS,1)+C(KS,2)
      IF (D.EQ.0.) KS=KS+1
```

```
      DO 140 MQ=1,NM
140   A(IL,MQ)=C(MONTR(MQ)+1,1)
      FF=FF+A(IL,1)
150   CONTINUE
160   IMAX=IL
      DO 300 MQ=1,NM
      CT=A(MONTR(MQ),MQ)
      IMIN=MONTR(MQ)+1
      DO 170 I=IMIN,IMAX
170   CT=CT+A(I,MQ)
      IF (MQ.NE.1) GO TO 220
      D=0.
      TF=0.
      CT=CT/E3
      KZ=LNGTH-1
      DO 180 K=1,KZ
      D=D+C(K,3)/E3
180   TF=TF+(C(K,1)+C(K,2))/E3
      SUM=D+TF+CT
      SMF=CT/(CT+TF)
C
C     ****************PRINT OUT OF SIMULATION RESULTS***************
C
      WRITE (9,190)
190   FORMAT (/,/,
     X'*************************************************************'
     X/,/,14X,'ANALYTE FRACTIONAL DISTRIBUTION')
      WRITE (9,200) D,TF,CT,SUM,SMF
200   FORMAT (/,2X,'ADSORBED',2X,'FREE ON COL',2X,'ELUTED',2X,
     X'TOTAL RECOVERED',2X,'FRAC FR ELUTED',/,1X,D10.5,1X,
     XD10.5,1X,D10.5,2X,D12.7,4X,D12.7)
      CA=DFLOAT(IMAX)/DFLOAT(MONTR(1))
      WRITE (9,210) IMAX,MONTR(1),CA
210   FORMAT (/,20X,'ITERATION STATISTICS',/,/,11X,'ITERATIONS',2X,
     X'MAX LENGTH',2X,'ITER/MAX LENGTH',/,
     X13X,I5,7X,I5,7X,D10.5)
220   WRITE (9,230) R1,G2,G3,G6,MONTR(MQ)
230   FORMAT (/,/,/,/,/,6X,'K3/VM',8X,'VE/VP',6X,'VP/VM',5X,'VE/VM',
     X'UE',4X,'LENGTH',/,3X,D12.7,2X,D9.4,2X,D9.4,2X,D9.4,2X,
     X'1.0',3X,I4)
      D=1./DFLOAT(MONTR(MQ))
      TF=D*D*G6/R1
      SUM=E3/DFLOAT(MONTR(MQ))
      WRITE (9,240) D,TF,SUM
240   FORMAT (/,7X,'UE/L',7X,'(UE/L)(K-1/K1K3(L))',7X,'LOAD',
     X/,4X,F10.8,8X,F10.7,8X,F10.6)
      D=DEXP(-1./TF)
      IF (MQ.NE.1) CT=CT/E3
      E2=100.*CT/D
      WRITE (9,250) D,CT,E2
250   FORMAT (/,18X,'IDEAL',6X,'MEASURED',10X,'% OF IDEAL',/,3X,
     X' FREE AREA',3X,D10.5,2X,D10.5,5X,F16.8)
      D=-1./DLOG(CT)
      E2=100.*D/TF
```

```
      WRITE (9,260) TF,D,E2
260   FORMAT (3X,' -1/LN F',4X,F10.6,2X,F10.6,6X,F16.8)
      WRITE (9,270)
270   FORMAT (/,18X,'TIME',11X,'RESPONSE',/)
      INC=INCRM(MQ)
      IMIN=IMIN-1
      DO 280 I=IMIN,IMAX,INC
      IF (A(I,MQ).LT..000000001) GO TO 280
      WRITE (9,290) I,A(I,MQ)
280   CONTINUE
290   FORMAT (12X,I10,7X,F14.10)
300   CONTINUE
400   CONTINUE
500   STOP
      END
```